



### 저작자표시-비영리-변경금지 2.0 대한민국

이용자는 아래의 조건을 따르는 경우에 한하여 자유롭게

- 이 저작물을 복제, 배포, 전송, 전시, 공연 및 방송할 수 있습니다.

다음과 같은 조건을 따라야 합니다:



저작자표시. 귀하는 원 저작자를 표시하여야 합니다.



비영리. 귀하는 이 저작물을 영리 목적으로 이용할 수 없습니다.



변경금지. 귀하는 이 저작물을 개작, 변형 또는 가공할 수 없습니다.

- 귀하는, 이 저작물의 재이용이나 배포의 경우, 이 저작물에 적용된 이용허락조건을 명확하게 나타내어야 합니다.
- 저작권자로부터 별도의 허가를 받으면 이러한 조건들은 적용되지 않습니다.

저작권법에 따른 이용자의 권리와 책임은 위의 내용에 의하여 영향을 받지 않습니다.

이것은 [이용허락규약\(Legal Code\)](#)을 이해하기 쉽게 요약한 것입니다.

[Disclaimer](#)





# Collision-Free Control for Formation Flying of Multiple Satellites Using Artificial Potential Field

Jiyoон Hwang

The Graduate School  
Yonsei University  
Department of Astronomy

# Collision-Free Control for Formation Flying of Multiple Satellites Using Artificial Potential Field

A Master's Thesis  
Submitted to the Department of Astronomy  
and the Graduate School of Yonsei University  
in partial fulfillment of the  
requirements for the degree of  
Master of Astronomy

Jiyoон Hwang

December 2018



This certifies that the master's thesis  
of Jiyoong Hwang is approved.

---

Thesis Supervisor: Chandeok Park

---

Sang-Young Park: Thesis Committee Member #1

---

Kwangwon Lee: Thesis Committee Member #2

The Graduate School  
Yonsei University  
December 2018



## Acknowledgments

*To my family, friends, and the professors  
I sincerely express my gratitude  
for guiding me through this journey.*

# Contents

<b>Acknowledgments.....</b>	<b>1</b>
<b>Contents.....</b>	<b>i</b>
<b>List of Figures .....</b>	<b>iv</b>
<b>List of Tables.....</b>	<b>ix</b>
<b>Abstract .....</b>	<b>x</b>
<b>1. Introduction.....</b>	<b>1</b>
<b>1.1 Research Background .....</b>	<b>1</b>
1.1.1 Formation Flying .....	1
1.1.2 Artificial Potential Field .....	2
<b>1.2 Thesis Objectives .....</b>	<b>4</b>
<b>1.3 Thesis Organization.....</b>	<b>5</b>
<b>2. Enhanced APF Method for Satellites Formation Flying .....</b>	<b>7</b>
<b>2.1 Problem Formulation .....</b>	<b>7</b>
<b>2.2 Potential Function for Formation Flying .....</b>	<b>10</b>
2.2.1 Structural Potential Function .....	11

2.2.2	Repulsive Potential Function.....	15
2.2.3	Formation Potential Function .....	19
2.2.4	Stability Analysis.....	27
<b>2.3</b>	<b>Rotational Potential Function .....</b>	<b>29</b>
2.3.1	Rotational Force Function in 2-D.....	30
2.3.2	Rotational Potential Function in 3-D.....	33
<b>2.4</b>	<b>Continuous Control Law Based on Lyapunov Theorem .....</b>	<b>49</b>
<b>3.</b>	<b>Numerical Simulations and Analysis .....</b>	<b>54</b>
<b>3.1</b>	<b>Formation Keeping.....</b>	<b>54</b>
3.1.1	When Virtual Leader Does Not Avoid Obstacles .....	54
3.1.2	When Virtual Leader Avoids Obstacles .....	76
<b>3.2</b>	<b>Multiple Reconfigurations .....</b>	<b>81</b>
<b>3.3</b>	<b>Improvement of Local Minima Problem.....</b>	<b>85</b>
<b>4.</b>	<b>Sliding Surface Application .....</b>	<b>91</b>
<b>4.1</b>	<b>Sliding Mode Controller Design.....</b>	<b>91</b>
<b>4.2</b>	<b>Simulation Results .....</b>	<b>97</b>
<b>5.</b>	<b>Conclusions .....</b>	<b>103</b>



<b>5.1 Summary and Contributions.....</b>	<b>103</b>
<b>5.2 Future Work .....</b>	<b>104</b>
<b>References .....</b>	<b>106</b>
<b>국문요약 .....</b>	<b>110</b>

## List of Figures

Figure 1.3.1 Thesis roadmap.....	6
Figure 2.1.1 Representation of ECI frame and relative frames.....	9
Figure 2.2.1 Possible location of the $k$ -th satellites for $k \in \{1,2,3,4\}$ (black dots) on the circle with a radius of $R$ centered on the virtual leader (a four-side star) in the $yz$ -plane using only structural potential function.....	14
Figure 2.2.2 Possible location of the $k$ -th satellites for $k \in \{1,2,3,4\}$ (black dots) on the circle with a radius of $R$ centered on the virtual leader (a four-side star) in the $yz$ -plane using the structural potential function and the repulsive potential function .....	16
Figure 2.3.1 Local minimum problem in the conventional APF approach.....	30
Figure 2.3.2 Rotational force around an obstacle and a satellite's trajectory .....	32
Figure 2.3.3 Reference frame $C$ and local coordinate frame $B$ .....	36
Figure 2.3.4 A rotated ellipse with a semi-major axis of $a'$ and a semi-minor axis of $b'$ and rotated $h'&n'$ -axes by an angle $\theta$ from $h&n$ -axes.....	42
Figure 2.3.5 Modified ellipse when $\sin 2\theta < 0$ .....	48
Figure 3.1.1a Trajectories of four satellites (solid line), obstacle (grey face), reference trajectory of the virtual leader (dashed line), initial & final position of virtual leader ( $\Delta$ ) and four satellites ( $\square$ ) .....	56
Figure 3.1.1b Lines between four satellites (solid line), obstacle (grey face), reference trajectory of the virtual leader (dashed line), instantaneous position of virtual leader ( $\Delta$ ) and four satellites ( $\square$ ) .....	57

Figure 3.1.2 Minimum Euclidean distance changes between four satellites.....	57
Figure 3.1.3 Relative distances between virtual leader and four satellites (solid line) in square formation and radius of circle R=6 m (dashed line) .....	58
Figure 3.1.4 Relative distances between satellites (solid line), side length of square, $62 \approx 8.485$ m (dashed line), and diagonal length of square, 12 m (dashed line) .....	58
Figure 3.1.5a Trajectories of five satellites (solid line), obstacle (grey face), reference trajectory of the virtual leader (dashed line), initial & final position of virtual leader ( $\Delta$ ) and five satellites ( $\square$ ) .....	60
Figure 3.1.5b Lines between five satellites (solid line), obstacle (grey face), reference trajectory of the virtual leader (dashed line), instantaneous position of virtual leader ( $\Delta$ ) and five satellites ( $\square$ ) .....	61
Figure 3.1.6 Minimum Euclidean distance changes between five satellites .....	62
Figure 3.1.7 Relative distances between virtual leader and five satellites (solid line) in pentagon formation and radius of circle R=6 m (dashed line).....	62
Figure 3.1.8 Relative distances between satellites (solid line), side length of pentagon, $12\cos54^\circ \approx 7.053$ m (dashed line), and diagonal length of pentagon, $(6 + 6\sqrt{5})\cos(54^\circ) \approx 11.413$ m (dashed line) .....	63
Figure 3.1.9a Trajectories of six satellites (solid line), obstacle (grey face), reference trajectory of the virtual leader (dashed line), initial & final position of virtual leader ( $\Delta$ ) and six satellites ( $\square$ ) .....	65

Figure 3.1.9b Lines between six satellites (solid line), obstacle (grey face), reference trajectory of the virtual leader (dashed line), instantaneous position of virtual leader ( $\Delta$ ) and six satellites ( $\square$ ) .....	65
Figure 3.1.10 Minimum Euclidean distance changes between six satellites.....	66
Figure 3.1.11 Relative distances between virtual leader and six satellites (solid line) in hexagon formation and radius of circle $R=6$ m (dashed line) .....	66
Figure 3.1.12 Relative distances between satellites (solid line), side length of hexagon, 6 m (dashed line), and diagonal length of pentagon, $6\sqrt{3} \approx 10.392$ m & 12 m (dashed line) .....	67
Figure 3.1.13a Trajectories of four satellites (solid line), obstacle (grey face), reference trajectory of the virtual leader (dashed line), initial & final position of virtual leader ( $\Delta$ ) and four satellites ( $\square$ ) .....	69
Figure 3.1.13b Lines between four satellites (solid line), obstacle (grey face), reference trajectory of the virtual leader (dashed line), instantaneous position of virtual leader ( $\Delta$ ) and four satellites ( $\square$ ) .....	69
Figure 3.1.14 Minimum Euclidean distance changes between four satellites.....	70
Figure 3.1.15 Relative distances between virtual leader and four satellites (solid line) in regular tetrahedron formation and radius of circle $R=6$ m (dashed line) .....	70
Figure 3.1.16 Relative distances between satellites (solid line), side length of tetrahedron, $6\sqrt{4/3}\approx9.798$ m (dashed line) .....	71

Figure 3.1.17 Trajectories of four satellites (solid line), seven obstacles (grey face), reference trajectory of the virtual leader (dashed line), initial & final position of virtual leader ( $\Delta$ ) and four satellites ( $\square$ ) in two different views (upper & lower graphs).....	74
Figure 3.1.18 Minimum Euclidean distance changes between four satellites and the obstacles' surface .....	75
Figure 3.1.19 Relative distances between virtual leader and four satellites (solid line) in a square formation and radius of circle $R=6$ m (dashed line) .....	75
Figure 3.1.20 Relative distances between satellites (solid line), side length of square, $62 \approx 8.49$ m (dashed line), and diagonal length of square, 12 m (dashed line) .....	76
Figure 3.1.21a Trajectories of four satellites (solid line), obstacle (grey face), reference trajectory of the virtual leader (dashed line), initial & final position of virtual leader ( $\Delta$ ) and four satellites ( $\square$ ) .....	78
Figure 3.1.21b Lines between four satellites (solid line), obstacle (grey face), reference trajectory of the virtual leader (dashed line), instantaneous position of virtual leader ( $\Delta$ ) and four satellites ( $\square$ ) .....	79
Figure 3.1.22 Minimum Euclidean distance changes between four satellites.....	79
Figure 3.1.23 Relative distances between virtual leader and four satellites (solid line) in a square formation and radius of circle $R=6$ m (dashed line) .....	80
Figure 3.1.24 Relative distances between satellites (solid line), side length of square, $62 \approx 8.49$ m (dashed line), and diagonal length of square, 12 m (dashed line) .....	80
Figure 3.2.1a Trajectories of five satellites (solid line), obstacle (grey face), reference	

trajectory of the virtual leader (dashed line), initial & final position of virtual leader ( $\Delta$ ) and five satellites ( $\square$ ) .....	82
Figure 3.2.1b Lines between five satellites (solid line), obstacle (grey face), reference trajectory of the virtual leader (dashed line), instantaneous position of virtual leader ( $\Delta$ ) and five satellites ( $\square$ ) .....	83
Figure 3.2.2 Relative distances from the obstacle to four satellites (solid line) and the fifth satellite (bold dotted line).....	83
Figure 3.2.3 Relative distances between virtual leader and five satellites (solid line).....	84
Figure 3.2.4 Relative distances between five satellites (solid line), side length of pentagon, 7.053 m (dashed line) & diagonal length of pentagon, 11.413 m (dashed line) for 0~900 sec and side length of square, 8.485 m (dashed line) & diagonal length of square, 12 m (dashed line) after 900 sec .....	84
Figure 3.3.1 Trajectories of the satellite by Method A (solid line) & Method B (dashed line), initial position ( $\Delta$ ) & final position ( $\circ$ ) of the satellite, the target point (grey star), and obstacle (grey face) .....	90
Figure 3.3.2 Relative distances between the obstacle and the satellites by Method A (solid line) & Method B (dashed line) .....	90
Figure 4.2.1a Trajectories of four satellites (solid line), obstacle (grey face), reference trajectory of the virtual leader (dashed line), initial & final position of virtual leader ( $\Delta$ ) and four satellites ( $\square$ ) .....	100

Figure 4.2.1b Lines between four satellites (solid line), obstacle (grey face), reference trajectory of the virtual leader (dashed line), instantaneous position of virtual leader ( $\Delta$ ) and four satellites ( $\square$ ) .....	101
Figure 4.2.2 Relative distances between the obstacle and four satellites.....	101
Figure 4.2.3 Relative distances between virtual leader and four satellites (solid line) in a regular tetrahedron formation and radius of circle $R=6$ m (dashed line) .....	102
Figure 4.2.4 Relative distances between satellites (solid line), side length of tetrahedron, 9.798 m (dashed line) .....	102

## List of Tables

Table 3.1.1. Minimum relative distance with obstacle, final relative distance with virtual leader, and maximum final relative error with other satellites.....	72
--	----

## Abstract

### Collision-Free Control for Formation Flying of Multiple Satellites Using Artificial Potential Field

Hwang, Jiyoong

Dept. of Astronomy

The Graduate School

Yonsei University

This thesis presents satellite formation flying trajectory design and control based on virtual structure while avoiding obstacles using the artificial potential field (APF). To derive virtual structure formation control laws based on the APF, a formation potential function is defined, which enables multiple satellites to maintain a polygonal or tetrahedral formation. As an efficient method to circumvent the local minimum which often occurs in APF-based approach, a rotational potential function is newly derived in a local coordinate frame in the APF framework. In order to design and control the formation flying trajectory considering collision avoidance, gradient-based control laws are derived from a total potential function which is defined by combining the formation and the rotational potential function. The proposed control law goes through stability analysis by Lyapunov stability theorem and Barbalat's lemma.

The developed continuous control laws are tested numerically in formation keeping and reconfiguration examples subject to Hills-Clohessy-Wiltshire (HCW) dynamics. Simulation results show that the proposed approach successfully controls the trajectory of

autonomous satellites in the desired formation while avoiding collisions without falling into the local minimum, which is favorably compared with another APF-based approach. Further improving the formation flying performance and robustness, we add a Sliding Mode Control (SMC) to the APF technique. Simulation results show that the enhanced control law enables multiple satellites to better maintain their desired formation even in the presence of disturbances.

The novelty of this thesis lies that it derives a new potential function that allows collision avoidance maneuvers with less convergence to a local minimum. By integrating the newly defined potential functions for collision avoidance and formation control, the control laws can be designed based on the APF that guarantees the stability of the control system. Also, by defining the potential functions as above, the SMC is applicable to further improve the performance of the control laws.

---

Keywords: Artificial Potential Function (APF), Collision Avoidance, Formation Flying,  
Sliding Mode Control (SMC)

# 1. Introduction

## 1.1 Research Background

### 1.1.1 Formation Flying

Formation flying (FF) is an idea that multiple spacecraft fly while maintaining a specific formation to carry out their common missions cooperatively [1]. This concept is motivated by considering that formation flying can significantly reduce the budget and increase the incidence of successful missions. Instead of a single (complicated and huge) spacecraft, multiple (simple and small) spacecraft can carry out the same tasks economically [2, 3]. Furthermore, multiple spacecraft in rigorously coordinated formation can perform demanding missions that are difficult to achieve with a single spacecraft. Some examples are virtual telescopes, 3-D mapping and NASA's Magnetospheric Multiscale (MMS) mission in which four spacecraft fly in a tetrahedral shape [4, 5, 6]. These advantages motivate even unmanned air vehicles (UAV), robots and autonomous underwater vehicles to also employ coordinated formation maneuver [7, 8, 9, 10, 11].

A variety of formation flying can be sorted as leader-following, behavioral, and virtual structure approaches [12]. In the leader-following approach, a pair of leader and follower form in a group to cooperatively perform their common missions. In the behavioral approach, satellites do not follow a specified formation, but typically move through sensing and reacting with each other [13]. Adjacent satellites can communicate, and feedback control is possible between them, which allows flexible control under external disturbances. However, it is difficult to analyze this type of formation flying mathematically. In the virtual structure approach, satellites maneuver in a group, keeping a single rigid shape. An imaginary satellite can be added to the group, which plays a complementary role at the strategic position in the virtual structure. More connections between satellites via the virtual satellite or virtual leader enable a stronger formation while maneuvering, and the virtual

satellite never breaks as it is literally imaginary. As satellites maintain the pre-determined configuration, this approach is straightforward to prescribe behaviors of satellites. However, the virtual structure approach is designed not to consider possible applications such as formation reconfiguration and obstacle avoidance [14, 15]. In the case of missions that perform these maneuvers, the behavioral approach should also be used.

As the approaches mentioned above have pros and cons, alternative ones have been proposed that complement their shortcomings by combining the existing ones [16, 17]. The Rezaee et al. integrated the virtual structure approach and the behavioral approach in two-dimensional space to propose a novel method. A virtual leader is positioned at the center of the circle, and the other satellites are designed to locate equidistantly on the circle. As the satellites approach obstacles, they adopt the behavioral approach and avoid the obstacles, not maintaining the shape. However, this approach has not been applied to three-dimensional space.

### 1.1.2 Artificial Potential Field

It is also necessary to consider collision avoidance while maintaining formation flying [18]. In this research, we use Artificial Potential Field (APF) as the behavioral approach to consider obstacle avoidance and formation reconfiguration maneuvers in formation flying. The APF method is suitable for real-time control because its formulas and calculations are relatively simple and intuitive, and the stability of the control system can be guaranteed [19, 20]. These can be advantages for small satellites that lack hardware performance [21]. The APF is applied to designing a controller quickly to reflect environmental changes in real time and to ensure stability of the control system [22, 23].

Artificial Potential Field (APF) method is an obstacle avoidance technique in which the gradient of the potential field is applied to the actuator of the satellite as an artificial force. A repulsive potential field is set around the obstacles, and an attractive potential field is set at the target point so that satellites reach the target while avoiding obstacles through the

gradient of the integrated potential field. The artificial potential function and its gradient are expressed as an explicit function of the current position, the target point, and the position of obstacles. The APF method does not calculate the global solution, but the local solution. Since the positions of obstacles are expressed as an explicit function and the computational burden is relatively low, feedback control can be configured by reflecting the information of the states of obstacles in real time [24].

However, the APF often leads to a local minimum when the attractive and the repulsive potential function are combined, so that satellites fall at an unintended local minimum before reaching the target point. Also, GNRON (Goals Non-reachable with Obstacles Nearby) problem can happen, where satellites cannot approach the target point because of the repulsive force generated from the obstacle. Some algorithms have been proposed to solve this issue [25, 26, 27, 28, 29, 30, 31].

Reference [25] resolves the local minima issue by setting a virtual target point within the scope of visual region where it is possible to fall into the undesired local minimum. Here, the visual region refers to all the regions that the actuator can observe including obstacles. The actuator enables satellites to reach the real target point through the virtual target point defined in the visual region, avoiding the local minimum. Reference [26] introduces an algorithm that avoids local minima by applying Simulated Annealing (SA) to the APF. SA is a general stochastic meta-algorithm for the global optimization problem, which gives a relatively good approximation to the global optimization of a given function in an extensive search space. In reference [27], a superquadric function is applied to an avoidance potential function of the APF; as the distance between the satellite and obstacles grows farther, the avoidance potential function is defined so that it becomes closer to the sphere including the entire obstacle. As the distance decreases, conversely, the avoidance potential function is defined so that it becomes closer to the actual shape of the obstacle which has a finite-size geometric shape. This approach can alleviate the local minima problem and secure wider flight space of the spacecraft. Reference [17] presented a new approach to obstacle

avoidance in the APF instead of the conventional repulsive potential function. They designed a rotational force function in two-dimensional space that makes the satellite detour the obstacle instead of moving in the opposite direction from the obstacle. The virtual target approach is the safest way to avoid falling into the local minima, but it is unclear how to set virtual target points. In the case of SA approach, the computational complexity is increased by an additional algorithm, and the advantages of the original APF technique can be faded. The approach using the superquadric function can lower the probability of convergence to the local minima, but cannot escape from the local minima if obstacles, satellites, and target are in a straight line. The approach using the rotational force function is a simple way of not creating a local minimum, but since it is not a complete APF-based controller, stability cannot be guaranteed. Also, it is difficult to apply rotational force function into a three-dimensional space.

Based on the above techniques, if a rotational potential function can be obtained from the rotational force function, APF-based control laws can ensure the stability of control system and make avoiding convergence to local minima while taking advantage of straightforward and intuitive formulas of the APF. However, there has been no research to obtain the rotational potential function in a three-dimensional space.

## 1.2 Thesis Objectives

Since formation flying is mainly used for small satellites and complicated maneuvers may be required, control algorithms with low computational burden are appropriate for formation control. To consider collision avoidance maneuver additionally, we need an integrated algorithm. The APF can be a suitable technique to meet these requirements, but the method has a local minimum problem.

This research mainly aims to develop an algorithm for trajectory design and control of multiple satellites based on the APF for collision-free formation flying without converging to a local minimum. Inspired by [17], artificial potential functions for formation flying are newly proposed, and the rotational potential function which prevents satellites from being stuck at a local minimum is derived for collision avoidance in a newly defined local frame. After defining all potential functions for collision-free formation flying, control laws are derived to ensure the stability of the control system. The control law is validated by numerical simulations in the formation keeping and reconfiguration examples. In addition, we also develop a robust control law by employing Sliding Mode Control (SMC) to maintain more stable and consistent formation in the presence of disturbances. The control law can be easily expanded to nonlinear control because it is designed in the APF system. By expressing formation flying and obstacle avoidance maneuvers with an integrated potential function, the control law can be represented by a single equation for the proposed algorithm to be simpler and more convenient. In conclusion, the proposed algorithm mitigates local minimum problem through the rotational potential function and achieves the control objectives, which is suitable for formation control of small satellites.

### 1.3 Thesis Organization

In the rest of this thesis, we first derive the control law for formation flying based on the APF and the virtual structure. Then, we present a newly proposed collision avoidance technique and derive the gradient based control law for collision-free path planning (Chapter 2). Next, numerical simulations present the application of the developed control law to various formation flying examples (Chapter 3). Chapter 4 shows the augmentation of SMC to the developed control law to improve performance and robustness. Chapter 5

summarizes the discussion and concludes with future research plan. The thesis roadmap is shown in Figure 1.3.1.

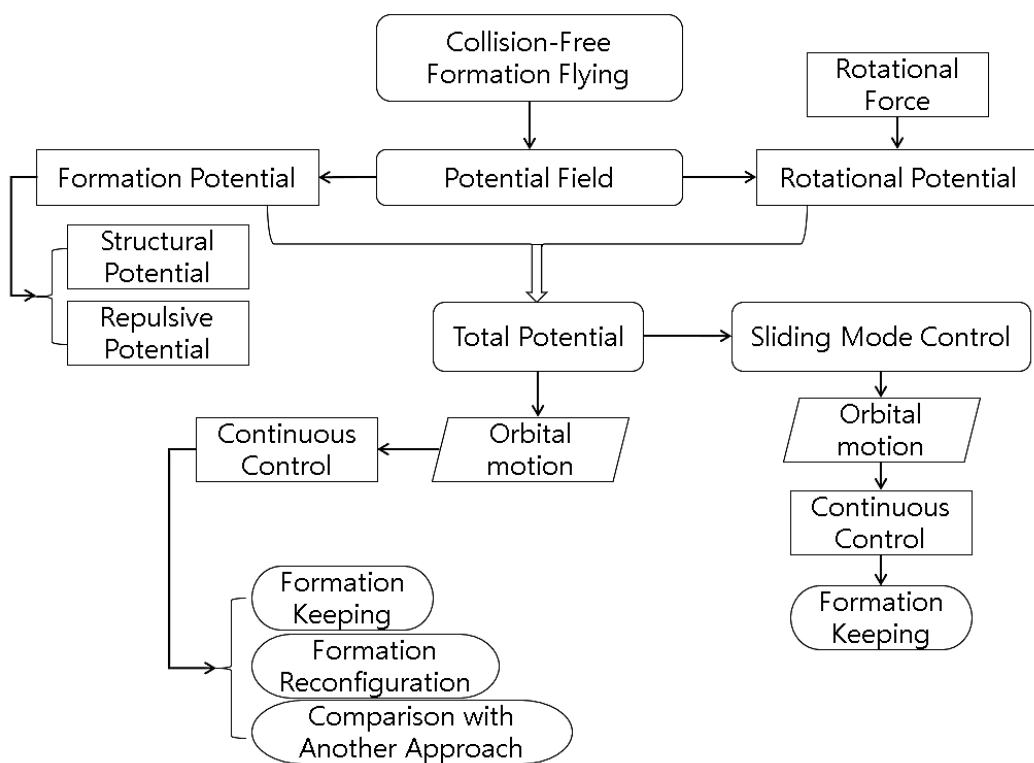


**Figure 1.3.1** Thesis roadmap

## 2. Enhanced APF Method for Satellites Formation Flying

Consider multiple satellites maneuvering in proximity to spacecraft or planets while maintaining a specific formation. This chapter presents a new technique of formation flying with obstacles avoidance by utilizing the virtual structure and the APF.

### 2.1 Problem Formulation

We use Hills-Clohessy-Wiltshire (HCW) equations of motion derived from the Earth Centered Inertial (ECI) frame to describe relative motion of satellites in the Low Earth Orbit (LEO). HCW equations are linearized equations describing the relative orbital motion on condition that both chief and deputy satellites are point masses and that the chief is in a circular orbit and that there is no other external force except spherically symmetric gravity force [32, 33]. HCW equations are presented as:

$$\begin{aligned}\ddot{x} &= 2w_0\dot{y} + 3w_0^2x \\ \ddot{y} &= -2w_0\dot{x} \\ \ddot{z} &= -w_0^2z\end{aligned}\tag{2.1.1}$$

where the  $x$ -axis is along the radius vector of the chief, the  $z$ -axis is along the normal vector to the chief orbit plane, and the  $y$ -axis follows the right-handed system (see Figure 2.1.1).  $w_0$  is the angular velocity of the chief's orbital motion and defined as:

$$w_0 = \sqrt{\frac{\mu}{a_c^3}}\tag{2.1.2}$$



where  $a_c$  is the radius of the chief's circular orbit and  $\mu = GM_E$ .  $G$  is the gravitational constant and  $M_E$  is the mass of the Earth.

The equations of motion with the control input is stated as:

$$\begin{aligned}\ddot{\mathbf{r}} &= f(\mathbf{r}, \dot{\mathbf{r}}) + \mathbf{u} \\ \mathbf{r} &= [x, y, z]^T, \quad \dot{\mathbf{r}} = [\dot{x}, \dot{y}, \dot{z}]^T, \quad \ddot{\mathbf{r}} = [\ddot{x}, \ddot{y}, \ddot{z}]^T \\ f(\mathbf{r}, \dot{\mathbf{r}}) &= [2w_0\dot{y} + 3w_0^2x, -2w_0\dot{x}, -w_0^2z]^T \\ \mathbf{u} &= [u_x, u_y, u_z]^T\end{aligned}\tag{2.1.3}$$

In this thesis, we aim to implement the formation flying of multiple satellites in the  $xyz$  coordinate system, originating from a spacecraft in orbit.

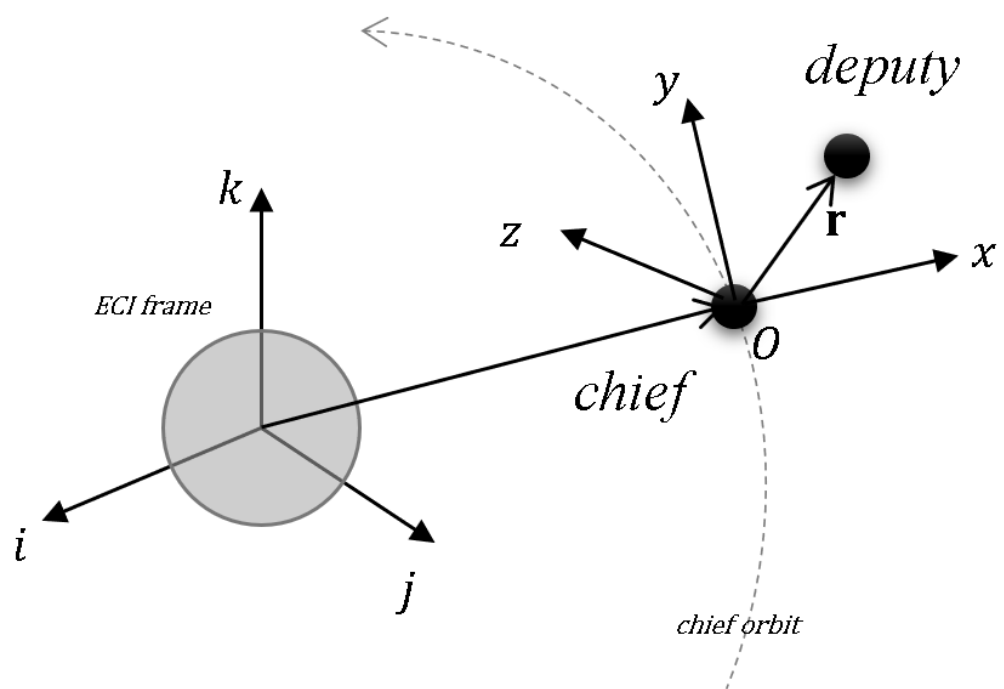


**Figure 2.1.1** Representation of ECI frame and relative frames

## 2.2 Potential Function for Formation Flying

The APF technique is a path planning method utilizing characteristics of physical systems in which the low potential means more stable. The APF artificially constructs the potential field in the configuration space and set the potential to zero at the target point. The gradient of the potential function acts as a force to move a satellite in the direction that the potential decreases to zero [22].

The artificial potential function typically consists of attractive and avoidance potential function. The former leads the satellite to the target point and the latter avoids obstacles. The attractive potential function should be designed to guarantee convergence to the target point. This convergence can be guaranteed by using Lyapunov stability theorem. In the Lyapunov stability theorem, a scalar energy-like function is created for the system, and the stability of the system (convergence to the equilibrium point) is ensured if this function satisfies some sufficient conditions [34]. The stability of the equilibrium point (the zero-potential point) is ensured by constructing the artificial potential function to satisfy the definition of Lyapunov function.

**Lyapunov stability theorem.** *Let origin  $\mathbf{r} = 0$  be the equilibrium point of a system  $\dot{\mathbf{r}} = g(\mathbf{r})$ . If the function  $V(\mathbf{r})$  is positive definite locally in  $\mathbf{R}^n$  and has continuous partial derivatives, and if its time derivative is negative semi-definite locally in  $\mathbf{R}^n$ , i.e.,*

$$\begin{cases} \text{If } V(0) = 0 \text{ and } V(\mathbf{r}) > 0 \quad \forall \mathbf{r} \in \mathbf{R}^n - \{0\} \\ \text{If } \dot{V}(0) = 0 \text{ and } \dot{V}(\mathbf{r}) \leq 0 \quad \forall \mathbf{r} \in \mathbf{R}^n - \{0\} \end{cases}$$

*then,  $V(\mathbf{r})$  is said to be a Lyapunov function for the system and the system is stable.*

In this research, we consider the formation flying of multiple satellites considering obstacle avoidance. For formation flying, a structural potential function and a repulsive

potential function are designed by utilizing the concept of the attractive potential function and virtual structure in Section 2.2.1 and Section 2.2.2 [17]. An integrated potential function for formation flying is described in Section 2.2.3. Stability analysis on control system based on the APF is presented in Section 2.2.4. For obstacle avoidance, a rotational potential function is distinctly developed with typical avoidance potential function such as the repulsive function in Section 2.3 [27].

### 2.2.1 Structural Potential Function

Various formations can be implemented through the virtual structure approach. In this research, however, we consider formation flying in which  $N$  satellites fly while maintaining polygonal or polyhedral shapes. Two types of potential functions of each satellite are defined for formation flying. It is assumed that all satellites are point masses. The first is a structural potential function to place a satellite on a circle/sphere with a radius of  $R$  and the second is a repulsive potential function to maintain the desired distance between the satellites on the circle/sphere.

Before defining the structural potential function which is necessary to locate the satellite on the circle/sphere, a (non-existent) virtual leader is located at the center of circle/sphere to maintain a rigid formation. The virtual leader determines the movement of the entire formation group, and the actual maneuvering satellites maintain an equal distance to the other satellites on the circle/sphere with a radius of  $\alpha$  centered on the virtual leader.

To locate satellites on the sphere, a positive definite structural potential function of the  $k$ -th satellite ( $k \in \{1, 2, \dots, N\}$ ) is defined as:

$$V_{structure,k} = \frac{1}{4} \lambda_{str} ((\mathbf{r}_k - \mathbf{r}_{VL}) \cdot (\mathbf{r}_k - \mathbf{r}_{VL}) - R^2)^2 \quad (2.2.1)$$

where  $\mathbf{r}_k = [x_k, y_k, z_k]^T$  denotes the position vector of the  $k$ -th maneuvering satellite,  $\mathbf{r}_{VL} = [x_{VL}, y_{VL}, z_{VL}]^T$  denotes the position vector of the virtual leader.  $\lambda_{str}$  is a positive scaling factor of the structural potential function, and  $R$  is the radius of sphere.  $V_{structure,k}$  becomes zero only if the  $k$ -th satellite is placed on the sphere. Otherwise,  $V_{structure,k}$  is always bigger than zero.

The time derivative of the structural potential function should be:

$$\dot{V}_{structure,k} = \lambda_{str}(\dot{\mathbf{r}}_k - \dot{\mathbf{r}}_{VL}) \cdot (\mathbf{r}_k - \mathbf{r}_{VL}) \cdot ((\mathbf{r}_k - \mathbf{r}_{VL}) \cdot (\mathbf{r}_k - \mathbf{r}_{VL}) - R^2) \quad (2.2.2)$$

where  $\dot{\mathbf{r}}_k = [\dot{x}_k, \dot{y}_k, \dot{z}_k]^T$  denotes the velocity vector of the  $k$ -th maneuvering satellite, and  $\dot{\mathbf{r}}_{VL} = [\dot{x}_{VL}, \dot{y}_{VL}, \dot{z}_{VL}]^T$  denotes the velocity vector of the virtual leader.

If we set the velocity of the  $k$ -th maneuvering satellite as [17]:

$$\dot{\mathbf{r}}_k = \dot{\mathbf{r}}_{VL} - (\mathbf{r}_k - \mathbf{r}_{VL}) \cdot ((\mathbf{r}_k - \mathbf{r}_{VL}) \cdot (\mathbf{r}_k - \mathbf{r}_{VL}) - R^2) \quad (2.2.3)$$

then, the time derivative of the structural potential function will be negative definite as:

$$\begin{aligned} \dot{V}_{structure,k} &= -\lambda_{str}(\mathbf{r}_k - \mathbf{r}_{VL}) \cdot (\mathbf{r}_k - \mathbf{r}_{VL}) \cdot ((\mathbf{r}_k - \mathbf{r}_{VL}) \cdot (\mathbf{r}_k - \mathbf{r}_{VL}) - R^2)^2 \\ &\leq 0 \end{aligned} \quad (2.2.4)$$

If the  $k$ -th satellite is controlled to maintain the required velocity of Eq. (2.2.3), the structural potential function can satisfy the definition of Lyapunov function and guarantees the stability.

The structural potential function is defined slightly different from Eq. (2.2.1) to form a polygonal shape on a plane instead of forming a polyhedral shape on a sphere. The structural potential function of the  $k$ -th maneuvering satellite for the formation on a circle with a radius of  $R$  centered on the virtual leader in the  $yz$ -plane is defined as follows.

The structural potential function of the  $k$ -th satellite is defined positive definite as:

$$V_{structure,k} = \frac{1}{4} \lambda_{str} [((y_k - y_{VL})^2 + (z_k - z_{VL})^2 - R^2)^2 + 2(x_k - x_{VL})^2] \quad (2.2.5)$$

The time derivative of the proposed potential function will be:

$$\begin{aligned} \dot{V}_{structure,k} = & \lambda_{str} [((\dot{y}_k - \dot{y}_{VL})(y_k - y_{VL}) + (\dot{z}_k - \dot{z}_{VL})(z_k - z_{VL})) \\ & \cdot ((y_k - y_{VL})^2 + (z_k - z_{VL})^2 - R^2) \\ & + (\dot{x}_k - \dot{x}_{VL})(x_k - x_{VL})] \end{aligned} \quad (2.2.6)$$

The required velocity of the  $k$ -th maneuvering satellite is defined as:

$$\begin{aligned} \dot{x}_k &= \dot{x}_{VL} - (x_k - x_{VL}) \\ \dot{y}_k &= \dot{y}_{VL} - (y_k - y_{VL})((y_k - y_{VL})^2 + (z_k - z_{VL})^2 - R^2) \\ \dot{z}_k &= \dot{z}_{VL} - (z_k - z_{VL})((y_k - y_{VL})^2 + (z_k - z_{VL})^2 - R^2) \end{aligned} \quad (2.2.7)$$

With Eq. (2.2.7), the time derivative of the structural potential function will be negative definite as:

$$\begin{aligned} \dot{V}_{structure,k} = & -\lambda_{str} [((y_k - y_{VL})(y_k - y_{VL}) + (z_k - z_{VL})(z_k - z_{VL})) \\ & \cdot ((y_k - y_{VL})^2 + (z_k - z_{VL})^2 - \alpha^2)^2 \\ & + (x_k - x_{VL})(x_k - x_{VL})] \\ & \leq 0 \end{aligned} \quad (2.2.8)$$

The structural potential function and the required velocity have been defined so that satellites can be located on a circle or a sphere. However, with the structural potential function only, it is difficult to control satellites to form a polygonal shape. Accordingly, the distance between the satellites needs to be adjusted to fulfill the desired shape using the repulsive potential function (see Figure 2.2.1).

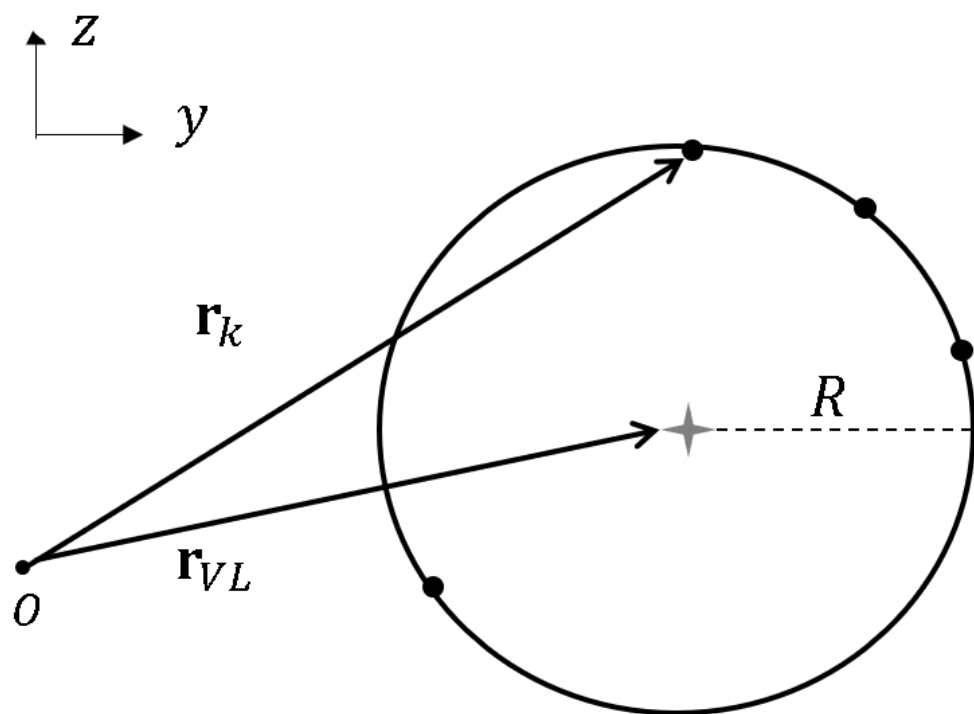


**Figure 2.2.1** Possible location of the  $k$ -th satellites for  $k \in \{1, 2, 3, 4\}$  (black dots) on the circle with a radius of  $R$  centered on the virtual leader (a four-side star) in the  $yz$ -plane using only structural potential function

## 2.2.2 Repulsive Potential Function

After placing satellites on a circle or a sphere with the virtual leader at the center, we need to adjust distances between the satellites to achieve the desired formation (see Figure 2.2.2). In this research, the formations of a regular polygon and regular tetrahedron are considered. To maintain the distances between satellites, every satellite is considered as an electric charge, and the distances are expanded by the Coulomb's law that the objects with the same electric charge generate repulsion [17]. Note that the repulsive potential function of the satellite generates a repulsive force to the other satellites which have the same charge except the virtual leader. Let  $N$  be the number of maneuvering satellites and  $\mathbf{r}_{ki}$  be the relative distance from the  $i$ -th satellite to the  $k$ -th satellite,  $\mathbf{r}_{ki} = \mathbf{r}_k - \mathbf{r}_i$  where  $k \in \{1, 2, \dots, N\}$ ,  $i \in \{1, 2, \dots, N\}$  and  $i \neq k$ . The repulsive potential function of the  $k$ -th satellite is defined as:

$$V_{rep,k} = \lambda_{rep} q_k \sum_{i=1, i \neq k}^N q_i \sqrt{\frac{1}{\mathbf{r}_{ki} \cdot \mathbf{r}_{ki}}} \quad (2.2.9)$$

where  $q_k$  and  $q_i$  denote electric charges of the  $k$ -th and the  $i$ -th satellites, respectively, and  $\lambda_{rep}$  is a positive scaling factor of the repulsive potential function. If all satellites have the same charge, the repulsive potential function of all satellites maintains a positive value, and it prevents them from colliding with each other. As all of them have the same charge, they reach the equilibrium point when the distances with each other are kept equal. That is, they can maintain the shape of a regular polygon or tetrahedron.

The time derivative of the proposed potential function of the  $k$ -th satellite will be:

$$\begin{aligned} \dot{V}_{rep,k} &= -\lambda_{rep} q_k \sum_{i=1, i \neq k}^N q_i \frac{\dot{\mathbf{r}}_{ki} \cdot \mathbf{r}_{ki}}{\sqrt{(\mathbf{r}_{ki} \cdot \mathbf{r}_{ki})^3}} \\ &= -\lambda_{rep} q_k \sum_{i=1, i \neq k}^N q_i \frac{(\dot{\mathbf{r}}_k - \dot{\mathbf{r}}_i) \cdot \mathbf{r}_{ki}}{\sqrt{(\mathbf{r}_{ki} \cdot \mathbf{r}_{ki})^3}} \end{aligned} \quad (2.2.10)$$

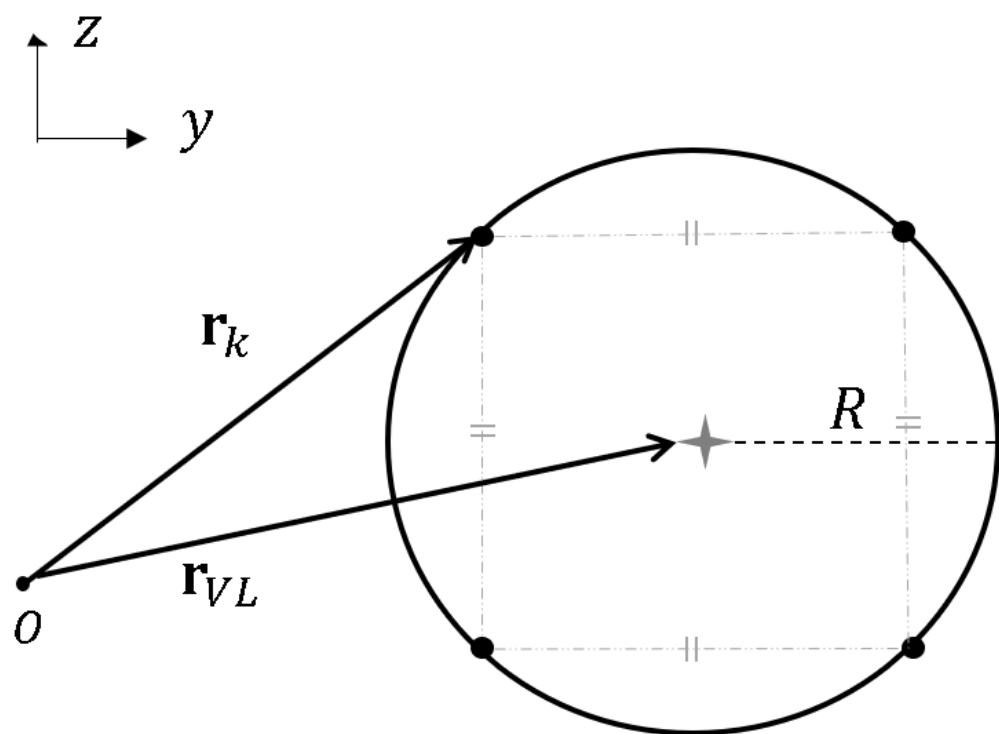


**Figure 2.2.2** Possible location of the  $k$ -th satellites for  $k \in \{1,2,3,4\}$  (black dots) on the circle with a radius of  $R$  centered on the virtual leader (a four-side star) in the  $yz$ -plane using the structural potential function and the repulsive potential function

Similar to the structural potential function, the required velocity of the  $k$ -th maneuvering satellite is defined as:

$$\dot{\mathbf{r}}_k = \sum_{i=1, i \neq k}^N \left( \dot{\mathbf{r}}_i + \frac{\mathbf{r}_{ki}}{\sqrt{(\mathbf{r}_{ki} \cdot \mathbf{r}_{ki})^3}} \right) \quad (2.2.11)$$

With Eq. (2.2.11), the time derivative of the repulsive potential function of the  $k$ -th satellite will be:

$$\dot{V}_{rep,k} = -\lambda_{rep} q_k \sum_{i=1, i \neq k}^N q_i \frac{1}{(\mathbf{r}_{ki} \cdot \mathbf{r}_{ki})^2} \quad (2.2.12)$$

The repulsive potential function maintains a negative value, but it is not a negative semi-definite function because we did not specify the equilibrium point in the repulsive potential function of each satellite. Instead of determining the desired position, letting coulomb's law balance the satellites naturally allows maintaining the formation without additional control. Even if one satellite fails on its way, the remaining satellites can reconfigure to another regular polygonal shape, which is demonstrated in examples in Chapter 3.

The proposed repulsive potential function enables satellites to maintain the desired polygonal shape if a sufficiently big structural potential function is given. If the structural function is too small compared with the repulsive potential function, it is difficult to locate satellites on the desired circle or sphere. However, in the case of polyhedral formation, which is a three-dimensional shape, it is challenging to maintain a solid formation only with the proposed repulsive potential function and the structural potential function; Coulomb force is insufficient to maintain equal distances in a regular polyhedron. For this reason, a regular tetrahedron is suitable for this method because the distances between all vertices are the same. Hence, this research deals with a regular tetrahedron to take advantage of the proposed technique.

To maintain a rigid shape of a regular tetrahedron during maneuvers, we slightly modify the previously defined repulsive potential function. Recall that a regular tetrahedron has

the same distance regardless of which of the two vertices you choose (i.e., equal length of every side). Using this property, we can create an equilibrium point in the repulsive potential function of each satellite so that every side of tetrahedron has equal length. With the virtual leader at the center of the regular tetrahedron, when the distance between the satellite and the virtual leader is set to be the radius of the sphere, the distance between the satellites is equally  $\frac{4R}{\sqrt{6}}$ . The repulsive potential function for regular tetrahedron formation is defined as follows using this value.

To make four satellites form a regular tetrahedron on a sphere with a radius of  $R$ , the repulsive potential function of the  $k$ -th satellite is defined as:

$$V_{rep,k} = \lambda_{rep} q_k \sum_{i=1, i \neq k}^N q_i \sqrt{\left( \frac{1}{\|\mathbf{r}_{ki}\|} - \frac{1}{4R/\sqrt{6}} \right) \cdot \left( \frac{1}{\|\mathbf{r}_{ki}\|} - \frac{1}{4R/\sqrt{6}} \right)} \quad (2.2.13)$$

It is specified that every satellite has the same positive charge,  $q_1 = q_2 = q_3 = q_4 > 0$ . When the magnitude of the relative distance between the  $k$ -th satellite and the  $i$ -th satellite,  $\|\mathbf{r}_{ki}\|$  becomes  $\frac{4R}{\sqrt{6}}$ , the repulsive potential function of the  $k$ -th satellite becomes zero. Thus, the repulsive potential function is positive definite.

The time derivative of the proposed potential function of the  $k$ -th satellite is given as:

$$\dot{V}_{rep,k} = \lambda_{rep} q_k \sum_{i=1, i \neq k}^N q_i \frac{\left( \frac{1}{\|\mathbf{r}_{ki}\|} - \frac{\sqrt{6}}{4R} \right)}{\left| \frac{1}{\|\mathbf{r}_{ki}\|} - \frac{\sqrt{6}}{4R} \right|} \left( -\frac{\dot{\mathbf{r}}_{ki}}{\|\mathbf{r}_{ki}\|^2} \right) \quad (2.2.14)$$

Velocity of the  $k$ -th maneuvering satellite is defined as:

$$\dot{\mathbf{r}}_k = \sum_{i=1, i \neq k}^N \left( \dot{\mathbf{r}}_i + \left( \frac{1}{\|\mathbf{r}_{ki}\|} - \frac{\sqrt{6}}{4R} \right) \frac{1}{\|\mathbf{r}_{ki}\|^2} \right) \quad (2.2.15)$$

With Eq. (2.2.15), the time derivative of the repulsive potential function of the  $k$ -th satellite is defined as:

$$\dot{V}_{rep,k} = -\lambda_{rep} q_k \sum_{i=1, i \neq k}^N q_i \left| \frac{1}{\|\mathbf{r}_{ki}\|} - \frac{\sqrt{6}}{4R} \right| \frac{1}{\|\mathbf{r}_{ki}\|^4} \leq 0 \quad (2.2.16)$$

The proposed repulsive potential function of the  $k$ -th satellite is negative definite.

### 2.2.3 Formation Potential Function

In this section, we integrate the potential functions for formation flying into one function and derive control laws for formation control without considering collision avoidance. The structural potential function ( $V_{structure}$ ) allows the satellite to be located on a sphere or circle with a specific radius, and the repulsive potential function ( $V_{rep}$ ) allows the satellite to be located equidistantly with other satellites on the sphere or circle. The function that is the sum of the structural potential function and the repulsive potential function is defined as a formation potential function ( $V_{form}$ ).

$$V_{form,k} = V_{structure,k} + V_{rep,k} \quad (2.2.17)$$

We derive the required velocity for two cases, formation flying in the  $yz$ -plane and formation flying in a regular tetrahedron shape.

#### (1) Formation flying in the $yz$ -plane

When  $N$  satellites form a regular polygonal shape in the  $yz$ -plane, the formation potential function of the  $k$ -th satellite is defined as:

$$\begin{aligned} V_{form,k} &= V_{structure,k} + V_{rep,k} \\ &= \frac{1}{4} \lambda_{str} [((y_k - y_{VL})^2 + (z_k - z_{VL})^2 - R^2)^2 + 2(x_k - x_{VL})^2] \\ &\quad + \lambda_{rep} q_k \sum_{i=1, i \neq k}^N q_i \sqrt{\frac{1}{\mathbf{r}_{ki} \cdot \mathbf{r}_{ki}}} \end{aligned} \quad (2.2.18)$$

The time derivative of the proposed potential function of the  $k$ -th satellite will be:

$$\begin{aligned}
 \dot{V}_{form,k} &= \dot{V}_{structure,k} + \dot{V}_{rep,k} \\
 &= \lambda_{str} [((\dot{y}_k - \dot{y}_{VL})(y_k - y_{VL}) + (\dot{z}_k - \dot{z}_{VL})(z_k - z_{VL})) \\
 &\quad \cdot ((y_k - y_{VL})^2 + (z_k - z_{VL})^2 - R^2) \\
 &\quad + (\dot{x}_k - \dot{x}_{VL})(x_k - x_{VL})] - \lambda_{rep} q_k \sum_{i=1, i \neq k}^N q_i \frac{(\dot{\mathbf{r}}_k - \dot{\mathbf{r}}_i) \cdot \mathbf{r}_{ki}}{\sqrt{(\mathbf{r}_{ki} \cdot \mathbf{r}_{ki})^3}}
 \end{aligned} \tag{2.2.19}$$

The required velocity of the  $k$ -th maneuvering satellite is defined as:

$$\begin{aligned}
 \dot{\mathbf{r}}_k = & \left[ \begin{array}{l} \dot{x}_{VL} - (x_k - x_{VL}) \\ \dot{y}_{VL} - (y_k - y_{VL})((y_k - y_{VL})^2 + (z_k - z_{VL})^2 - R^2) \\ \dot{z}_{VL} - (z_k - z_{VL})((y_k - y_{VL})^2 + (z_k - z_{VL})^2 - R^2) \end{array} \right] \\
 & + \sum_{i=1, i \neq k}^N \left( \dot{\mathbf{r}}_i + \frac{\mathbf{r}_{ki}}{\sqrt{(\mathbf{r}_{ki} \cdot \mathbf{r}_{ki})^3}} \right)
 \end{aligned} \tag{2.2.20}$$

The velocity vector is broken down into each component,  $[\dot{x}_k, \dot{y}_k, \dot{z}_k]^T$  and expressed as follows:

$$\begin{aligned}
 \dot{x}_k &= \dot{x}_{VL} - (x_k - x_{VL}) \\
 \dot{y}_k &= \dot{y}_{VL} - (y_k - y_{VL}) \cdot ((y_k - y_{VL})^2 + (z_k - z_{VL})^2 - R^2) \\
 &\quad + \sum_{i=1, i \neq k}^N \left( \dot{y}_i + \frac{(y_k - y_i)}{\sqrt{(\mathbf{r}_{ki} \cdot \mathbf{r}_{ki})^3}} \right) \\
 \dot{z}_k &= \dot{z}_{VL} - (z_k - z_{VL}) \cdot ((y_k - y_{VL})^2 + (z_k - z_{VL})^2 - R^2) \\
 &\quad + \sum_{i=1, i \neq k}^N \left( \dot{z}_i + \frac{(z_k - z_i)}{\sqrt{(\mathbf{r}_{ki} \cdot \mathbf{r}_{ki})^3}} \right)
 \end{aligned} \tag{2.2.21}$$

With the proposed velocity vector, the time derivative of formation potential function of  $k$ -th satellite will be:

$$\begin{aligned}
 \dot{V}_{form,k} &= \dot{V}_{structure,k} + \dot{V}_{rep,k} \\
 &= -\lambda_{str} [((y_k - y_{VL})(y_k - y_{VL}) + (z_k - z_{VL})(z_k - z_{VL})) \\
 &\quad \cdot ((y_k - y_{VL})^2 + (z_k - z_{VL})^2 - R^2)^2 \\
 &\quad + (x_k - x_{VL})(x_k - x_{VL})] - \lambda_{rep} q_k \sum_{i=1, i \neq k}^N q_i \frac{1}{(\mathbf{r}_{ki} \cdot \mathbf{r}_{ki})^2} \\
 &\leq 0
 \end{aligned} \tag{2.2.22}$$

## (2) Formation flying in a regular tetrahedron shape

The formation potential function of the  $k$ -th satellite for a regular tetrahedron formation is defined positive definite as:

$$\begin{aligned}
 V_{form,k} &= V_{structure,k} + V_{rep,k} \\
 &= \frac{1}{4} \lambda_{str} ((\mathbf{r}_k - \mathbf{r}_{VL}) \cdot (\mathbf{r}_k - \mathbf{r}_{VL}) - R^2)^2 \\
 &\quad + \lambda_{rep} q_k \sum_{i=1, i \neq k}^N q_i \sqrt{\left( \frac{1}{\|\mathbf{r}_{ki}\|} - \frac{1}{4R/\sqrt{6}} \right) \cdot \left( \frac{1}{\|\mathbf{r}_{ki}\|} - \frac{1}{4R/\sqrt{6}} \right)}
 \end{aligned} \tag{2.2.23}$$

The time derivative of the formation potential function of the  $k$ -th satellite will be:

$$\begin{aligned}
 \dot{V}_{form,k} &= \dot{V}_{structure,k} + \dot{V}_{rep,k} \\
 &= \lambda_{str} (\dot{\mathbf{r}}_k - \dot{\mathbf{r}}_{VL}) \cdot (\mathbf{r}_k - \mathbf{r}_{VL}) \cdot ((\mathbf{r}_k - \mathbf{r}_{VL}) \cdot (\mathbf{r}_k - \mathbf{r}_{VL}) - R^2) \\
 &\quad + \lambda_{rep} q_k \sum_{i=1, i \neq k}^N q_i \frac{\left( \frac{1}{\|\mathbf{r}_{ki}\|} - \frac{\sqrt{6}}{4R} \right)}{\left| \frac{1}{\|\mathbf{r}_{ki}\|} - \frac{\sqrt{6}}{4R} \right|} \left( -\frac{\mathbf{r}_{ki}}{\|\mathbf{r}_{ki}\|^3} \cdot \dot{\mathbf{r}}_{ki} \right)
 \end{aligned} \tag{2.2.24}$$

The required velocity of the  $k$ -th maneuvering satellite is defined as:

$$\begin{aligned}\dot{\mathbf{r}}_k &= \dot{\mathbf{r}}_{VL} - (\mathbf{r}_k - \mathbf{r}_{VL}) \cdot ((\mathbf{r}_k - \mathbf{r}_{VL}) \cdot (\mathbf{r}_k - \mathbf{r}_{VL}) - R^2) \\ &\quad + \sum_{i=1, i \neq k}^N \left( \dot{\mathbf{r}}_i + \left( \frac{1}{\|\mathbf{r}_{ki}\|} - \frac{\sqrt{6}}{4R} \right) \cdot \frac{\mathbf{r}_{ki}}{\|\mathbf{r}_{ki}\|^2} \right)\end{aligned}\quad (2.2.25)$$

With the proposed velocity vector, the time derivative of formation potential function of  $k$ -th satellite will be a negative definite function as:

$$\begin{aligned}\dot{V}_{form,k} &= \dot{V}_{structure,k} + \dot{V}_{rep,k} \\ &= -\lambda_{str}(\mathbf{r}_k - \mathbf{r}_{VL}) \cdot (\mathbf{r}_k - \mathbf{r}_{VL}) \cdot ((\mathbf{r}_k - \mathbf{r}_{VL}) \cdot (\mathbf{r}_k - \mathbf{r}_{VL}) - R^2)^2 \\ &\quad - \lambda_{rep} q_k \sum_{i=1, i \neq k}^N q_i \left| \frac{1}{\|\mathbf{r}_{ki}\|} - \frac{\sqrt{6}}{4R} \right| \left( -\frac{1}{\|\mathbf{r}_{ki}\|^3} \right) \\ &\leq 0\end{aligned}\quad (2.2.26)$$

The process so far seems plausible, but if the control laws are designed to have the required velocity defined above without speed limit and are implemented by numerical simulations, the speed of the satellite is increased so rapidly that it might be unrealistic when considering actual maneuvers. Therefore, for more realistic maneuvering, the velocity term is added to the formation potential function, which maintains the satellite speed low and enables delicate maneuvers. Even if the satellite speed is not limited, the APF technique always keeps the potential function lower, so adding a velocity term to the formation potential function enables the satellite to move at a slower speed than before.

The formation potential function including the  $k$ -th satellite's velocity term is defined as:

$$V_{form,k} = V_{structure,k} + V_{rep,k} + 0.5\lambda_v \dot{\mathbf{r}}_k \cdot \dot{\mathbf{r}}_k \quad (2.2.27)$$

where  $\dot{\mathbf{r}}_k = [\dot{x}_k, \dot{y}_k, \dot{z}_k]^T$  is the velocity vector of the  $k$ -th satellite and  $\lambda_v$  is a positive scaling factor of the velocity term.

In the same way as before, we derive the required acceleration of the  $k$ -th satellite for the two cases, formation flying in the  $yz$ -plane and formation flying in a regular tetrahedron shape.

### (3) Formation flying in the $yz$ -plane with velocity term

When  $N$  satellites form a regular polygonal shape in the  $yz$ -plane, the formation potential function of the  $k$ -th satellite is defined as:

$$\begin{aligned}
 V_{form,k} &= V_{structure,k} + V_{rep,k} + 0.5\lambda_v \dot{\mathbf{r}}_k \cdot \dot{\mathbf{r}}_k \\
 &= \frac{1}{4}\lambda_{str}[((y_k - y_{VL})^2 + (z_k - z_{VL})^2 - R^2)^2 + 2(x_k - x_{VL})^2] \\
 &\quad + \lambda_{rep} q_k \sum_{i=1, i \neq k}^N q_i \sqrt{\frac{1}{\mathbf{r}_{ki} \cdot \mathbf{r}_{ki}}} + 0.5\lambda_v \dot{\mathbf{r}}_k \cdot \dot{\mathbf{r}}_k
 \end{aligned} \tag{2.2.28}$$

Before deriving the time derivative of the formation potential function, a critical assumption is needed. We assume that the current velocity of the other satellites and the virtual leader are zero when defining the potential function of the  $k$ -th satellite because, in practice, it is challenging to know the velocity vector of other satellites in real-time. It may be a strong assumption, but it is necessary to make the time derivative of the  $k$ -th satellite's formation potential function negative semi-definite. Make sure that we assume that all position information is known to each other.

The time derivative of the proposed potential function of the  $k$ -th satellite will be:

$$\begin{aligned}
 \dot{V}_{form,k} &= \dot{V}_{structure,k} + \dot{V}_{rep,k} + \lambda_v \dot{\mathbf{r}}_k \cdot \ddot{\mathbf{r}}_k \\
 &= \dot{\mathbf{r}}_k \cdot (\nabla V_{structure,k} + \nabla V_{rep,k}) + \lambda_v \dot{\mathbf{r}}_k \cdot \ddot{\mathbf{r}}_k \\
 &= \dot{\mathbf{r}}_k \cdot (\nabla V_{structure,k} + \nabla V_{rep,k} + \lambda_v \ddot{\mathbf{r}}_k)
 \end{aligned} \tag{2.2.29}$$

Here,  $\ddot{\mathbf{r}}_k = [\ddot{x}_k, \ddot{y}_k, \ddot{z}_k]^T$  denotes the acceleration vector of the  $k$ -th satellite and  $\nabla = \left[ \frac{\partial}{\partial x}, \frac{\partial}{\partial y}, \frac{\partial}{\partial z} \right]^T$  denotes the vector differential operator.  $\nabla V_{structure,k}$  is the gradient of the structural potential function and  $\nabla V_{rep,k}$  is the gradient of the repulsive potential function.

$$\begin{aligned} \nabla V_{structure,k} &= \lambda_{str} [((y_k - y_{VL}) + (z_k - z_{VL})) \\ &\quad \cdot ((y_k - y_{VL})^2 + (z_k - z_{VL})^2 - R^2) + (x_k - x_{VL})] \end{aligned} \quad (2.2.30)$$

$$\nabla V_{rep,k} = -\lambda_{rep} q_k \sum_{i=1, i \neq k}^N q_i \frac{\mathbf{r}_{ki}}{\sqrt{(\mathbf{r}_{ki} \cdot \mathbf{r}_{ki})^3}} \quad (2.2.31)$$

The required acceleration vector of the  $k$ -th maneuvering satellite is defined as:

$$\ddot{\mathbf{r}}_k = - \left( \nabla V_{structure,k} + \nabla V_{rep,k} + \frac{\lambda_{vk}}{\lambda_v} \dot{\mathbf{r}}_k \right) \quad (2.2.32)$$

where  $\lambda_{vk}$  is a positive parameter that slows down the speed with a larger value.

The required acceleration vector is broken down into each component  $[\ddot{x}_k, \ddot{y}_k, \ddot{z}_k]^T$  and expressed as follows:

$$\begin{aligned} \ddot{x}_k &= - \left\{ (x_k - x_{VL}) - \lambda_{rep} q_k \sum_{i=1, i \neq k}^N q_i \frac{(x_k - x_i)}{\sqrt{(\mathbf{r}_{ki} \cdot \mathbf{r}_{ki})^3}} + \frac{\lambda_{vk}}{\lambda_v} \dot{x}_k \right\} \\ \ddot{y}_k &= - \left\{ (y_k - y_{VL}) ((y_k - y_{VL})^2 + (z_k - z_{VL})^2 - R^2) \right. \\ &\quad \left. - \lambda_{rep} q_k \sum_{i=1, i \neq k}^N q_i \frac{(y_k - y_i)}{\sqrt{(\mathbf{r}_{ki} \cdot \mathbf{r}_{ki})^3}} + \frac{\lambda_{vk}}{\lambda_v} \dot{y}_k \right\} \\ \ddot{z}_k &= - \left\{ (z_k - z_{VL}) ((y_k - y_{VL})^2 + (z_k - z_{VL})^2 - R^2) \right. \\ &\quad \left. - \lambda_{rep} q_k \sum_{i=1, i \neq k}^N q_i \frac{(z_k - z_i)}{\sqrt{(\mathbf{r}_{ki} \cdot \mathbf{r}_{ki})^3}} + \frac{\lambda_{vk}}{\lambda_v} \dot{z}_k \right\} \end{aligned} \quad (2.2.33)$$

With the proposed acceleration vector, the time derivative of formation potential function of  $k$ -th satellite will be:

$$\begin{aligned}\dot{V}_{form,k} &= \dot{\mathbf{r}}_k \cdot (\nabla V_{structure,k} + \nabla V_{rep,k} + \lambda_v \ddot{\mathbf{r}}_k) \\ &= -\lambda_{vk} \dot{\mathbf{r}}_k \cdot \dot{\mathbf{r}}_k \\ &\leq 0\end{aligned}\tag{2.2.34}$$

#### (4) Formation flying in a regular tetrahedron shape with velocity term

The formation potential function of a regular tetrahedron formation is defined positive definite as:

$$\begin{aligned}V_{form,k} &= V_{structure,k} + V_{rep,k} + 0.5\lambda_v \dot{\mathbf{r}}_k \cdot \dot{\mathbf{r}}_k \\ &= \frac{1}{4}\lambda_{str}((\mathbf{r}_k - \mathbf{r}_{VL}) \cdot (\mathbf{r}_k - \mathbf{r}_{VL}) - R^2)^2 \\ &\quad + \lambda_{rep} q_k \sum_{i=1, i \neq k}^N q_i \sqrt{\left(\frac{1}{\|\mathbf{r}_{ki}\|} - \frac{1}{4R/\sqrt{6}}\right) \cdot \left(\frac{1}{\|\mathbf{r}_{ki}\|} - \frac{1}{4R/\sqrt{6}}\right)} \\ &\quad + 0.5\lambda_v \dot{\mathbf{r}}_k \cdot \dot{\mathbf{r}}_k\end{aligned}\tag{2.2.35}$$

The time derivative of the formation potential function of the  $k$ -th satellite will be:

$$\begin{aligned}\dot{V}_{form,k} &= \dot{V}_{structure,k} + \dot{V}_{rep,k} + \lambda_v \dot{\mathbf{r}}_k \cdot \ddot{\mathbf{r}}_k \\ &= \dot{\mathbf{r}}_k \cdot (\nabla V_{structure,k} + \nabla V_{rep,k} + \lambda_v \ddot{\mathbf{r}}_k) \\ &= \lambda_{str}(\dot{\mathbf{r}}_k - \dot{\mathbf{r}}_{VL}) \cdot (\mathbf{r}_k - \mathbf{r}_{VL}) \cdot ((\mathbf{r}_k - \mathbf{r}_{VL}) \cdot (\mathbf{r}_k - \mathbf{r}_{VL}) - R^2) \\ &\quad + \lambda_{rep} q_k \sum_{i=1, i \neq k}^N q_i \frac{\left(\frac{1}{\|\mathbf{r}_{ki}\|} - \frac{\sqrt{6}}{4R}\right)}{\left|\frac{1}{\|\mathbf{r}_{ki}\|} - \frac{\sqrt{6}}{4R}\right|} \left(-\frac{\mathbf{r}_{ki}}{\|\mathbf{r}_{ki}\|^3} \cdot \dot{\mathbf{r}}_{ki}\right)\end{aligned}\tag{2.2.36}$$

where  $\nabla V_{structure,k}$  is the gradient of the structural potential function and  $\nabla V_{rep,k}$  is the gradient of the repulsive potential function.

$$\nabla V_{structure,k} = \lambda_{str}(\mathbf{r}_k - \mathbf{r}_{VL}) \cdot ((\mathbf{r}_k - \mathbf{r}_{VL}) \cdot (\mathbf{r}_k - \mathbf{r}_{VL}) - R^2) \quad (2.2.37)$$

$$\nabla V_{rep,k} = -\lambda_{rep} q_k \sum_{i=1, i \neq k}^N q_i \frac{\left( \frac{1}{\|\mathbf{r}_{ki}\|} - \frac{\sqrt{6}}{4R} \right)}{\left| \frac{1}{\|\mathbf{r}_{ki}\|} - \frac{\sqrt{6}}{4R} \right|} \frac{\mathbf{r}_{ki}}{\|\mathbf{r}_{ki}\|^3} \quad (2.2.38)$$

The required acceleration vector of the  $k$ -th maneuvering satellite is defined as:

$$\begin{aligned} \ddot{\mathbf{r}}_k &= - \left( \nabla V_{structure,k} + \nabla V_{rep,k} + \frac{\lambda_{vk}}{\lambda_v} \dot{\mathbf{r}}_k \right) \\ &= - \left( \lambda_{str}(\mathbf{r}_k - \mathbf{r}_{VL}) \cdot ((\mathbf{r}_k - \mathbf{r}_{VL}) \cdot (\mathbf{r}_k - \mathbf{r}_{VL}) - R^2) \right. \\ &\quad \left. - \lambda_{rep} q_k \sum_{i=1, i \neq k}^N q_i \frac{\left( \frac{1}{\|\mathbf{r}_{ki}\|} - \frac{\sqrt{6}}{4R} \right)}{\left| \frac{1}{\|\mathbf{r}_{ki}\|} - \frac{\sqrt{6}}{4R} \right|} \frac{\mathbf{r}_{ki}}{\|\mathbf{r}_{ki}\|^3} + \frac{\lambda_{vk}}{\lambda_v} \dot{\mathbf{r}}_k \right) \end{aligned} \quad (2.2.39)$$

With the proposed acceleration vector, the time derivative of formation potential function of  $k$ -th satellite will be a negative semi-definite function as:

$$\begin{aligned} \dot{V}_{form,k} &= \dot{\mathbf{r}}_k \cdot (\nabla V_{structure,k} + \nabla V_{rep,k} + \lambda_v \ddot{\mathbf{r}}_k) \\ &= -\lambda_{vk} \dot{\mathbf{r}}_k \cdot \dot{\mathbf{r}}_k \\ &\leq 0 \end{aligned} \quad (2.2.40)$$

Using the required accelerations in (3) and (4), we can derive the control law for formation control of the  $k$ -th satellite as:

$$\mathbf{u}_k = \ddot{\mathbf{r}}_k - f_k(\mathbf{r}_k, \dot{\mathbf{r}}_k) \quad (2.2.41)$$

where  $f_k(\mathbf{r}_k, \dot{\mathbf{r}}_k) = [2w_0\dot{y} + 3w_0^2x, -2w_0\dot{x}, -w_0^2z]^T$  denotes the HCW dynamic equation and  $\mathbf{u}_k = [u_{k,x}, u_{k,y}, u_{k,z}]^T$  denotes the control input.

## 2.2.4 Stability Analysis

In this section, we analyze the stability of the control system in cases (3) and (4) derived from Section 2.2.3.

In case (4), the formation potential function is zero at the equilibrium point and is positive definite. Its time derivative is negative semi-definite. Therefore, it is Lyapunov function.

In case (3), as described in Section 2.2.3, the formation potential function is not positive definite because the function is not set to zero at the equilibrium point because of the repulsive potential function. Thus, Lyapunov stability theorem is not applicable in case (3).

Instead, we analyze the stability of the system in case (3) according to Lyapunov-Like Lemma which is a corollary of Barbalat's Lemma [34].

**Barbalat's Lemma.** *If the differentiable function  $f(t)$  has a finite limit as  $t \rightarrow \infty$ , and if  $\dot{f}$  is uniformly continuous (or  $\ddot{f}$  is bounded), then  $\dot{f}(t) \rightarrow 0$  as  $t \rightarrow \infty$ .*

**Lyapunov-Like Lemma.** *If a scalar function  $V(\mathbf{r}, t)$  satisfies the following conditions*

$$\begin{cases} V(\mathbf{r}, t) \text{ is lower bounded} \\ \dot{V}(\mathbf{r}, t) \text{ is negative semi - definite} \\ \dot{V}(\mathbf{r}, t) \text{ is uniformly continuous in time} \end{cases}$$

*then  $\dot{V}(\mathbf{r}, t) \rightarrow 0$  as  $t \rightarrow \infty$ .*

To apply Barbalat's Lemma to our stability analysis, we can use corollary called “Lyapunov-Like Lemma” [34]:

From the lemma,  $V(\mathbf{r}, t)$  converges to a finite limiting value  $V_\infty$ , such that  $V_\infty \leq V(\mathbf{r}(0), 0)$ .

Using the conditions in Lyapunov-Like Lemma, we analyze the stability of case (3). The formation potential function of case (3) is defined as:

$$\begin{aligned} V_{form,k} &= \frac{1}{4} \lambda_{str} [((y_k - y_{VL})^2 + (z_k - z_{VL})^2 - R^2)^2 + 2(x_k - x_{VL})^2] \\ &\quad + \lambda_{rep} q_k \sum_{i=1, i \neq k}^N q_i \frac{1}{\|\mathbf{r}_{ki}\|} + 0.5 \lambda_v \|\dot{\mathbf{r}}_k\|^2 \\ &\geq 0 \end{aligned} \quad (2.2.42)$$

The formation potential function is lower bounded, and its time derivative is given by

$$\begin{aligned} \dot{V}_{form,k} &= -\lambda_{vk} \dot{\mathbf{r}}_k \cdot \dot{\mathbf{r}}_k \\ &= -\lambda_{vk} \|\dot{\mathbf{r}}_k\|^2 \\ &\leq 0 \end{aligned} \quad (2.2.43)$$

The time derivative of the formation potential function is negative semi-definite. This implies that  $V_{form,k}(t) \leq V_{form,k}(0)$ , and therefore  $(y_k - y_{VL})$ ,  $(z_k - z_{VL})$ ,  $(x_k - x_{VL})$ ,  $\frac{1}{\|\mathbf{r}_{ki}\|}$ , and  $\dot{\mathbf{r}}_k$  are bounded locally in  $\mathbf{R}^n$ .

To check the uniform continuity of  $\dot{V}_{form,k}$ , the time derivative of  $\dot{V}_{form,k}$  is derived using Eq. (2.2.32).

$$\begin{aligned} \ddot{V}_{form,k} &= -2\lambda_{vk} \ddot{\mathbf{r}}_k \cdot \dot{\mathbf{r}}_k \\ &= -2\lambda_{vk} \dot{\mathbf{r}}_k \cdot \left( -\left( \nabla V_{structure,k} + \nabla V_{rep,k} + \frac{\lambda_{vk}}{\lambda_v} \dot{\mathbf{r}}_k \right) \right) \end{aligned} \quad (2.2.44)$$

where

$$\nabla V_{rep,k} = -\lambda_{rep} q_k \sum_{i=1, i \neq k}^N q_i \frac{1}{\|\mathbf{r}_{ki}\|^2} \quad (2.2.45)$$

Equation (2.2.44) shows that  $\dot{V}_{form,k}$  is bounded, since  $(y_k - y_{VL})$ ,  $(z_k - z_{VL})$ ,  $(x_k - x_{VL})$ ,  $\frac{1}{\|\mathbf{r}_{ki}\|}$ , and  $\dot{\mathbf{r}}_k$  were shown to be bounded for  $\forall \mathbf{r}_k \in \mathbf{R}^n$ . Thus,  $\dot{V}_{form,k}$  is

uniformly continuous. Application of Barbalat's Lemma indicates that  $\dot{\mathbf{r}}_k \rightarrow 0$  as  $t \rightarrow \infty$  and then  $V_{form,k}$  approaches a finite limiting value,  $\lim_{t \rightarrow \infty} V_{form,k}(t) = V_{\infty,k}$  which is smaller than  $V_{form,k}(0)$ . It concludes that the local stability of the control system is ensured.

## 2.3 Rotational Potential Function

Collision avoidance is essential for autonomous maneuvers. A standard potential function for collision avoidance is designed to move in the opposite direction to the obstacle, such as an avoidance potential function ( $V_{avoid}$ ) [27].

$$V_{avoid} = c_1 \frac{\exp(-c_2 d)}{d} \quad (2.3.1)$$

where  $d$  denotes the relative distance between a satellite and an obstacle and  $c_1 & c_2$  are positive constants. As the satellite approaches the obstacle, the avoidance potential function increases exponentially; thus the force which is a gradient of the potential is applied in the opposite direction to the direction of the obstacle. However, the proposed collision avoidance potential function has a significant drawback. If the obstacle is located symmetrically on the trajectory of the satellite, the force to avoid obstacles and the force to reach the target (attractive force) are combined in a line. This situation leads to canceling out the total force and makes an undesired local minimum (see Figure 2.3.1). This situation causes the satellite to be stuck at the local minimum.

In order to solve this issue, a newly defined “rotational potential function” is presented for collision avoidance in this section. The rotational potential function operates to detour obstacles through behavioral approach using real-time states of all satellites. Unlike the conventional avoidance potential function, it does not merely operate in the opposite

direction of the obstacle, but it works actively to avoid the obstacles. In Section 2.3.2, we will describe the process of how to obtain this rotational potential function which is derived from the rotational force function in Section 2.3.1.

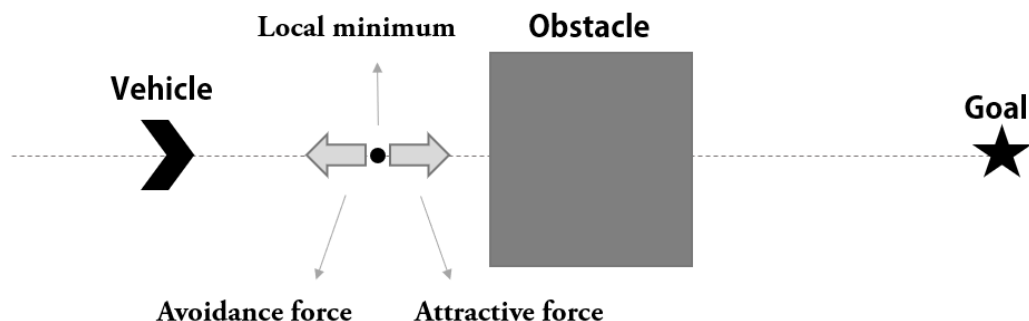


**Figure 2.3.1** Local minimum problem in the conventional APF approach

### 2.3.1 Rotational Force Function in 2-D

To derive the rotational potential function, we define a two-dimensional force function that enables satellites to detour around the obstacle without collisions [17]. Assume that a rectangular obstacle whose side parallel to the  $x$ -axis is  $2a$  whose side parallel to the  $y$ -axis is  $2b$  is located at  $[x_0, y_0]^T$  on the  $xy$ -plane.

As can be seen in Figure 2.3.2, an ellipse equation having the minimum width including all the vertices of the rectangular obstacle can be defined as Eq. (2.3.2).

$$\frac{(x - x_0)^2}{2a^2} + \frac{(y - y_0)^2}{2b^2} = 1 \quad (2.3.2)$$

The required velocity vector of the  $k$ -th satellite ( $\dot{\mathbf{r}}_k$ ) is set to move in the clockwise tangential direction of the ellipse.

$$\begin{aligned}\dot{\mathbf{r}}_k &= \dot{x}_k \hat{x} + \dot{y}_k \hat{y} \\ \dot{x}_k &= \frac{a}{b} (y_k - y_0) \\ \dot{y}_k &= -\frac{b}{a} (x_k - x_0)\end{aligned}\quad (2.3.3)$$

where  $\mathbf{r}_k = [x_k, y_k]^T$  denotes a position vector of the  $k$ -th satellite in the  $xy$ -plane.

Using Eq. (2.3.3), an artificial force vector ( $\mathbf{f}_{rot}$ ) that makes the  $k$ -th satellite move in the clockwise tangential direction of the ellipse is defined as:

$$\begin{aligned}\mathbf{f}_{rot} &= f_{rot,x} \hat{x} + f_{rot,y} \hat{y} \\ f_{rot,x} &= \frac{a}{b} (y_k - y_0) \\ f_{rot,y} &= -\frac{b}{a} (x_k - x_0)\end{aligned}\quad (2.3.4)$$

A detailed derivation process is shown in [17]. By moving the satellite in the tangential direction of the ellipse, the force vector does not cancel out the attractive force vector in a straight line. In other words, the satellite can avoid obstacles without getting into a local minimum. The rotational force function ( $\mathbf{F}_{rot}$ ) in two-dimensional space can be defined using Eq. (2.3.4) to make the satellite bypass the obstacle with greater force as it becomes closer to the obstacle.

$$\mathbf{F}_{rot} = \lambda_r \frac{\mathbf{f}_{rot}}{\|\mathbf{f}_{rot}\|} \exp(-\lambda_{rot} d_k) \quad (2.3.5)$$

where  $d_k$  denotes a relative distance between the  $k$ -th satellite and the obstacle.  $\lambda_{rot}$  is a design parameter which determines how steeply force is increased according to relative distance change. As  $\lambda_{rot}$  increases, the force increases more steeply when the satellite

approaches the obstacle.  $\lambda_r$  is a scaling factor of the rotational force function. The force vector in Eq. (2.3.4) determine the direction of the rotational force function.  $\lambda_r$  and the relative distance determine the magnitude of the function.

Up to this point, we have defined the rotational force function that enables satellites to avoid obstacles in two-dimensional space. Because this research focuses on collision avoidance during formation flying, an efficient avoidance technique making use of three-dimensional Euclidean space is required. In the next section, a rotational “potential” function is newly derived which can apply to the APF. The rotational potential function utilizes three-dimensional Euclidean space and the rotational force function defined in Eq. (2.3.5).

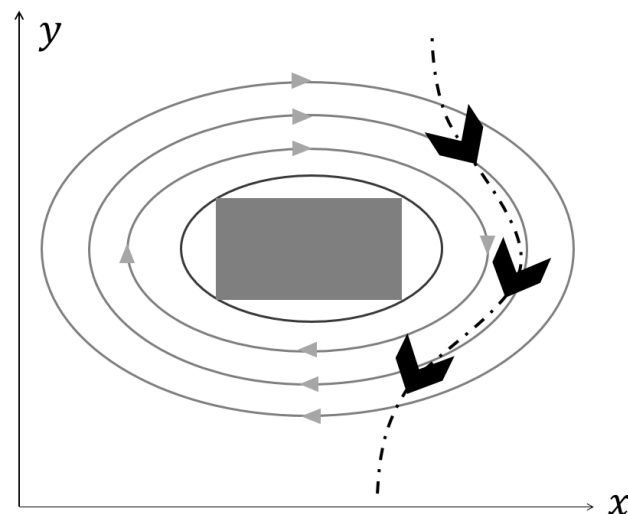


**Figure 2.3.2** Rotational force around an obstacle and a satellite’s trajectory near the obstacle

### 2.3.2 Rotational Potential Function in 3-D

The process of deriving the rotational potential function in three-dimensional Euclidean space is described in four steps:

**STEP 1.** Define a 3-D local coordinate frame centered on the obstacle

**STEP 2.** Select a plane which makes a shorter collision-free path in the local frame

**STEP 3.** Derive a rotational force function in the plane selected in STEP 2

**STEP 4.** Derive a rotational potential function from STEP 3

In order to apply the rotational force function defined in 2-D to the three-dimensional Euclidean space, the 3-D coordinate frame centered on the obstacle is defined. We select a 2-D plane of the 3-D frame and apply the rotational force function to that plane. Which plane makes a satellite go on a shorter path without collision is a criterion for selecting a 2-D plane.

#### **STEP 1. Define a 3-D local coordinate frame centered on the obstacle**

Assume that a reference frame ( $\mathbf{C}$ ) with origin at  $O$  consists of  $x$ ,  $y$ , and  $z$ -axes.

$$\mathbf{C} : \{\hat{x}, \hat{y}, \hat{z}\}$$

Let  $\mathbf{r}_{obs} = (r_{obs,x}, r_{obs,y}, r_{obs,z})$  be the position vector of an obstacle,  $\mathbf{r} = (r_x, r_y, r_z)$  be the position vector of a satellite and  $\mathbf{r}_G = (r_{G,x}, r_{G,y}, r_{G,z})$  be the position vector of target point. We create a local 3-D coordinate frame around the obstacle to making the

satellite easier to avoid the obstacle. The origin of this local 3-D frame ( $\mathbf{B}$ ) is set to the center of mass of the obstacle,  $O' = \mathbf{r}_{obs} - O$ , assuming that the density of the obstacle is uniform. The three orthogonal axes of the local 3-D coordinates are defined as  $h, n$  &  $i$ -axes (see Figure 2.3.3).  $\hat{h}$  is set to the unit direction vector from the obstacle to the satellite.  $\hat{n}$  is set to the unit vector of the cross product of  $\hat{h}$  and the target vector from the origin  $O'$ . Lastly,  $\hat{i}$  is set to the unit vector of the cross product of  $\hat{h}$  and  $\hat{n}$ .

$$\begin{aligned}\mathbf{B} : & \{\hat{h}, \hat{n}, \hat{i}\} \\ \hat{h} &= \frac{\mathbf{r} - \mathbf{r}_{obs}}{|\mathbf{r} - \mathbf{r}_{obs}|} \\ \hat{n} &= \frac{\hat{h} \times (\mathbf{r}_G - \mathbf{r}_{obs})}{|\hat{h} \times (\mathbf{r}_G - \mathbf{r}_{obs})|} \\ \hat{i} &= \frac{\hat{n} \times \hat{h}}{|\hat{n} \times \hat{h}|}\end{aligned}\tag{2.3.6}$$

If the cross product of  $(\mathbf{r} - \mathbf{r}_{obs})$  and  $(\mathbf{r}_G - \mathbf{r}_{obs})$  becomes zero, that is, when the obstacle is located on the straight line connecting the position of the satellite and the target point, we make it nonzero by adding an arbitrary vector with the magnitude of  $10^{-6}\text{m}$  to  $(\mathbf{r}_G - \mathbf{r}_{obs})$ .

Once the local coordinate frame  $\mathbf{B}$  has been determined, define the transformation matrices ( $T$ ) that transforms from the reference frame ( $\mathbf{C}$ ) to the local coordinate frame ( $\mathbf{B}$ ).

$$T = \begin{bmatrix} \hat{h}_x & \hat{h}_y & \hat{h}_z \\ \hat{n}_x & \hat{n}_y & \hat{n}_z \\ \hat{i}_x & \hat{i}_y & \hat{i}_z \end{bmatrix}\tag{2.3.7}$$

Using the transformation matrices, position vector of the satellite in the local frame ( ${}^B\mathbf{r}$ ) is expressed as:

$${}^B\mathbf{r} = T \cdot (\mathbf{r} - \mathbf{r}_{obs})\tag{2.3.8}$$

Position vector of the target point in the local frame ( ${}^B\mathbf{r}_G$ ) is expressed as:

$${}^B\mathbf{r}_G = T \cdot (\mathbf{r} - \mathbf{r}_{obs}) \quad (2.3.9)$$

Velocity vector of the satellite in the local frame ( ${}^B\dot{\mathbf{r}}$ ) is expressed as:

$${}^B\dot{\mathbf{r}} = T \cdot (\dot{\mathbf{r}} - \dot{\mathbf{r}}_{obs}) \quad (2.3.10)$$

## STEP 2. Select a plane which makes a shorter collision-free path in the local frame

Next, suppose that the rectangular obstacle  $\mathbf{r}_{obs} = (r_{obs,x}, r_{obs,y}, r_{obs,z})$  with lengths of  $(2a, 2b, 2c)$  of one side located in frame  $\mathcal{C}$ . Same with the previously defined in the rotational force function, an ellipsoid with the smallest volume enclosing the rectangle is defined and expressed as:

$$\frac{(x - r_{obs,x})^2}{2a^2} + \frac{(y - r_{obs,y})^2}{2b^2} + \frac{(z - r_{obs,z})^2}{2c^2} = 1 \quad (2.3.11)$$

To represent the ellipsoid equation in frame  $\mathcal{B}$ , an arbitrary position  $[x, y, z]^T$  in frame  $\mathcal{C}$  is represented by a vector  $[h, n, i]^T$  in frame  $\mathcal{B}$  through transformation.

$$\begin{bmatrix} x - r_{obs,x} \\ y - r_{obs,y} \\ z - r_{obs,z} \end{bmatrix} = T^{-1} \begin{bmatrix} h \\ n \\ i \end{bmatrix} \quad (2.3.12)$$

where  $T^{-1}$  is the inverse matrix of transformation matrix  $T$ .

$T^{-1}$  becomes the transpose of  $T$  and is substituted as Eq. (2.3.13) for simpler calculation.

$$T^{-1} = \begin{bmatrix} \hat{h}_x & \hat{h}_y & \hat{h}_z \\ \hat{n}_x & \hat{n}_y & \hat{n}_z \\ \hat{i}_x & \hat{i}_y & \hat{i}_z \end{bmatrix}^T = \begin{bmatrix} \hat{h}_x & \hat{n}_x & \hat{i}_x \\ \hat{h}_y & \hat{n}_y & \hat{i}_y \\ \hat{h}_z & \hat{n}_z & \hat{i}_z \end{bmatrix} = \begin{bmatrix} \alpha_1 & \alpha_2 & \alpha_3 \\ \alpha_4 & \alpha_5 & \alpha_6 \\ \alpha_7 & \alpha_8 & \alpha_9 \end{bmatrix} \quad (2.3.13)$$

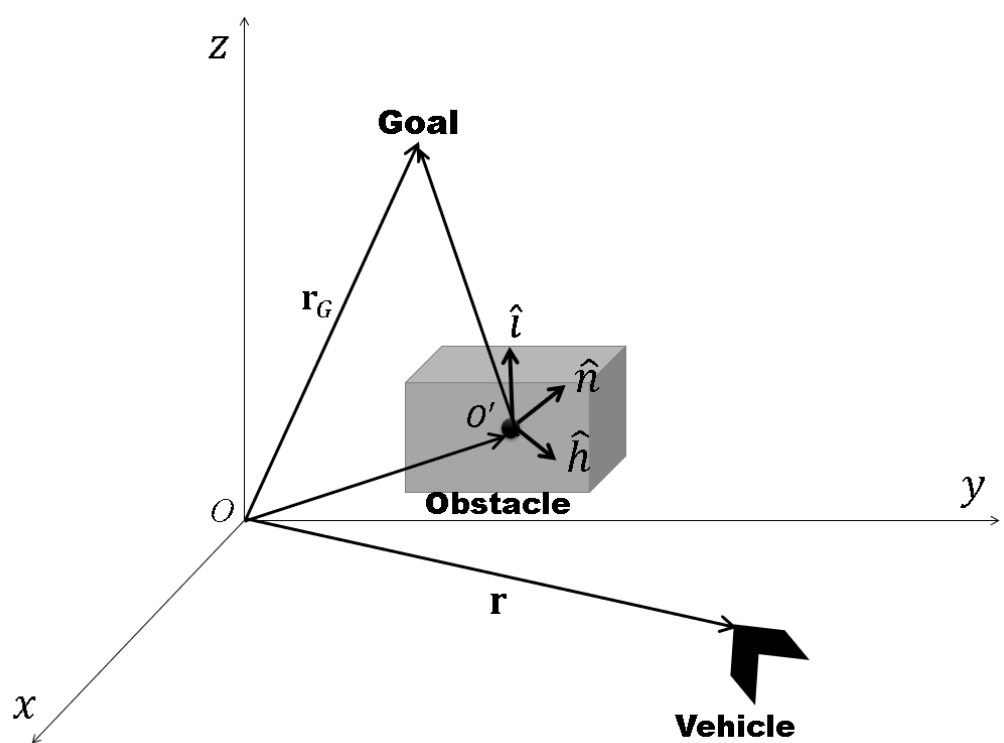


**Figure 2.3.4** Reference frame  $C$  and local coordinate frame  $B$



Put the Eq. (2.3.13) into the Eq. (2.3.12).

$$\begin{bmatrix} x - r_{obs,x} \\ y - r_{obs,y} \\ z - r_{obs,z} \end{bmatrix} = \begin{bmatrix} \alpha_1 & \alpha_2 & \alpha_3 \\ \alpha_4 & \alpha_5 & \alpha_6 \\ \alpha_7 & \alpha_8 & \alpha_9 \end{bmatrix}^B \begin{bmatrix} h \\ n \\ i \end{bmatrix} \quad (2.3.14)$$

Expansion of the above Eq. (2.3.14) yields:

$$\begin{aligned} x - r_{obs,x} &= \alpha_1 h + \alpha_2 n + \alpha_3 i \\ y - r_{obs,y} &= \alpha_4 h + \alpha_5 n + \alpha_6 i \\ z - r_{obs,z} &= \alpha_7 h + \alpha_8 n + \alpha_9 i \end{aligned} \quad (2.3.15)$$

The obstacle ellipsoid can be expressed in frame  $B$  as follows:

$$\frac{(\alpha_1 h + \alpha_2 n + \alpha_3 i)^2}{2a^2} + \frac{(\alpha_4 h + \alpha_5 n + \alpha_6 i)^2}{2b^2} + \frac{(\alpha_7 h + \alpha_8 n + \alpha_9 i)^2}{2c^2} = 1 \quad (2.3.16)$$

After representing the ellipsoid equation of the obstacle in frame  $B$ , we select a 2-D plane and derive the rotational force function in that plane. To choose a proper 2-D plane, we configured an algorithm to select a plane that can be avoided with a shorter distance between the  $hn$ -plane and  $hi$ -plane. Note that since the satellite is on the  $h$ -axis, only the plane containing the  $h$ -axis is available.

First, select  $hn$ -plane and  $hi$ -plane, and get an ellipse equation that is the intersection of the ellipsoid and each plane. Then, obtain a semi-major axis and semi-minor axis of each ellipse. Compare the ratio of the length of the semi-major axis to the semi-minor axis and select the plane with the smaller ratio because the satellite can escape faster for the less asymmetric ellipse. The calculation procedure of the semi-major axis and the semi-minor axis is described in detail in STEP 3.

### STEP 3. Derive a rotational force function in the plane selected in STEP 2

Assume that the  $hn$ -plane is selected. We need to find the ellipse equation in the  $hn$ -plane by obtaining the intersection of the obstacle ellipsoid and the  $hn$ -plane so that it is possible to apply the rotational force function in the  $hn$ -plane. The  $hn$ -plane is expressed as an equation of  $i = 0$ . Therefore, the intersection with the ellipsoid is given by solving simultaneous equations as follows:

$$\left\{ \begin{array}{l} \frac{(\alpha_1 h + \alpha_2 n + \alpha_3 i)^2}{2a^2} + \frac{(\alpha_4 h + \alpha_5 n + \alpha_6 i)^2}{2b^2} + \frac{(\alpha_7 h + \alpha_8 n + \alpha_9 i)^2}{2c^2} = 1 \\ i = 0 \end{array} \right. \quad (2.3.17)$$

Solving the simultaneous equations gives the following equation:

$$\frac{(\alpha_1 h + \alpha_2 n)^2}{2a^2} + \frac{(\alpha_4 h + \alpha_5 n)^2}{2b^2} + \frac{(\alpha_7 h + \alpha_8 n)^2}{2c^2} = 1 \quad (2.3.18)$$

Equation (2.3.18) can be rearranged as:

$$\begin{aligned} & \left( \frac{\alpha_1^2}{2a^2} + \frac{\alpha_4^2}{2b^2} + \frac{\alpha_7^2}{2c^2} \right) h^2 + \left( \frac{\alpha_2^2}{2a^2} + \frac{\alpha_5^2}{2b^2} + \frac{\alpha_8^2}{2c^2} \right) n^2 \\ & + 2 \left( \frac{\alpha_1 \alpha_2}{2a^2} + \frac{\alpha_4 \alpha_5}{2b^2} + \frac{\alpha_7 \alpha_8}{2c^2} \right) hn = 1 \end{aligned} \quad (2.3.19)$$

If coefficients of Eq. (2.3.19) are substituted by

$$\begin{aligned} A &= \left( \frac{\alpha_1^2}{2a^2} + \frac{\alpha_4^2}{2b^2} + \frac{\alpha_7^2}{2c^2} \right) \\ B &= 2 \left( \frac{\alpha_1 \alpha_2}{2a^2} + \frac{\alpha_4 \alpha_5}{2b^2} + \frac{\alpha_7 \alpha_8}{2c^2} \right) \\ C &= \left( \frac{\alpha_2^2}{2a^2} + \frac{\alpha_5^2}{2b^2} + \frac{\alpha_8^2}{2c^2} \right) \end{aligned} \quad (2.3.20)$$

then, Eq. (2.3.19) is simplified as follows:

$$Ah^2 + Cn^2 + Bhn = 1 \quad (2.3.21)$$

If the coefficient of the  $hn$ -term is non-zero, the ellipse is not aligned with the  $h$ -axis and  $n$ -axis. It implies that the ellipse is rotated about the  $h$ -axis and  $n$ -axis. Before

analyzing the equation in detail, we need to know a rotated ellipse equation with a simple example.

Suppose that an ellipse equation in the reference frame is defined as:

$$\frac{x^2}{a^2} + \frac{y^2}{b^2} = 1 \quad (2.3.22)$$

where  $a$  is a semi-major axis and  $b$  is a semi-minor axis.

If the ellipse is rotated counterclockwise by an angle of  $\theta$  about the  $x$ -axis, the rotated ellipse equation is obtained as follows by simple calculation:

$$\frac{(x\cos\theta + y\sin\theta)^2}{a^2} + \frac{(x\sin\theta - y\cos\theta)^2}{b^2} = 1 \quad (2.3.23)$$

Back to our problem, to apply the rotational force function defined in Section 2.3.1, we should know the semi-major axis and semi-minor axis of the rotated ellipse. It is difficult to immediately know the angle of rotation and the semi-major & semi-minor axis of the ellipse just by Eq. (2.3.21). Thus, we tilt the original axes to align the tilted ellipse with the axes and derive an equation of the non-tilted ellipse (see Figure 2.3.4). To obtain these values, we go through the following process.

Let  $\theta$  be the rotated angle measured in the counterclockwise direction from the  $h$ -axis. Let  $h'$ -axis and  $n'$ -axis be the axes that are rotated counterclockwise from the  $h$ -axis and the  $n$ -axis by  $\theta$ , respectively. Then,  $h'$  and  $n'$  can be obtained as follows:

$$h' = h\cos\theta + n\sin\theta, \quad n' = -h\sin\theta + n\cos\theta \quad (2.3.24)$$

Conversely,  $h$  and  $n$  are expressed as follows:

$$h = h'\cos\theta - n'\sin\theta, \quad n = h'\sin\theta + n'\cos\theta \quad (2.3.25)$$

Using Eq. (2.3.25), the ellipse equation in Eq. (2.3.21) is summarized as follows:

$$A'h'^2 + C'n'^2 + B'h'n' = 1 \quad (2.3.26)$$

where the coefficients of each term are defined as:

$$\begin{aligned} A' &= A \cos^2 \theta + B \sin \theta \cos \theta + C \sin^2 \theta \\ C' &= A \sin^2 \theta - B \sin \theta \cos \theta + C \cos^2 \theta \\ B' &= 2(C - A) \sin \theta \cos \theta + B(\cos^2 \theta - \sin^2 \theta) \end{aligned} \quad (2.3.27)$$

The value of  $\theta$  where  $h'n'$ -term becomes zero ( $B' = 0$ ) is:

$$\theta = \frac{1}{2} \tan^{-1}\left(\frac{B}{A - C}\right), \theta \in \left(-\frac{\pi}{2}, \frac{\pi}{2}\right) \quad (2.3.28)$$

At the point of ( $A - C = 0$ ) where Eq. (2.3.28) is not defined,  $\theta$  is  $\pm \frac{\pi}{4}$ .

As we obtained the equation for the non-tilted ellipse, the semi-major axis ( $a'$ ) and semi-minor axis ( $b'$ ) of the ellipse are obtained as follows by simple calculation:

$$a' = \sqrt{\frac{1}{A'}}, b' = \sqrt{\frac{1}{C'}} \quad (2.3.29)$$

Then, the ellipse equation that is rotated by  $\theta$  is expressed in the  $hn$ -plane as:

$$\frac{(h \cos \theta + n \sin \theta)^2}{a'^2} + \frac{(h \sin \theta - n \cos \theta)^2}{b'^2} = 1 \quad (2.3.30)$$

Using Eq. (2.3.30) and Eq. (2.3.3), we can obtain the following simultaneous equations:

$$\begin{aligned} \dot{h}_k \cos \theta + \dot{n}_k \sin \theta &= \frac{a'}{b'}(h_k \sin \theta - n_k \cos \theta) \\ \dot{h}_k \sin \theta - \dot{n}_k \cos \theta &= -\frac{b'}{a'}(h_k \cos \theta + n_k \sin \theta) \end{aligned} \quad (2.3.31)$$

By solving Eq. (2.3.31), the required velocity vector  $(\dot{h}_k, \dot{n}_k)$  of the  $k$ -th satellite to move in the clockwise tangential direction of the ellipse is derived as:

$$\dot{h}_k = \left( \frac{a'}{b'} + \frac{b'}{a'} \right) \cos \theta \sin \theta h_k + \left( \frac{b'}{a'} \sin^2 \theta - \frac{a'}{b'} \cos^2 \theta \right) n_k \quad (2.3.32)$$

$$\dot{n}_k = \left( \frac{a'}{b'} \sin^2 \theta + \frac{b'}{a'} \cos^2 \theta \right) h_k + \left( \frac{b'}{a'} - \frac{a'}{b'} \right) \cos \theta \sin \theta n_k$$

Using Eq. (2.3.32), a force vector ( $\mathbf{f}_{rot,hn}$ ) of the  $k$ -th satellite in the  $hn$ -plane for avoidance maneuver is defined as:

$$\begin{aligned} \mathbf{f}_{rot,hn} &= f_{rot,h} \hat{h} + f_{rot,n} \hat{n} \\ f_{rot,h} &= c_1 h_k + c_2 n_k \\ f_{rot,n} &= c_3 h_k + c_4 n_k \end{aligned} \tag{2.3.33}$$

where

$$\begin{aligned} c_1 &= \left( \frac{a'}{b'} + \frac{b'}{a'} \right) \cos \theta \sin \theta, & c_3 &= \left( \frac{a'}{b'} \sin^2 \theta + \frac{b'}{a'} \cos^2 \theta \right) \\ c_2 &= \left( \frac{b'}{a'} \sin^2 \theta - \frac{a'}{b'} \cos^2 \theta \right), & c_4 &= \left( \frac{b'}{a'} - \frac{a'}{b'} \right) \cos \theta \sin \theta \end{aligned}$$

Using Eq. (2.3.33), the rotational force function ( $\mathbf{F}_{rot,hn}$ ) of  $k$ -th satellite in the  $hn$ -plane is defined as:

$$\mathbf{F}_{rot,hn} = \lambda_r \frac{\mathbf{f}_{rot,hn}}{\|\mathbf{f}_{rot,hn}\|} \exp(-\lambda_{rot} d_k) \tag{2.3.34}$$

where  $d_k$  denotes a relative distance between the  $k$ -th satellite and the obstacle and we define it specifically in STEP 4.  $\lambda_{rot}$  is a parameter which determines how steeply force is increased according to relative distance change.  $\lambda_r$  is a scaling factor of the rotational force function. As the satellite moves away from the obstacle, the force becomes exponentially smaller.

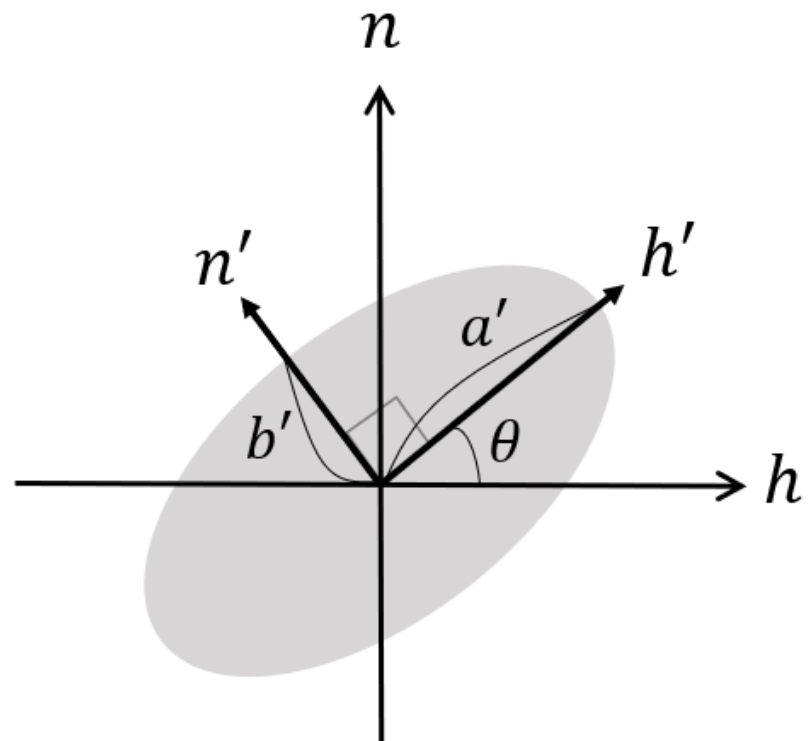


**Figure 2.3.5** A rotated ellipse with a semi-major axis of  $a'$  and a semi-minor axis of  $b'$  and rotated  $h'$ & $n'$ -axes by an angle  $\theta$  from  $h$ & $n$ -axes

#### STEP 4. Derive a rotational potential function from STEP 3

In STEP 4, we derive a rotational potential function from the rotational force function in Eq. (2.3.34). The rotational force function of the  $k$ -th satellite is defined as:

$$\begin{aligned} \mathbf{F}_{rot,hn} &= F_{rot,h}\hat{h} + F_{rot,n}\hat{n} \\ F_{rot,h} &= \lambda_r \frac{(c_1 h_k + c_2 n_k)}{\sqrt{(c_1 h_k + c_2 n_k)^2 + (c_3 h_k + c_4 n_k)^2}} \exp(-\lambda_{rot} d_k) \\ F_{rot,n} &= \lambda_r \frac{(c_3 h_k + c_4 n_k)}{\sqrt{(c_1 h_k + c_2 n_k)^2 + (c_3 h_k + c_4 n_k)^2}} \exp(-\lambda_{rot} d_k) \end{aligned} \quad (2.3.35)$$

Note that the  $k$ -th satellite is located on the positive  $h$ -axis, and the rotational force function is recalculated at each moment when satellite needs to avoid obstacles. Thus, the coordinates of the  $k$ -th satellite is set as  $[h_k, 0, 0]^T$  in the local coordinate frame for a positive value of  $h_k$ . If we assign  $n_k = 0$ , the rotational force function is defined as:

$$\begin{aligned} F_{rot,h} &= \lambda_r \frac{c_1 h_k}{\sqrt{(c_1 h_k)^2 + (c_3 h_k)^2}} \exp(-\lambda_{rot} d_k) \\ &= \lambda_r \frac{c_1}{\sqrt{c_1^2 + c_3^2}} \exp(-\lambda_{rot} d_k) \\ F_{rot,n} &= \lambda_r \frac{c_3 h_k}{\sqrt{(c_1 h_k)^2 + (c_3 h_k)^2}} \exp(-\lambda_{rot} d_k) \\ &= \lambda_r \frac{c_3}{\sqrt{c_1^2 + c_3^2}} \exp(-\lambda_{rot} d_k) \end{aligned} \quad (2.3.36)$$

where  $d_k$  denotes the distance between the  $k$ -th satellite and the obstacle ellipse:

$$d_k = h_k - \frac{1}{\sqrt{A}} \quad (2.3.37a)$$

The distance ( $d_k$ ) is obtained from the simultaneous equations as follows:

$$\begin{cases} Ah^2 + Cn^2 + Bhn = 1 \\ n = 0 \end{cases} \quad (2.3.37b)$$

To derive the rotational potential function, we use the following theorem based on the APF that a negative gradient of potential becomes an artificial force [27].

**Artificial force theorem.** *Negative gradient of potential  $V$  becomes an artificial force  $F$  which indicates a direction of motion, i.e.,  $F = -\nabla V$ .*

The rotational potential function of the  $k$ -th satellite can be obtained from the rotational force function using the Artificial force theorem:

$$\begin{aligned}\mathbf{F}_{rot,hn} &= -\nabla^* V_{rot,k} \\ V_{rot,k} &= - \int F_{rot,h} dh_k - \int F_{rot,n} dn_k\end{aligned}\tag{2.3.38}$$

where  $\nabla^* = \left[ \frac{\partial}{\partial h}, \frac{\partial}{\partial n}, \frac{\partial}{\partial i} \right]^T$  denotes the vector differential operator.

Using Eq. (2.3.38), the rotational potential function is derived as:

$$\begin{aligned}V_{rot,k} &= - \int F_{rot,h} dh_k - \int F_{rot,n} dn_k \\ &= \lambda_r \left( \frac{c_1}{\lambda_{rot}} - c_3 n_k \right) \frac{\exp(-\lambda_{rot} d_k)}{\sqrt{c_1^2 + c_3^2}}\end{aligned}\tag{2.3.39}$$

In Eq. (2.3.39),  $n_k$  is not set to zero because the value of the rotational potential function is changed after avoidance maneuvers according to the satellite's changed position. As we set the rotational force is applied in the clockwise direction around the obstacle, the satellite moves in the negative  $n$ -axis direction. Thus, the value of  $n_k$  is less than or equal to zero, which means  $(-c_3 n_k)$  is a positive value because  $c_3 = \left( \frac{a'}{b} \sin^2 \theta + \frac{b'}{a'} \cos^2 \theta \right)$  is a positive value. If  $c_1$  is a positive value, the rotational potential function ( $V_{rot,k}$ ) can be  $V_{rot,k} \geq 0$ . Using the trigonometric identity,  $c_1$  is given by

$$\begin{aligned}
 c_1 &= \left( \frac{a'}{b'} + \frac{b'}{a'} \right) \cos\theta \sin\theta \\
 &= \frac{1}{2} \left( \frac{a'}{b'} + \frac{b'}{a'} \right) \sin 2\theta
 \end{aligned} \tag{2.3.40}$$

The sign of the coefficient  $c_1$  depends on  $\sin 2\theta$  as follows:

$$\begin{cases} \sin 2\theta \geq 0 & \text{if } 0 \leq \theta \leq \frac{\pi}{2} \\ \sin 2\theta < 0 & \text{if } \frac{3\pi}{2} < \theta < 2\pi \end{cases} \tag{2.3.41}$$

To make  $\theta$  in a certain range of  $0 \leq \theta \leq \frac{\pi}{2}$  so that  $\sin 2\theta$  holds a positive value, we modify the ellipse.

The original ellipse equation in the  $hn$ -plane is  $Ah^2 + Cn^2 + Bh_n = 1$  (Eq. 2.3.21) which is the rotated ellipse equation with an angle of  $\theta$  from  $\frac{h^2}{a'^2} + \frac{n^2}{b'^2} = 1$ . However, when  $\sin 2\theta$  is negative ( $\sin 2\theta < 0$ ), we regard the rotated ellipse is rotated by  $(\theta - \frac{\pi}{2})$  from  $\frac{h^2}{b'^2} + \frac{n^2}{a'^2} = 1$  that the semi-major axis ( $b'$ ) and semi-minor axis ( $a'$ ) are reversed from the original ellipse (Figure 2.3.5). Accordingly, the rotational force function should be changed as below:

$$\begin{aligned}
 F_{rot,h} &= \lambda_r \frac{c_5}{\sqrt{c_5^2 + c_6^2}} \exp(-\lambda_{rot} D_k) \\
 F_{rot,n} &= \lambda_r \frac{c_6}{\sqrt{c_5^2 + c_6^2}} \exp(-\lambda_{rot} D_k) \\
 &\quad \text{if } \frac{\pi}{2} < \theta < \pi
 \end{aligned} \tag{2.3.42}$$

where the coefficients  $c_5$  and  $c_6$  are stated as follows:



$$\begin{aligned}
 c_5 &= \left( \frac{a'}{b'} + \frac{b'}{a'} \right) \cos\left(\theta - \frac{\pi}{2}\right) \sin\left(\theta - \frac{\pi}{2}\right) \\
 &= \frac{1}{2} \left( \frac{a'}{b'} + \frac{b'}{a'} \right) \sin 2\left(\theta - \frac{\pi}{2}\right) \\
 c_6 &= \frac{b'}{a'} \sin^2\left(\theta - \frac{\pi}{2}\right) + \frac{a'}{b'} \cos^2\left(\theta - \frac{\pi}{2}\right)
 \end{aligned} \tag{2.3.43}$$

$D_k$  denotes the distance between the  $k$ -th satellite and the obstacle ellipse, which is defined in the same way as Eq. (2.3.37a):

$$D_k = h_k - \frac{1}{\sqrt{C}} \tag{2.3.44}$$

In this case, the rotational potential function ( $V_{rot,k}$ ) is changed as follows:

$$\begin{aligned}
 V_{rot,k} &= - \int F_{rot,h} dh_k - \int F_{rot,n} dn_k \\
 &= \lambda_r \left( \frac{c_5}{\lambda_{rot}} - c_6 n_k \right) \frac{\exp(-\lambda_{rot} D_k)}{\sqrt{c_5^2 + c_6^2}}
 \end{aligned} \tag{2.3.45}$$

The following definition can be obtained based on the process so far.

**Definition 2.3.** Let  $\theta$  be an angle between  $h$ -axis and  $h'$ -axis. Let  $d = h - \frac{1}{\sqrt{A}}$  and  $D = h - \frac{1}{\sqrt{C}}$ . The rotational potential function ( $V_{rot}$ ) is defined as:

$$\begin{cases} V_{rot} = \lambda_r \left( \frac{c_1}{\lambda_{rot}} - c_3 n \right) \frac{\exp(-\lambda_{rot} d)}{\sqrt{c_1^2 + c_3^2}} & \text{if } \sin 2\theta \geq 0 \\ V_{rot} = \lambda_r \left( \frac{c_5}{\lambda_{rot}} - c_6 n \right) \frac{\exp(-\lambda_{rot} D)}{\sqrt{c_5^2 + c_6^2}} & \text{if } \sin 2\theta < 0 \end{cases}$$

where  $c_1 = \frac{1}{2} \left( \frac{a'}{b'} + \frac{b'}{a'} \right) \sin 2\theta$ ,  $c_3 = \left( \frac{a'}{b'} \sin^2 \theta + \frac{b'}{a'} \cos^2 \theta \right)$ ,  $c_5 = \frac{1}{2} \left( \frac{a'}{b'} + \frac{b'}{a'} \right) \sin 2 \left( \theta - \frac{\pi}{2} \right)$ ,  $c_6 = \frac{b'}{a'} \sin^2 \left( \theta - \frac{\pi}{2} \right) + \frac{a'}{b'} \cos^2 \left( \theta - \frac{\pi}{2} \right)$

Hence, the rotational potential function has a positive value and can be applied to the APF control technique.

We have defined both the rotational force function and the rotational potential function in the  $hn$ -plane. Now we are going to represent the functions in the reference frame  $\mathbf{C}$ . The coordinate transformation matrices ( $T^{-1}$ ) in Eq. (2.3.13) from the local coordinate frame  $\mathbf{B}$  to the reference frame  $\mathbf{C}$  can be used. If we transform from the  $hn$ -plane to the reference frame  $\mathbf{C}$ , the rotational force function is defined in the reference frame  $\mathbf{C}$  as follows:

$$\mathbf{F}_{rot} = T^{-1} \cdot [\mathbf{F}_{rot,hn}, 0]^T \quad (2.3.46)$$

In this section, we defined the 3-D local coordinate frame using the states of the satellite. We defined the rotational force function and the rotational potential function that are calculated each moment when the satellite needs for collision avoidance maneuvers in the local coordinate frame. The functions for collision avoidance are ready, we derive control laws for collision-free formation control in the Section 2.4.

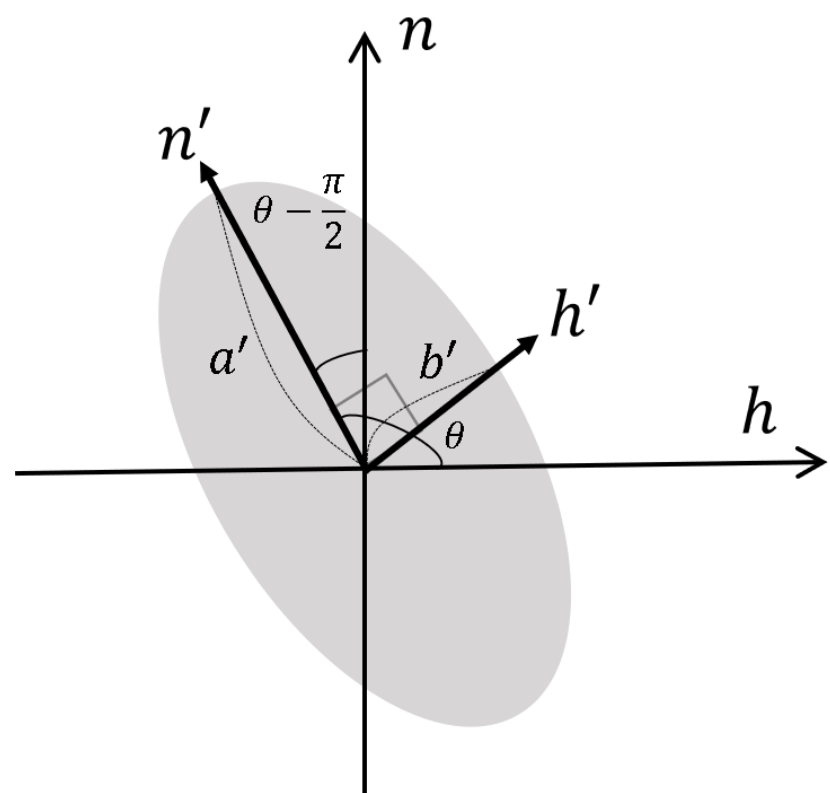


**Figure 2.3.6** Modified ellipse when  $\sin 2\theta < 0$

## 2.4 Continuous Control Law Based on Lyapunov Theorem

We have presented a strategy for collision-free formation control based on the APF. We defined the structural potential function and the repulsive potential function for formation control. Also, we defined the rotational potential function for the collision avoidance maneuver. Using these potential functions, we define continuous control laws in HCW dynamics.

Before deriving control laws, we define the equations of motion of the  $k$ -th satellite.

$$\begin{aligned} \ddot{\mathbf{r}}_k &= f_k(\mathbf{r}_k, \dot{\mathbf{r}}_k) + \mathbf{u}_k \\ \mathbf{r}_k &= [x_k, y_k, z_k]^T, \dot{\mathbf{r}}_k = [\dot{x}_k, \dot{y}_k, \dot{z}_k]^T \\ f_k(\mathbf{r}_k, \dot{\mathbf{r}}_k) &= [2w_0\dot{y} + 3w_0^2x, -2w_0\dot{x}, -w_0^2z]^T \\ \mathbf{u}_k &= [u_{k,x}, u_{k,y}, u_{k,z}]^T \end{aligned} \tag{2.4.1}$$

where  $f_k(\mathbf{r}_k, \dot{\mathbf{r}}_k)$  denotes HCW dynamic equations and  $\mathbf{u}_k$  denotes the control input of the  $k$ -th satellite. In this chapter, we consider the relative motion of satellites to the spacecraft in a circular orbit at an altitude of 408 km. The angular velocity of the chief's orbital motion is defined as  $w_0 = \sqrt{GM_E/(R_E + 408)}$  where  $R_E$  is the Earth radius and  $M_E$  is the Earth mass.

To control  $N$  satellites maneuver in the formation of a regular polygon or a regular tetrahedron while avoiding collisions, the total potential function ( $V_{total,k}$ ) of the  $k$ -th satellite is defined as the sum of the formation potential function ( $V_{form,k}$ ) and the rotational potential function ( $V_{rot,k}$ ).

$$\begin{aligned} V_{total,k} &= V_{form,k} + V_{rot,k} \\ &= V_{structure,k} + V_{rep,k} + \lambda_v \dot{\mathbf{r}}_k \cdot \dot{\mathbf{r}}_k + V_{rot,k} \end{aligned} \tag{2.4.2}$$

The time derivative of the total potential function ( $\dot{V}_{total,k}$ ) of the  $k$ -th satellite will be:

$$\begin{aligned}\dot{V}_{total,k} &= \dot{V}_{structure,k} + \dot{V}_{rep,k} + \lambda_v \dot{\mathbf{r}}_k \cdot \ddot{\mathbf{r}}_k + \dot{V}_{rot,k} \\ &= \dot{\mathbf{r}}_k \cdot (\nabla V_{structure,k} + \nabla V_{rep,k}) + \lambda_v \dot{\mathbf{r}}_k \cdot \ddot{\mathbf{r}}_k + \dot{V}_{rot,k}\end{aligned}\quad (2.4.3)$$

where  $\nabla = \left[ \frac{\partial}{\partial x}, \frac{\partial}{\partial y}, \frac{\partial}{\partial z} \right]^T$  denotes the vector differential operator in the reference frame  $\mathcal{C}$ .

The time derivative of the rotational potential function can be derived as:

$$\begin{aligned}\dot{V}_{rot,k} &= \frac{dV_{rot,k}}{dt} \\ &= \dot{\mathbf{r}}_k \cdot \left( \frac{\partial V_{rot,k}}{\partial h} \left[ \frac{dh}{dx}, \frac{dh}{dy}, \frac{dh}{dz} \right]^T + \frac{\partial V_{rot,k}}{\partial n} \left[ \frac{dn}{dx}, \frac{dn}{dy}, \frac{dn}{dz} \right]^T \right. \\ &\quad \left. + \frac{\partial V_{rot,k}}{\partial i} \left[ \frac{di}{dx}, \frac{di}{dy}, \frac{di}{dz} \right]^T \right) \\ &= \dot{\mathbf{r}}_k \cdot T^{-1} \cdot \nabla^* V_{rot,k}\end{aligned}\quad (2.4.4)$$

where  $\nabla^* = \left[ \frac{\partial}{\partial h}, \frac{\partial}{\partial n}, \frac{\partial}{\partial i} \right]^T$  denotes the vector differential operator in the local coordinate frame  $\mathcal{B}$  and  $T^{-1}$  denotes the transformation matrices in Eq. (2.3.13).

Thus, the time derivative of the total potential function of the  $k$ -th satellite will be:

$$\begin{aligned}\dot{V}_{total,k} &= \dot{V}_{structure,k} + \dot{V}_{rep,k} + \lambda_v \dot{\mathbf{r}}_k \cdot \ddot{\mathbf{r}}_k + \dot{V}_{rot,k} \\ &= \dot{\mathbf{r}}_k \cdot (\nabla V_{structure,k} + \nabla V_{rep,k}) + \lambda_v \dot{\mathbf{r}}_k \cdot \ddot{\mathbf{r}}_k + \dot{\mathbf{r}}_k \cdot T^{-1} \cdot \nabla^* V_{rot,k} \\ &= \dot{\mathbf{r}}_k \cdot (\nabla V_{structure,k} + \nabla V_{rep,k} + T^{-1} \cdot \nabla^* V_{rot,k} + \lambda_v \cdot \ddot{\mathbf{r}}_k)\end{aligned}\quad (2.4.5)$$

where  $\ddot{\mathbf{r}}_k = [\ddot{x}_k, \ddot{y}_k, \ddot{z}_k]^T$  is the acceleration vector of the  $k$ -th satellite.

The required acceleration vector of the  $k$ -th satellite is defined as:

$$\ddot{\mathbf{r}}_k = - \left( \nabla V_{structure,k} + \nabla V_{rep,k} + T^{-1} \cdot \nabla^* V_{rot,k} + \frac{\lambda_{vk}}{\lambda_v} \dot{\mathbf{r}}_k \right) \quad (2.4.6)$$

Note that we previously defined ( $\mathbf{F}_{rot,hn} = -\nabla^* V_{rot,k}$ ) and ( $\mathbf{F}_{rot} = T^{-1} \cdot \mathbf{F}_{rot,hn}$ ). With the required acceleration vector, the time derivative of total potential function of  $k$ -th satellite will be defined negative semi-definite function as:

$$\begin{aligned}
 \dot{V}_{total,k} &= \dot{\mathbf{r}}_k \cdot (\nabla V_{structure,k} + \nabla V_{rep,k} + T^{-1} \cdot \nabla^* V_{rot,k} + \lambda_v \ddot{\mathbf{r}}_k) \\
 &= -\lambda_{vk} \dot{\mathbf{r}}_k \cdot \dot{\mathbf{r}}_k \\
 &= -\lambda_{vk} \|\dot{\mathbf{r}}_k\|^2 \\
 &\leq 0
 \end{aligned} \tag{2.4.7}$$

We can derive continuous control laws ( $\mathbf{u}_k$ ) for the  $k$ -th satellite using the required acceleration in Eq. (2.4.6).

$$\mathbf{u}_k = -\left(\nabla V_{structure,k} + \nabla V_{rep,k} + T \cdot \nabla^* V_{rot,k} + \frac{\lambda_{vk}}{\lambda_v} \dot{\mathbf{r}}_k\right) - f_k(\mathbf{r}_k, \dot{\mathbf{r}}_k) \tag{2.4.8}$$

where  $f_k(\mathbf{r}_k, \dot{\mathbf{r}}_k)$  denotes HCW dynamic equations.

$$f_k(\mathbf{r}_k, \dot{\mathbf{r}}_k) = [2w_0\dot{y} + 3w_0^2x, -2w_0\dot{x}, -w_0^2z]^T \tag{2.4.9}$$

In practice, if obstacles are detected in advance, it is safer to design a reference trajectory of the formation group considering the obstacles in the beginning. Therefore, in this research, when obstacles are not detected beforehand, a reference trajectory is designed without considering avoidance maneuvering. On the contrary to this, when an obstacle is detected beforehand, a reference trajectory is designed considering avoidance maneuvering. For this reason, we design a trajectory of the virtual leader, which is the reference trajectory of the group, based on the APF technique. In this research, we design a reference trajectory of a virtual leader 1) considering obstacles, and 2) not considering obstacles.

1) To construct a reference trajectory of a virtual leader without considering obstacles, a potential function ( $V_{VL,1}$ ) is defined as [27]:

$$V_{VL,1} = \lambda_p \|\mathbf{r}_{VL} - \mathbf{r}_{VL,goal}\| + \frac{1}{2} \lambda_v \dot{\mathbf{r}}_{VL} \cdot \dot{\mathbf{r}}_{VL} \tag{2.4.10}$$

where  $\mathbf{r}_{VL,goal}$  denotes virtual leader's target point,  $\dot{\mathbf{r}}_{VL}$  denotes virtual leader's velocity vector, and  $\lambda_p$  &  $\lambda_v$  are positive scaling factors.

The potential function ( $V_{VL,1}$ ) converges to zero when the virtual leader reaches the target point and the velocity reaches zero at the same time.

The time derivative of the proposed potential function ( $\dot{V}_{VL,1}$ ) will be:

$$\dot{V}_{VL,1} = \dot{\mathbf{r}}_{VL} \cdot \left( \lambda_p \frac{(\mathbf{r}_{VL} - \mathbf{r}_{VL,goal})}{\|\mathbf{r}_{VL} - \mathbf{r}_{VL,goal}\|} + \lambda_v \ddot{\mathbf{r}}_{VL} \right) \quad (2.4.11)$$

where  $\ddot{\mathbf{r}}_{VL}$  denotes the virtual leader's acceleration vector.

The required acceleration vector is defined as:

$$\ddot{\mathbf{r}}_{VL} = - \left( \frac{\lambda_p (\mathbf{r}_{VL} - \mathbf{r}_{VL,goal})}{\lambda_v \|\mathbf{r}_{VL} - \mathbf{r}_{VL,goal}\|} + \frac{\lambda_{vk,VL}}{\lambda_v} \dot{\mathbf{r}}_{VL} \right) \quad (2.4.12)$$

where  $\lambda_{vk,VL}$  is a positive parameter.

Time derivative of the potential function will be negative semi-definite as:

$$\begin{aligned} \dot{V}_{VL,1} &= -\lambda_{vk,VL} \dot{\mathbf{r}}_{VL} \cdot \dot{\mathbf{r}}_{VL} \\ &\leq 0 \end{aligned} \quad (2.4.13)$$

The control law of the virtual leader can be derived as:

$$\mathbf{u}_{VL,1} = - \left( \frac{\lambda_p (\mathbf{r}_{VL} - \mathbf{r}_{VL,goal})}{\lambda_v \|\mathbf{r}_{VL} - \mathbf{r}_{VL,goal}\|} + \frac{\lambda_{vk,VL}}{\lambda_v} \dot{\mathbf{r}}_{VL} \right) - f_k(\mathbf{r}_{VL}, \dot{\mathbf{r}}_{VL}) \quad (2.4.14)$$

2) To design a reference trajectory avoiding obstacles, the potential function ( $V_{VL,2}$ ) is defined as:

$$V_{VL,2} = \lambda_p \|\mathbf{r}_{VL} - \mathbf{r}_{VL,goal}\| + \frac{1}{2} \lambda_v \dot{\mathbf{r}}_{VL} \cdot \dot{\mathbf{r}}_{VL} + V_{rot,VL} \quad (2.4.15)$$

where  $V_{rot,VL}$  is defined about the virtual leader, not the  $k$ -th satellite.

The control law is defined as:



$$\begin{aligned}\mathbf{u}_{VL,2} = & - \left( \frac{\lambda_p (\mathbf{r}_{VL} - \mathbf{r}_{VL,goal})}{\lambda_v \|\mathbf{r}_{VL} - \mathbf{r}_{VL,goal}\|} + \frac{\lambda_{vk,VL}}{\lambda_v} \dot{\mathbf{r}}_{VL} + T^{-1} \cdot \nabla^* V_{rot,VL} \right) \\ & - f_k(\mathbf{r}_{VL}, \dot{\mathbf{r}}_{VL})\end{aligned}\quad (2.4.16)$$

where  $T^{-1}$  denotes the transformation matrices defined about the virtual leader, not the  $k$ -th satellite.

## 3. Numerical Simulations and Analysis

In this chapter, we implement some formation keeping and formation reconfiguration using the proposed control laws in HCW dynamics.

### 3.1 Formation Keeping

We check the performance of the proposed control laws in several formation keeping examples through numerical simulations. Designing a reference trajectory of the formation group was classified as not to avoid obstacles or to avoid obstacles.

#### 3.1.1 When Virtual Leader Does Not Avoid Obstacles

When designing the reference trajectory of the virtual leader without considering obstacles, the control law ( $\mathbf{u}_{VL}$ ) is set as follows:

$$\mathbf{u}_{VL} = \mathbf{u}_{VL,1}$$

We validate that  $N$  satellites maintain the formation of a square, pentagon, hexagon, and regular tetrahedron rigidly without colliding with obstacles using the proposed control laws. We aim to keep the satellites at least 5 m away from the obstacle surface.

#### Example (1) Square formation

Suppose that on a circle with a radius  $R = 6$  m centered on the virtual leader in the  $yz$ -plane, four satellites ( $\mathbf{r}_1, \mathbf{r}_2, \mathbf{r}_3, \mathbf{r}_4$ ) form a square shape while avoiding a rectangular parallelepiped obstacle with side lengths of (6,12,6) m. The obstacle is not moving in the

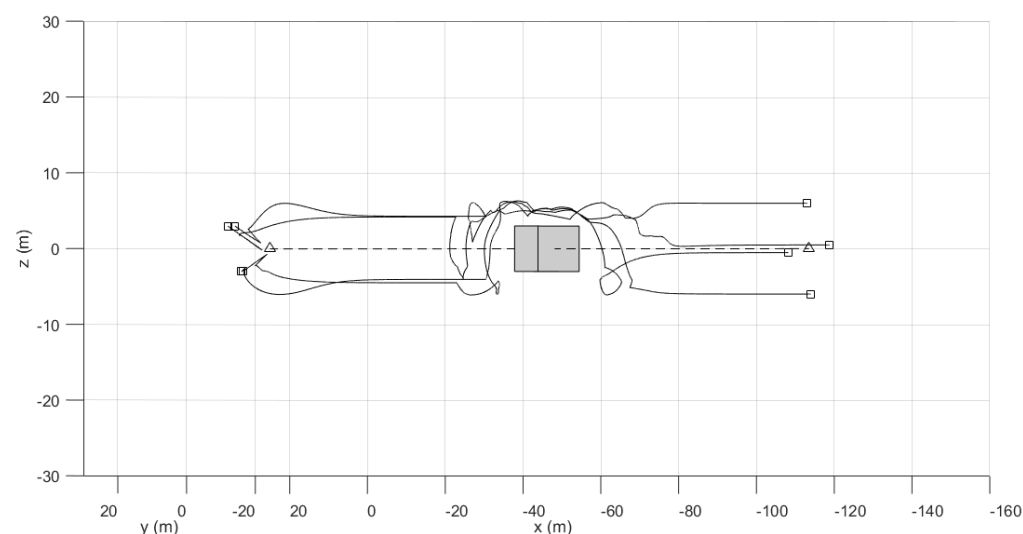
reference frame. Note that the four satellites should be in a square formation in no particular order.

The initial positions of the four satellites are set as  $\mathbf{r}_{1,0} = [2, 4, -3]^T$  m,  $\mathbf{r}_{2,0} = [4, 4, 3]^T$  m,  $\mathbf{r}_{3,0} = [5, 1, -3]^T$  m, and  $\mathbf{r}_{4,0} = [5, 1, -3]^T$  m. The initial position of the virtual leader is set as  $\mathbf{r}_{VL,0} = [2, 4, -3]^T$  m and the target point of the virtual leader is set as  $\mathbf{r}_{VL,goal} = [-140, 0, 0]^T$  m. The center of a stationary obstacle is set as  $\mathbf{r}_{obs} = [-70, -3, 0]^T$  m. Scaling factors and design parameters are set as  $\lambda_{str} = 0.5$ ,  $\lambda_{rep} = 0.2$ ,  $q_1 = q_2 = q_3 = q_4 = 10$ ,  $\lambda_{rot} = 0.13$ ,  $\lambda_r = 2$ ,  $\lambda_p = 0.1$ ,  $\lambda_v = 1.2$ ,  $\lambda_{vk,VL} = 1$ , and  $\lambda_{vk} = 7$ .

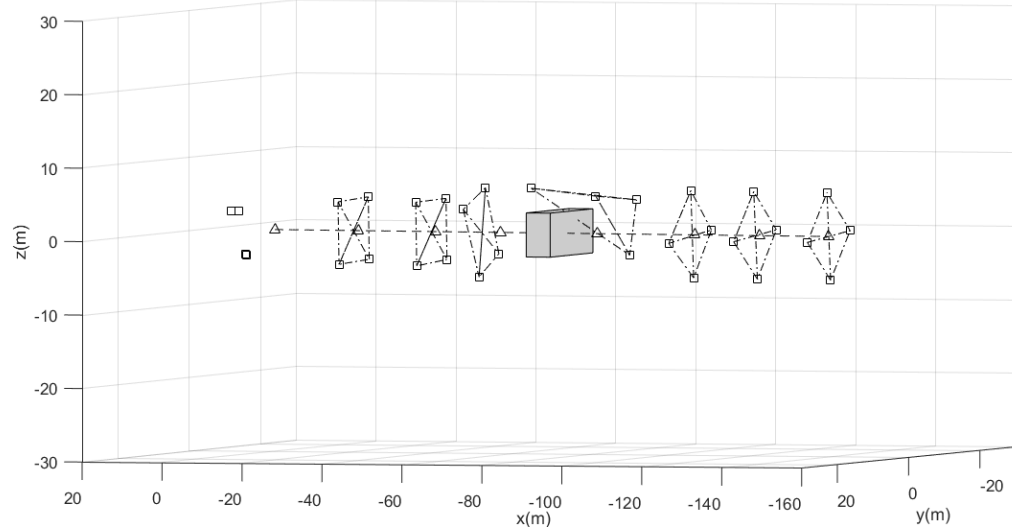
Figure 3.1.1a shows the trajectories of the four satellites for 1800 seconds. A dashed line represents the virtual leader's reference trajectory, and solid lines represent the four satellites. A grey rectangular parallelepiped represents the obstacle. Figure 3.1.2 shows the minimum Euclidean distance changes between the satellites and the obstacle's surface. As shown in Figure 3.1.1a and Figure 3.1.2, the four satellites safely avoid the obstacle with the distance greater than or equal to 5.646 m. All four satellites are avoiding in the same direction because of the force to maintain the formation, the virtual structure. Figure 3.1.1b shows the formation of four satellites ( $\square$ ) around the virtual leader ( $\Delta$ ) through solid lines between the satellites at 260 sec, 500 sec, 900 sec, 1000 sec, 1300 sec, 1500 sec, 1800 sec. Figure 3.1.3 shows the relative distance changes between the virtual leader and each satellite. The four satellites should maintain a distance of 6m (dashed line) which is the radius of the circle. Figure 3.1.4 shows the relative distance changes between the satellites,  $(\|\mathbf{r}_1 - \mathbf{r}_2\|, \|\mathbf{r}_1 - \mathbf{r}_3\|, \|\mathbf{r}_1 - \mathbf{r}_4\|, \|\mathbf{r}_2 - \mathbf{r}_3\|, \|\mathbf{r}_2 - \mathbf{r}_4\|, \|\mathbf{r}_3 - \mathbf{r}_4\|)$ . Because the four satellites need to form a square shape, the distance between two of them should be the length of one side of the square,  $6\sqrt{2} \approx 8.485$  m or the length of the diagonal, 12 m.

Figure 3.1.1b, Figure 3.1.3, and Figure 3.1.4 show that the four satellites maintained the square formation with some errors for all simulation times except when avoiding the

obstacle. The satellites do not collide with each other due to the repulsive forces. We calculated the distance error to see the formation maintenance performance at distances of 30 m or more from the obstacle. In Figure 3.1.3, the root mean square distance error with the virtual leader is 0.127 m, which is the result of ignoring the speed of the virtual leader when designing the control law. In Figure 3.1.4, the root mean square relative distance error is 0.041 m because the speed of the other satellites is ignored. The simulation results imply that distance errors are caused by not considering the tracking speed.



**Figure 3.1.1a** Trajectories of four satellites (solid line), obstacle (grey face), reference trajectory of the virtual leader (dashed line), initial & final position of virtual leader ( $\Delta$ ) and four satellites ( $\square$ )



**Figure 3.1.1b** Lines between four satellites (solid line), obstacle (grey face), reference trajectory of the virtual leader (dashed line), instantaneous position of virtual leader ( $\Delta$ ) and four satellites ( $\square$ )

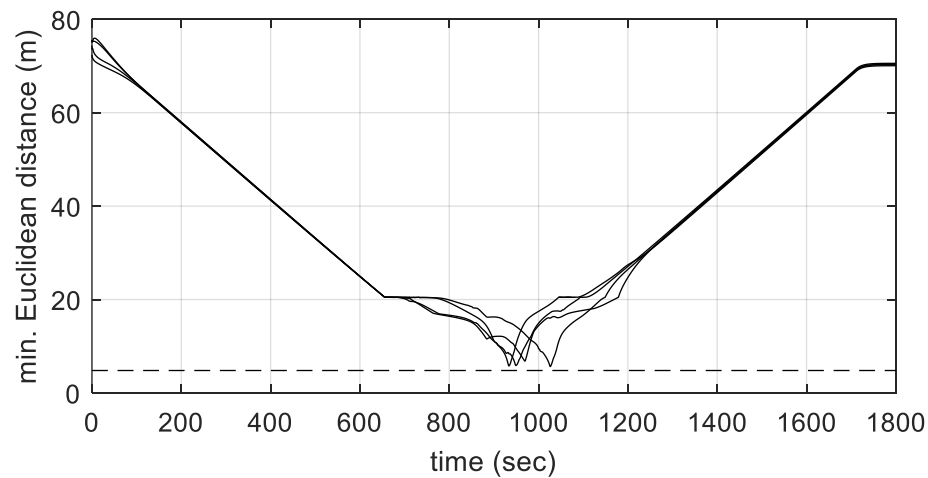


**Figure 3.1.2** Minimum Euclidean distance changes between four satellites and the obstacle's surface

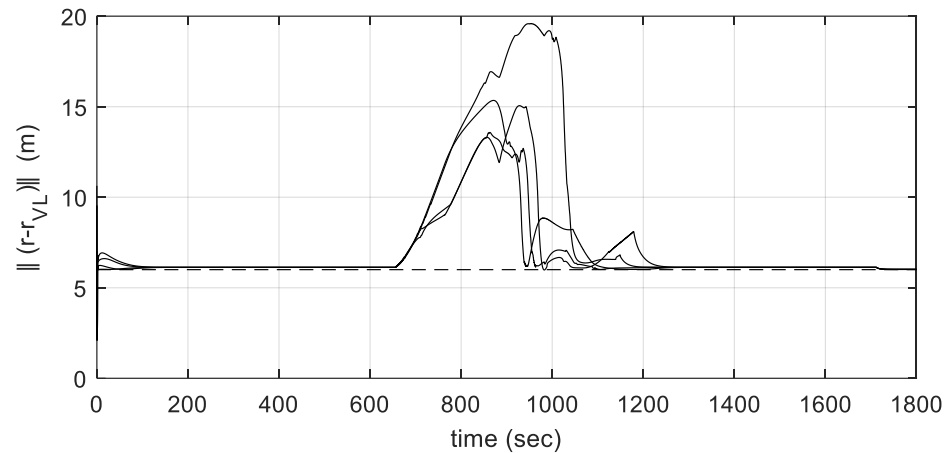


**Figure 3.1.3** Relative distances between virtual leader and four satellites (solid line) in square formation and radius of circle  $R = 6$  m (dashed line)

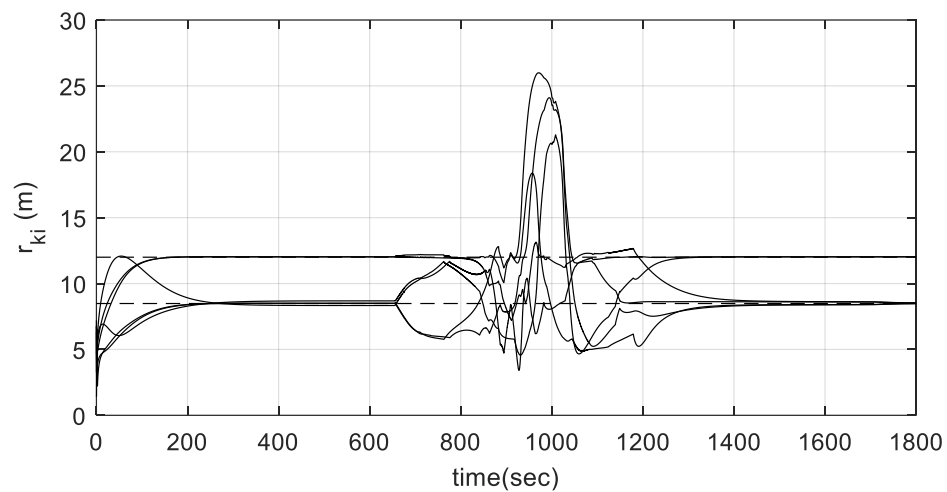


**Figure 3.1.4** Relative distances between satellites (solid line), side length of square,  $6\sqrt{2} \approx 8.485$  m (dashed line), and diagonal length of square, 12 m (dashed line)

### Example (2) Pentagon formation

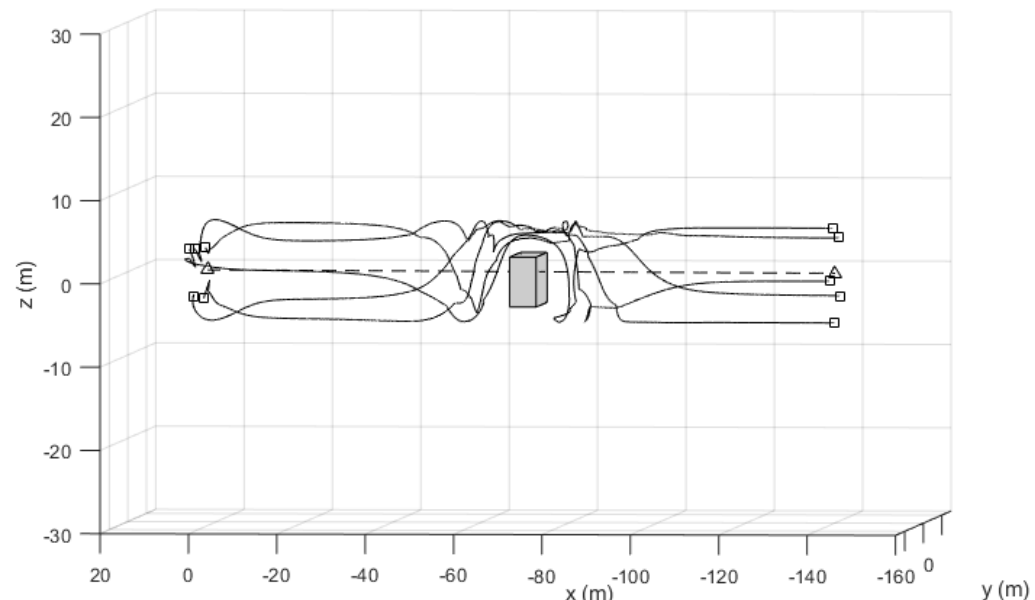
Suppose that on a circle with a radius of  $R = 6$  m centered on the virtual leader in the  $yz$ -plane, five satellites ( $\mathbf{r}_1, \mathbf{r}_2, \mathbf{r}_3, \mathbf{r}_4, \mathbf{r}_5$ ) form a pentagon shape while avoiding a rectangular parallelepiped obstacle with side lengths of (6,12,6) m. Note that the five satellites should be in a pentagon formation in any order.

The initial positions of the five satellites are set as  $\mathbf{r}_{1,0} = [5, 5, 3]^T$  m,  $\mathbf{r}_{2,0} = [2, 4, -3]^T$  m,  $\mathbf{r}_{3,0} = [4, 4, 3]^T$  m,  $\mathbf{r}_{4,0} = [5, 1, -3]^T$  m, and  $\mathbf{r}_{5,0} = [2, 2, 3]^T$  m. The initial position of the virtual leader is set as  $\mathbf{r}_{VL,0} = [3, -5, 0]^T$  m and the target point of the virtual leader is set as  $\mathbf{r}_{VL,goal} = [-140, 0, 0]^T$  m. The center of a stationary obstacle is set as  $\mathbf{r}_{obs} = [-70, -3, -1]^T$  m. Scaling factors and design parameters are set as  $\lambda_{str} = 0.5$ ,  $\lambda_{rep} = 0.3$ ,  $q_1 = q_2 = q_3 = q_4 = 10$ ,  $\lambda_{rot} = 0.13$ ,  $\lambda_r = 5$ ,  $\lambda_p = 0.1$ ,  $\lambda_v = 1.2$ ,  $\lambda_{vk,VL} = 1$ , and  $\lambda_{vk} = 7$ .

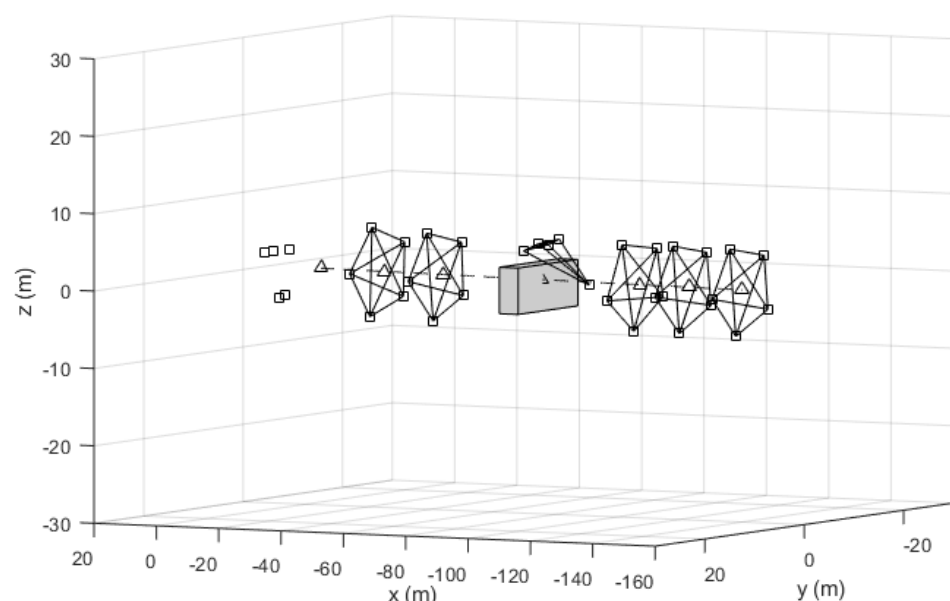
Figure 3.1.5a shows the trajectories of the five satellites for 1800 seconds. A dashed line represents the virtual leader's reference trajectory, and solid lines represent the five satellites. A grey rectangular parallelepiped represents the obstacle. Figure 3.1.6 shows the minimum Euclidean distance changes between the satellites and the obstacle's surface. As shown in Figure 3.1.5a and Figure 3.1.6, the five satellites safely avoid the obstacle with the distance greater than or equal to 6.431 m. All five satellites are avoiding in the same direction because of the force to maintain the formation.

Figure 3.1.5b shows the formation of five satellites (□) around the virtual leader (Δ) through solid lines between the satellites at 260 sec, 500 sec, 900 sec, 1300 sec, 1500 sec, 1800 sec. Figure 3.1.7 presents the distance changes between the virtual leader and each satellite. The five satellites should maintain a distance of 6 m (dashed line) which is the radius of the circle. Figure 3.1.8 shows the relative distance changes between the satellites, ( $\|\mathbf{r}_1 - \mathbf{r}_2\|, \|\mathbf{r}_1 - \mathbf{r}_3\|, \|\mathbf{r}_1 - \mathbf{r}_4\|, \|\mathbf{r}_1 - \mathbf{r}_5\|, \|\mathbf{r}_2 - \mathbf{r}_3\|, \|\mathbf{r}_2 - \mathbf{r}_4\|, \|\mathbf{r}_2 - \mathbf{r}_5\|, \|\mathbf{r}_3 - \mathbf{r}_4\|, \|\mathbf{r}_3 - \mathbf{r}_5\|, \|\mathbf{r}_4 - \mathbf{r}_5\|$ ,

$\|\mathbf{r}_3 - \mathbf{r}_4\|, \|\mathbf{r}_3 - \mathbf{r}_5\|, \|\mathbf{r}_4 - \mathbf{r}_5\|$ ). Because the five satellites need to form a pentagonal shape, the distance between two of them should be the length of one side of the pentagon,  $12\cos(54^\circ) \approx 7.053$  m or the length of the diagonal,  $(6 + 6\sqrt{5})\cos(54^\circ) \approx 11.413$  m. Figure 3.1.5b, Figure 3.1.7, and Figure 3.1.8 show that the five satellites maintain the pentagonal formation with some errors for all simulation times except when avoiding the obstacle. In Figure 3.1.7, the root mean square distance error with the virtual leader is 0.065 m. In Figure 3.1.8, the root mean square relative distance error is 0.047 m.



**Figure 3.1.5a** Trajectories of five satellites (solid line), obstacle (grey face), reference trajectory of the virtual leader (dashed line), initial & final position of virtual leader ( $\Delta$ ) and five satellites ( $\square$ )



**Figure 3.1.5b** Lines between five satellites (solid line), obstacle (grey face), reference trajectory of the virtual leader (dashed line), instantaneous position of virtual leader ( $\Delta$ ) and five satellites ( $\square$ )

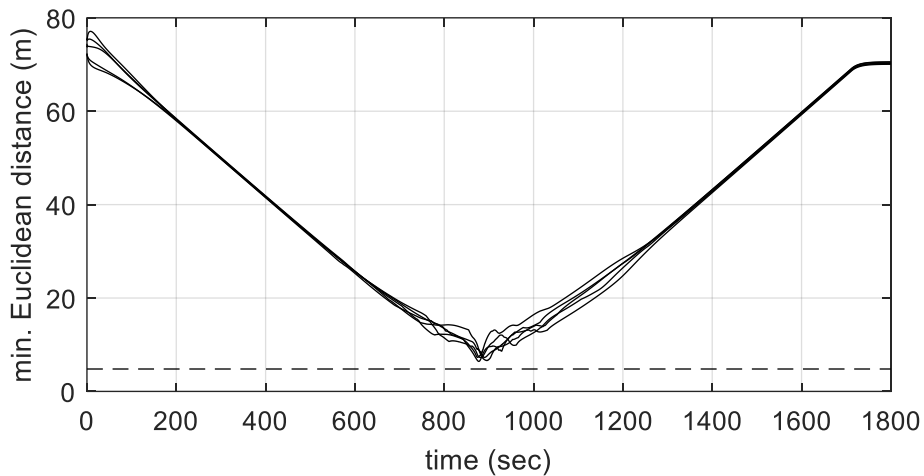


**Figure 3.1.6** Minimum Euclidean distance changes between five satellites and the obstacle's surface

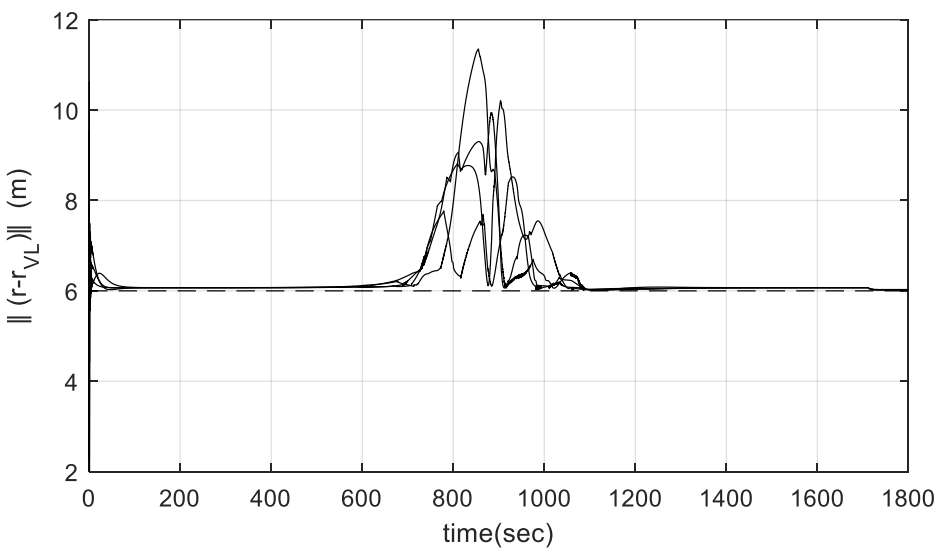


**Figure 3.1.7** Relative distances between virtual leader and five satellites (solid line) in pentagon formation and radius of circle  $R = 6$  m (dashed line)

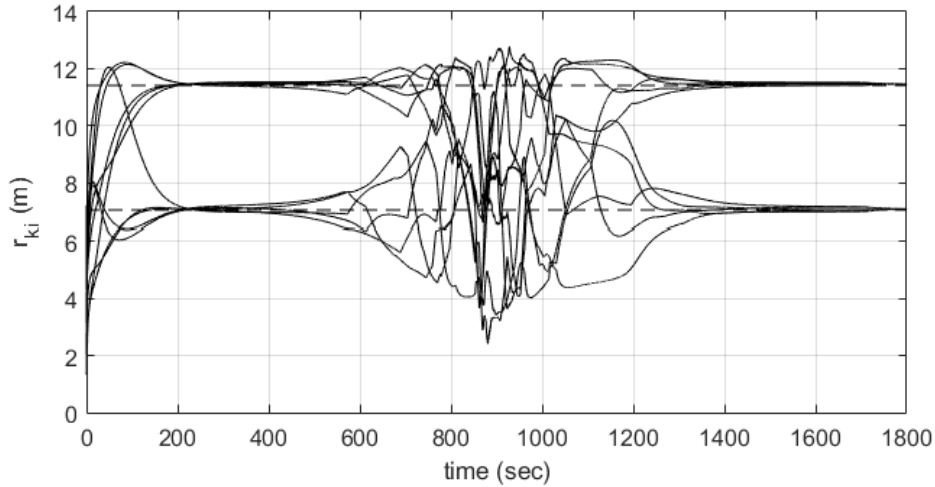


**Figure 3.1.8** Relative distances between satellites (solid line), side length of pentagon,  $12\cos(54^\circ) \approx 7.053$  m (dashed line), and diagonal length of pentagon,  $(6 + 6\sqrt{5})\cos(54^\circ) \approx 11.413$  m (dashed line)

### Example (3) Hexagon formation

Suppose that on a circle with a radius of  $R = 6$  m centered on the virtual leader in the  $yz$ -plane, six satellites ( $\mathbf{r}_1, \mathbf{r}_2, \mathbf{r}_3, \mathbf{r}_4, \mathbf{r}_5, \mathbf{r}_6$ ) form a hexagon shape while avoiding a rectangular parallelepiped obstacle with side lengths of (6,12,6) m. The obstacle is not moving in the reference frame. Note that the six satellites should be in hexagon formation in any order.

The initial positions of the six satellites are set as  $\mathbf{r}_{1,0} = [5, 5, 3]^T$  m,  $\mathbf{r}_{2,0} = [2, 4, -3]^T$  m,  $\mathbf{r}_{3,0} = [4, 4, 3]^T$  m,  $\mathbf{r}_{4,0} = [5, 1, -3]^T$  m,  $\mathbf{r}_{5,0} = [-5, -5, -3]^T$  m and  $\mathbf{r}_{6,0} = [-2, -4, 3]^T$  m. The initial position of the virtual leader is set as  $\mathbf{r}_{VL,0} = [3, -5, 0]^T$  m and the target point of the virtual leader is set as  $\mathbf{r}_{VL,goal} = [-140, 0, 0]^T$  m.

The center of a stationary obstacle is set as  $\mathbf{r}_{obs} = [-70, -3, -3]^T$  m. Scaling factors and design parameters are set as  $\lambda_{str} = 0.7$ ,  $\lambda_{rep} = 0.3$ ,  $q_1 = q_2 = q_3 = q_4 = 8$ ,  $\lambda_{rot} = 0.1$ ,  $\lambda_r = 4$ ,  $\lambda_p = 0.1$ ,  $\lambda_v = 1.2$ ,  $\lambda_{vk,VL} = 1$ , and  $\lambda_{vk} = 7$ .

Figure 3.1.9a shows the trajectories of the six satellites for 1800 seconds. A dashed line represents the virtual leader's reference trajectory, and solid lines represent the six satellites. A grey rectangular parallelepiped represents the obstacle. Figure 3.1.10 shows the minimum Euclidean distance changes between the satellites and the obstacle's surface. As shown in Figure 3.1.9a and Figure 3.1.10, the six satellites safely avoid the obstacle with the distance greater than or equal to 8.955 m. All six satellites are avoiding in the same direction because of the force to maintain the formation. Figure 3.1.9b shows the formation of six satellites ( $\square$ ) around the virtual leader ( $\Delta$ ) through lines between the satellites at 260 sec, 500 sec, 900 sec, 1300 sec, 1500 sec, 1800 sec. Figure 3.1.11 shows the distance changes between the virtual leader and each satellite. The six satellites should maintain a distance of 6 m (dashed line) which is the radius of the circle. Figure 3.1.12 shows the relative distance changes between the six satellites, ( $\|\mathbf{r}_1 - \mathbf{r}_2\|$ ,  $\|\mathbf{r}_1 - \mathbf{r}_3\|$ ,  $\|\mathbf{r}_1 - \mathbf{r}_4\|$ ,  $\|\mathbf{r}_1 - \mathbf{r}_5\|$ ,  $\|\mathbf{r}_1 - \mathbf{r}_6\|$ ,  $\|\mathbf{r}_2 - \mathbf{r}_3\|$ ,  $\|\mathbf{r}_2 - \mathbf{r}_4\|$ ,  $\|\mathbf{r}_2 - \mathbf{r}_5\|$ ,  $\|\mathbf{r}_2 - \mathbf{r}_6\|$ ,  $\|\mathbf{r}_3 - \mathbf{r}_4\|$ ,  $\|\mathbf{r}_3 - \mathbf{r}_5\|$ ,  $\|\mathbf{r}_3 - \mathbf{r}_6\|$ ,  $\|\mathbf{r}_4 - \mathbf{r}_5\|$ ,  $\|\mathbf{r}_4 - \mathbf{r}_6\|$ ,  $\|\mathbf{r}_5 - \mathbf{r}_6\|$ ). Because the six satellites need to form a hexagonal shape, the distance between two of them should be the length of one side of the hexagon, 6 m or the length of the diagonal,  $6\sqrt{3} \approx 10.392$  m or 12 m. Figure 3.1.9b, Figure 3.1.11, and Figure 3.1.12 show that the six satellites maintain the hexagonal formation with some errors for all simulation times except when avoiding the obstacle. In Figure 3.1.11, the root mean square distance error with the virtual leader is 0.045 m. In Figure 3.1.12, the root mean square relative distance error is 0.034 m.

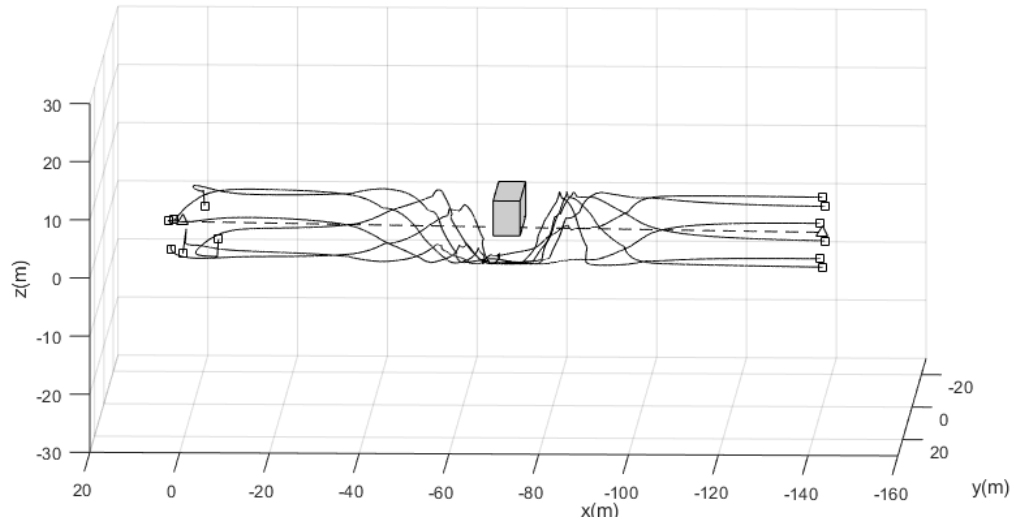


**Figure 3.1.9a** Trajectories of six satellites (solid line), obstacle (grey face), reference trajectory of the virtual leader (dashed line), initial & final position of virtual leader ( $\Delta$ ) and six satellites ( $\square$ )

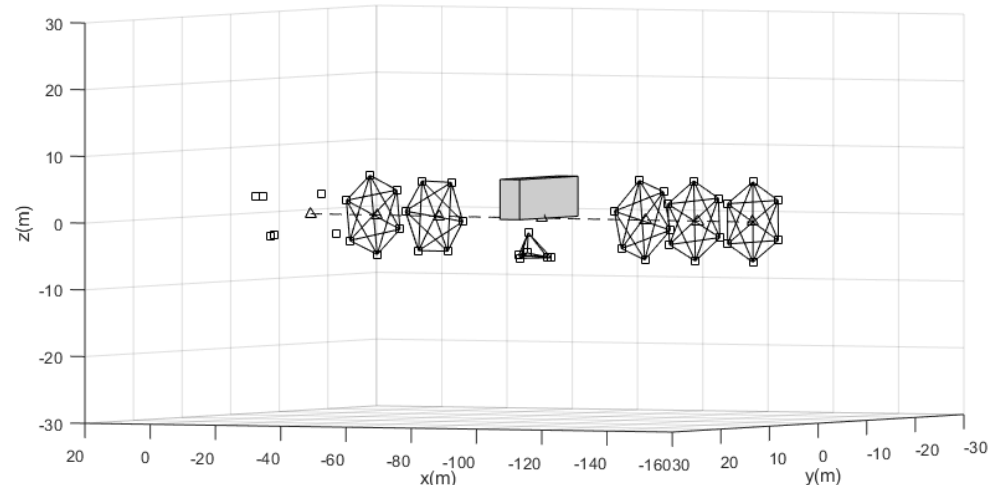


**Figure 3.1.9b** Lines between six satellites (solid line), obstacle (grey face), reference trajectory of the virtual leader (dashed line), instantaneous position of virtual leader ( $\Delta$ ) and six satellites ( $\square$ )

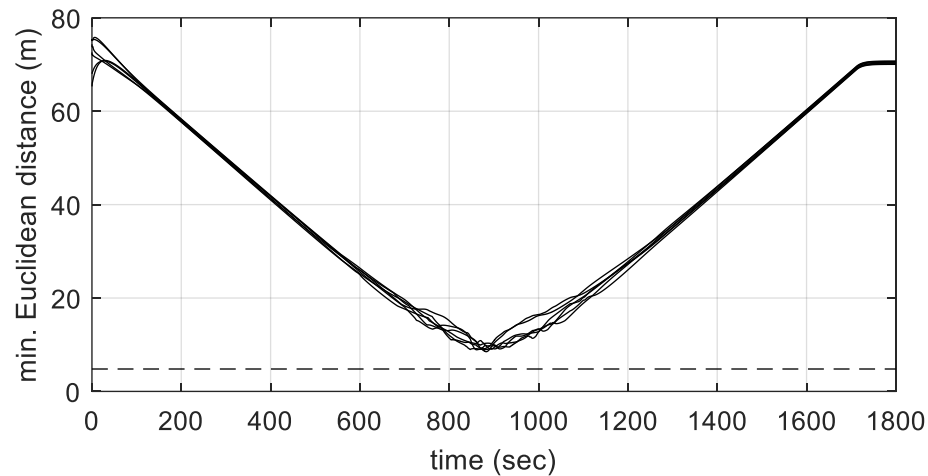


**Figure 3.1.10** Minimum Euclidean distance changes between six satellites and the obstacle's surface

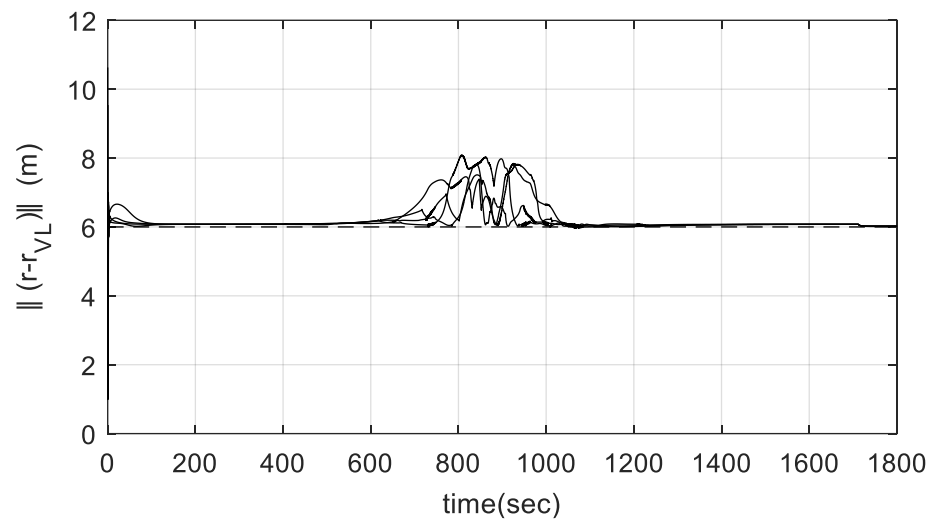


**Figure 3.1.11** Relative distances between virtual leader and six satellites (solid line) in hexagon formation and radius of circle  $R = 6$  m (dashed line)

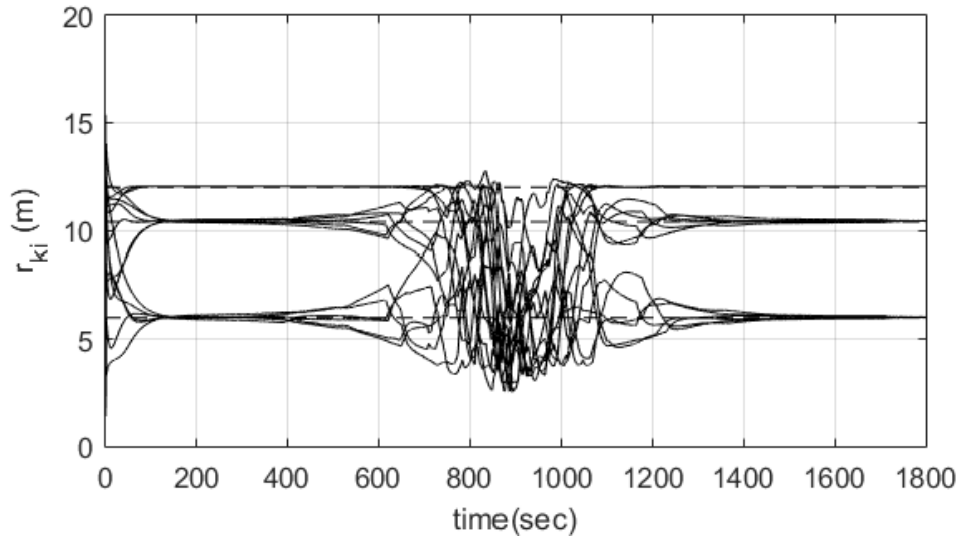


**Figure 3.1.12** Relative distances between satellites (solid line), side length of hexagon, 6 m (dashed line), and diagonal length of pentagon,  $6\sqrt{3} \approx 10.392$  m & 12 m (dashed line)

#### Example (4) Regular tetrahedron formation

Suppose that on a sphere with a radius of  $R = 6$  m centered on the virtual leader, four satellites ( $\mathbf{r}_1, \mathbf{r}_2, \mathbf{r}_3, \mathbf{r}_4$ ) form a regular tetrahedron shape while avoiding a rectangular parallelepiped obstacle with side lengths of (6,12,6) m. The obstacle is not moving in the reference frame. Note that the four satellites should be in tetrahedron formation in any order.

The initial positions of the four satellites are set as  $\mathbf{r}_{1,0} = [5, 5, 3]^T$  m,  $\mathbf{r}_{2,0} = [2, 4, -3]^T$  m,  $\mathbf{r}_{3,0} = [4, 4, 3]^T$  m,  $\mathbf{r}_{4,0} = [5, 1, -3]^T$  m. The initial position of the virtual leader is set as  $\mathbf{r}_{VL,0} = [-5, -5, 0]^T$  m and the target point of the virtual leader is set as  $\mathbf{r}_{VL,goal} = [-140, 0, 0]^T$  m. The center of a stationary obstacle is set as  $\mathbf{r}_{obs} =$

$[-70, -3, -3]^T$  m. Scaling factors and design parameters are set as  $\lambda_{str} = 0.12$ ,  $\lambda_{rep} = 0.75$ ,  $q_1 = q_2 = q_3 = q_4 = 10$ ,  $\lambda_{rot} = 0.3$ ,  $\lambda_r = 4$ ,  $\lambda_p = 0.1$ ,  $\lambda_v = 1.3$ ,  $\lambda_{vk,vL} = 1$ , and  $\lambda_{vk} = 7$ .

Figure 3.1.13a shows the trajectories of the four satellites for 1600 seconds. A dashed line represents the virtual leader's reference trajectory, and solid lines represent the four satellites. A grey rectangular parallelepiped represents the obstacle. Figure 3.1.14 shows the minimum Euclidean distance changes between the satellites and the obstacle's surface. As shown in Figure 3.1.13a and Figure 3.1.14, the four satellites safely avoid the obstacle with the distance greater than or equal to 7.615 m. All four satellites are avoiding in the same direction because of the force to maintain the formation, virtual structure. Figure 3.1.13b shows the formation of four satellites ( $\square$ ) around the virtual leader ( $\Delta$ ) through lines between the satellites at 60 sec, 300 sec, 600 sec, 860 sec, 1100 sec, 1300 sec, and 1600 sec. Figure 3.1.15 presents the distance changes between the virtual leader and each satellite. The four satellites should maintain a distance of 6 m (dashed line) which is the radius of the sphere. Figure 3.1.16 shows the relative distance changes between the satellites,  $(\|\mathbf{r}_1 - \mathbf{r}_2\|, \|\mathbf{r}_1 - \mathbf{r}_3\|, \|\mathbf{r}_1 - \mathbf{r}_4\|, \|\mathbf{r}_2 - \mathbf{r}_3\|, \|\mathbf{r}_2 - \mathbf{r}_4\|, \|\mathbf{r}_3 - \mathbf{r}_4\|)$ . Because the four satellites need to form a regular tetrahedron shape, the distance between two of them should be the length of one side of the tetrahedron,  $6 \times \frac{4}{\sqrt{6}} \approx 9.798$  m. Figure 3.1.13b, Figure 3.1.15, and Figure 3.1.16 show that the formation is maintained with some chattering for all simulation times except when avoiding the obstacle. The chattering occurs because we designed the control law to ignore the speed of the virtual leader and the other satellites. Unlike the polygonal formation examples, the relative distances between the virtual leader and each satellite are not biased because the control law for tetrahedral formation is defined so that the total potential function is zero when the satellites form in the desired shape.

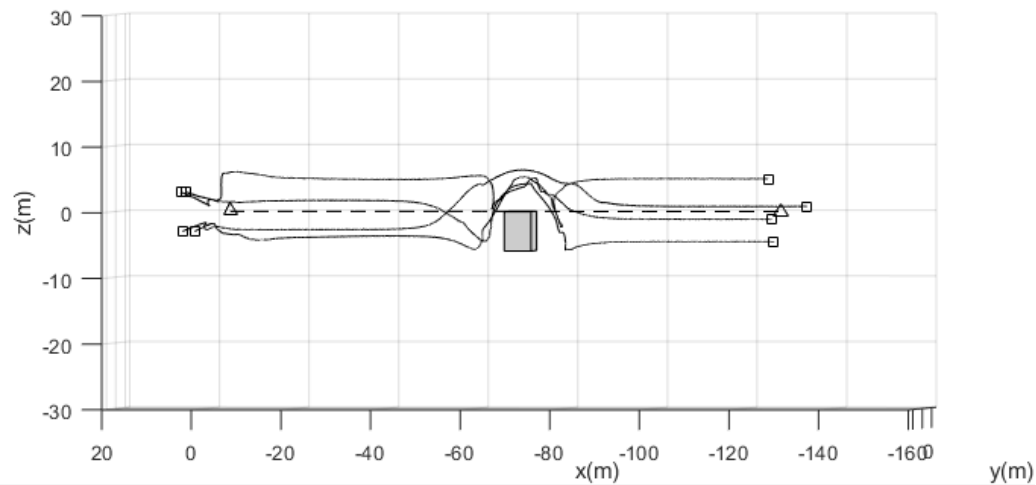


**Figure 3.1.13a** Trajectories of four satellites (solid line), obstacle (grey face), reference trajectory of the virtual leader (dashed line), initial & final position of virtual leader ( $\Delta$ ) and four satellites ( $\square$ )

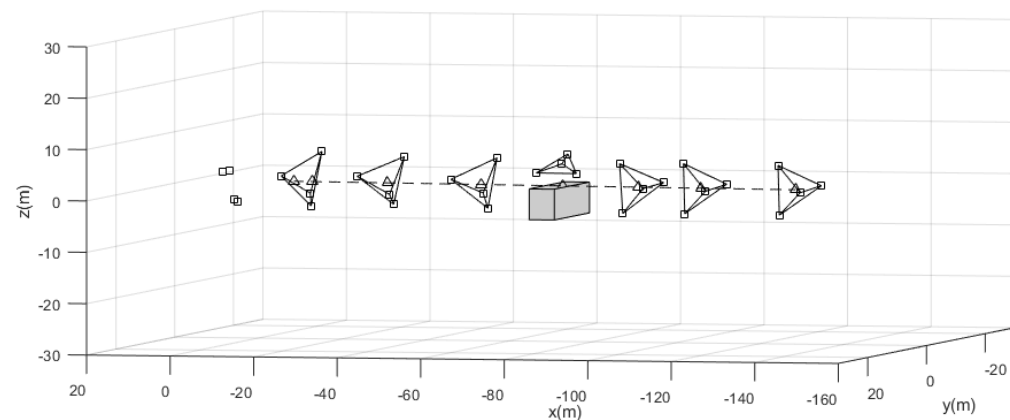


**Figure 3.1.13b** Lines between four satellites (solid line), obstacle (grey face), reference trajectory of the virtual leader (dashed line), instantaneous position of virtual leader ( $\Delta$ ) and four satellites ( $\square$ )

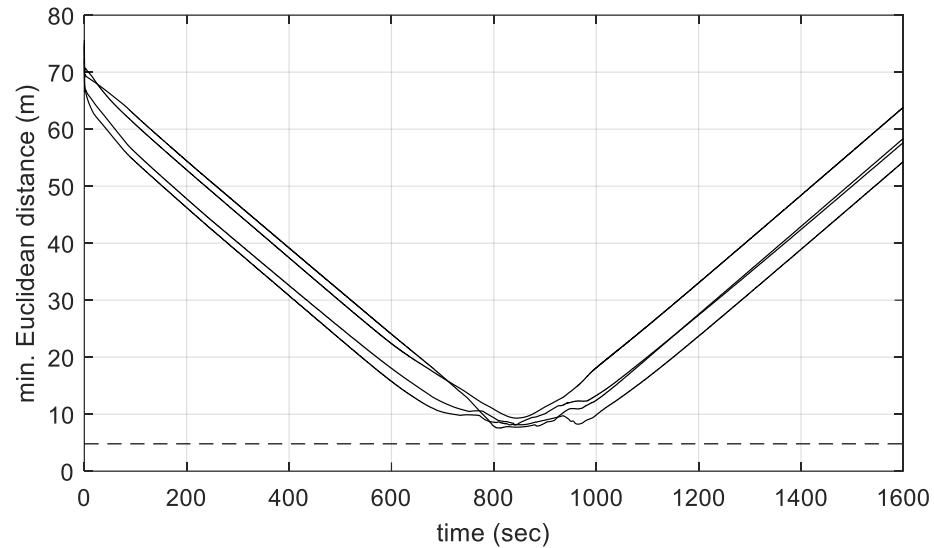


**Figure 3.1.14** Minimum Euclidean distance changes between four satellites and the obstacle's surface

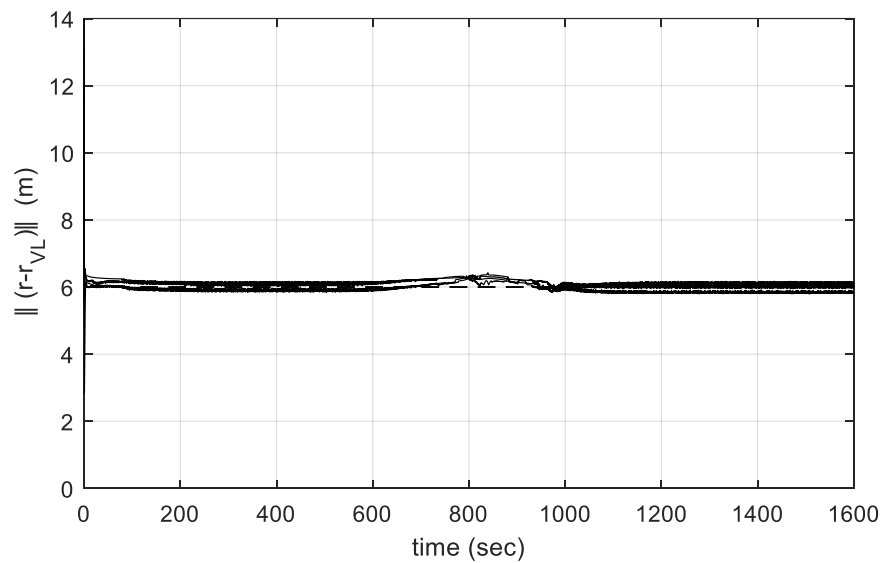


**Figure 3.1.15** Relative distances between virtual leader and four satellites (solid line) in regular tetrahedron formation and radius of circle  $R = 6$  m (dashed line)

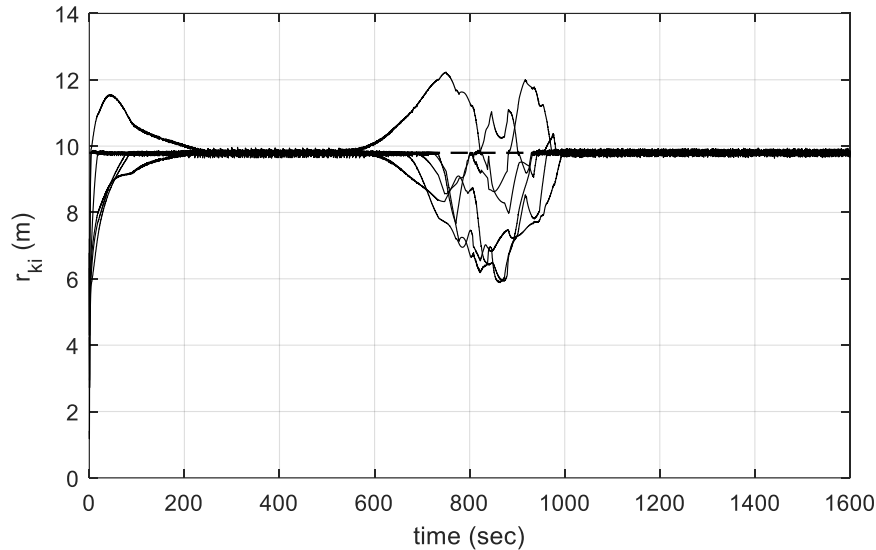


**Figure 3.1.16** Relative distances between satellites (solid line),  
side length of tetrahedron,  $6 \times \frac{4}{\sqrt{6}} \approx 9.798$  m (dashed line)

It is confirmed that multiple satellites maintain a certain formation while avoiding collisions using our control law. In all examples, the satellites avoid the obstacle, but the relative distance errors in the formation occur because our control law for the  $k$ -th satellite is defined ignoring the speed of the virtual leader and other satellites. The quantitative results obtained from the numerical simulations of these four examples (1) ~ (4) are summarized in Table 3.1.1. Table 3.1.1 presents the resultant minimum Euclidean distance between the obstacle surface and the satellites,  $\|\mathbf{r}_k - \mathbf{r}_{obs}\|_{min}$ , final maximum relative distance error with virtual leader,  $d\|\mathbf{r}_k - \mathbf{r}_{VL,goal}\|_{t=t_f, max} = \|\mathbf{r}_k - \mathbf{r}_{VL,goal}\|_{t=t_f, max} - 6$  m, and the maximum final relative distance error between each satellite,  $\|d\mathbf{r}_{ki}\|_{t=t_f, max}$  for  $k = 1, 2, \dots, N$ ,  $i = 1, 2, \dots, N$  ( $i \neq k$ )

In all examples, all satellites avoid the obstacles at a distance equal to or greater than 5.646 m, and the distance error between the virtual leader and the satellites at the final time was the largest at 0.135 m in the tetrahedron example. The final maximum relative distance error between each satellite is also largest in the tetrahedron example. The reason for the greatest distance error is that it is difficult to maintain a three-dimensional tetrahedron formation rather than a two-dimensional polygonal formation using our control law. Therefore, an additional strategy is needed for more rigid tetrahedron formation.

**Table 3.1.1.** Minimum relative distance with obstacle, final relative distance with virtual leader, and maximum final relative error with other satellites

Examples	$\ \mathbf{r}_k - \mathbf{r}_{obs}\ _{min}$ (m)	$d\ \mathbf{r}_k - \mathbf{r}_{VL,goal}\ _{t=t_f,max}$ (m)	$\ d\mathbf{r}_{ki}\ _{t=t_f,max}$ (m)
Square	5.646	0.017	0.036
Pentagon	6.431	0.021	0.051
Hexagon	8.955	0.020	0.043
Tetrahedron	7.615	0.135	0.108

Furthermore, Example (5) was configured to maintain a square formation in the presence of multiple obstacles to ensure that the obstacles were well avoided.

### **Example (5) Square formation with multiple obstacles**

Suppose that on a sphere with a radius of  $R = 6$  m centered on the virtual leader, four satellites ( $\mathbf{r}_1, \mathbf{r}_2, \mathbf{r}_3, \mathbf{r}_4$ ) form a square shape while avoiding seven rectangular parallelepiped obstacles with various sizes. The obstacles are not moving in the reference frame. The initial position of the virtual leader is set as  $\mathbf{r}_{VL,0} = [3, 0, 0]^T$  m and the target point of the virtual leader is set as  $\mathbf{r}_{VL,goal} = [-35, -80, 35]^T$  m. Note that the four satellites should be in square formation in any order. The distance between satellites and the obstacles was set to keep more than 5 m. We set for the satellites to maintain a square formation perpendicular to the direction in which the virtual leader moves.

Figure 3.1.17 shows the trajectories of the four satellites for 4000 seconds. A dashed line represents the virtual leader's reference trajectory, and solid lines represent the four satellites. Grey rectangular parallelepipeds represent the seven obstacles. Figure 3.1.18 shows the minimum Euclidean distance changes between the satellites and the seven obstacles' surface. Figure 3.1.18, the four satellites safely avoid all obstacles with the distance greater than or equal to 5.052 m. Figure 3.1.19 presents the distance changes between the virtual leader and each satellite. The four satellites should maintain a distance of 6 m (dashed line) which is the radius of the sphere. Figure 3.1.20 shows the relative distance changes between the satellites,  $(\|\mathbf{r}_1 - \mathbf{r}_2\|, \|\mathbf{r}_1 - \mathbf{r}_3\|, \|\mathbf{r}_1 - \mathbf{r}_4\|, \|\mathbf{r}_2 - \mathbf{r}_3\|, \|\mathbf{r}_2 - \mathbf{r}_4\|, \|\mathbf{r}_3 - \mathbf{r}_4\|)$ .

As the four satellites continuously avoid the seven obstacles, so both the distance between the satellites and the distances from the virtual leader increase. Therefore, the

satellites did not maintain the square shape well. However, all satellites avoid collisions with all obstacles at distances greater than the desired minimum distance.

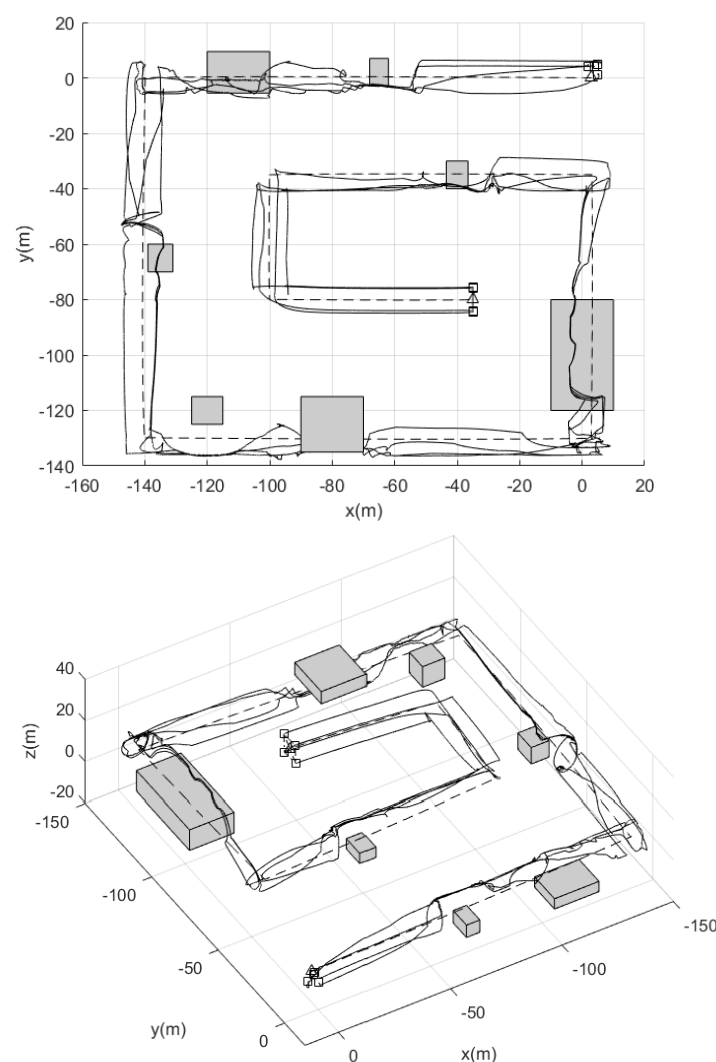


**Figure 3.1.17** Trajectories of four satellites (solid line), seven obstacles (grey face), reference trajectory of the virtual leader (dashed line), initial & final position of virtual leader ( $\Delta$ ) and four satellites ( $\square$ ) in two different views (upper & lower graphs)

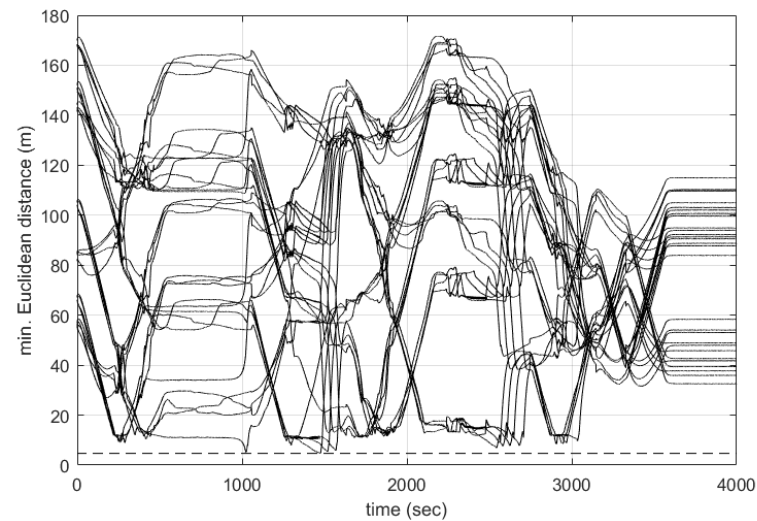


**Figure 3.1.18** Minimum Euclidean distance changes between four satellites and the obstacles' surface

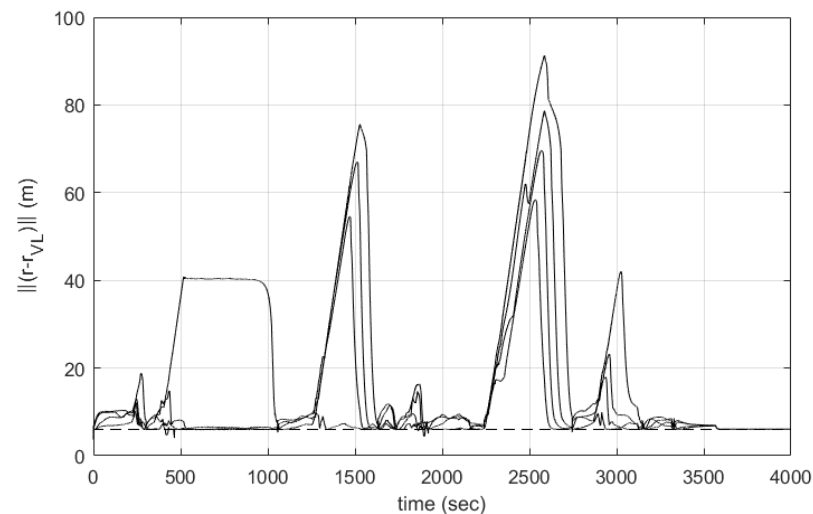


**Figure 3.1.19** Relative distances between virtual leader and four satellites (solid line) in a square formation and radius of circle  $R = 6$  m (dashed line)

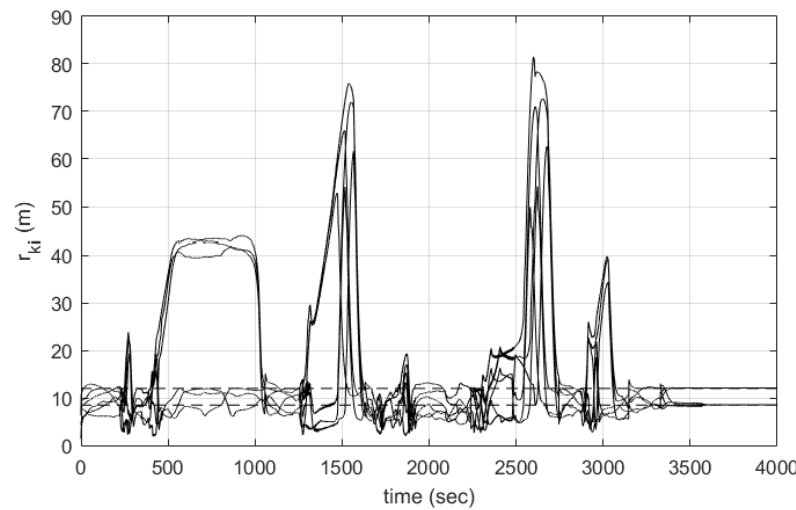


**Figure 3.1.20** Relative distances between satellites (solid line), side length of square,  $6\sqrt{2} \approx 8.49$  m (dashed line), and diagonal length of square, 12 m (dashed line)

### 3.1.2 When Virtual Leader Avoids Obstacles

If obstacles are detected in advance, it is safer to design the virtual leader's trajectory to avoid the obstacles. In this section, the control laws are implemented by numerical simulations in an example that the virtual leader avoids a large obstacle.

When designing the reference trajectory of the virtual leader considering obstacles, the control law ( $\mathbf{u}_{VL}$ ) is set as follows:

$$\mathbf{u}_{VL} = \mathbf{u}_{VL,2}$$

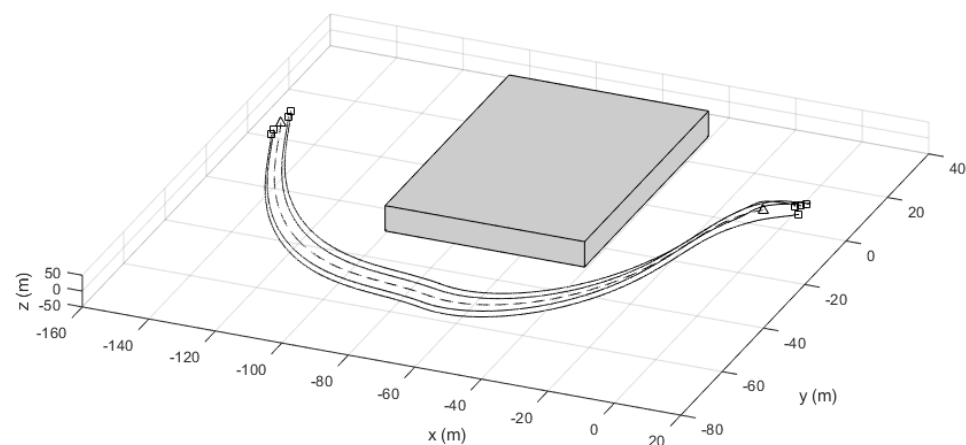
We validate that the satellites maintain a square formation without colliding with a large obstacle using our control law. We aim to keep the satellites at least 10 m away from the obstacle surface.

Suppose that on a circle with a radius of  $R = 6$  m centered on the virtual leader in the  $yz$ -plane, four satellites ( $\mathbf{r}_1, \mathbf{r}_2, \mathbf{r}_3, \mathbf{r}_4$ ) form a square shape while avoiding a rectangular parallelepiped obstacle with side lengths of (60,60,80) m.

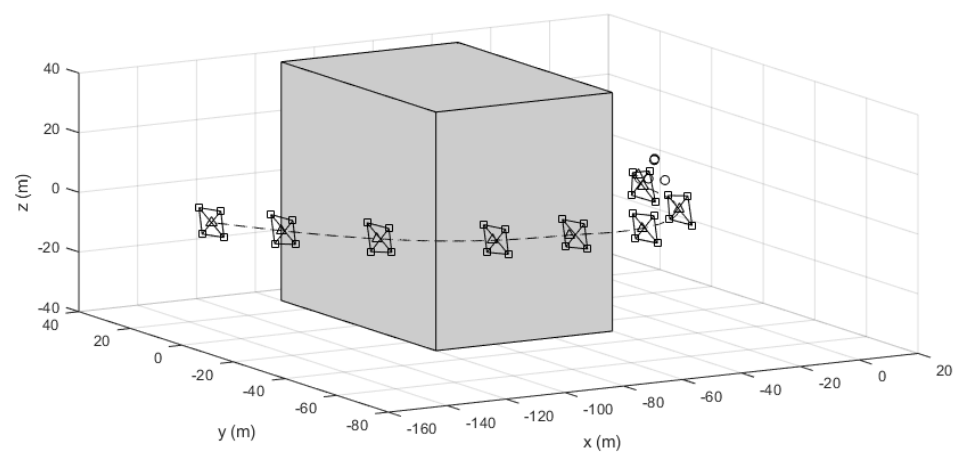
The initial positions of the four satellites are set as  $\mathbf{r}_{1,0} = [5, 5, 3]^T$  m,  $\mathbf{r}_{2,0} = [2, 4, -3]^T$  m,  $\mathbf{r}_{3,0} = [4, 4, 3]^T$  m, and  $\mathbf{r}_{4,0} = [5, 1, -3]^T$  m. The initial position of the virtual leader is set as  $\mathbf{r}_{VL,0} = [-5, 0, 0]^T$  m and the target point of the virtual leader is set as  $\mathbf{r}_{VL,goal} = [-150, 0, 0]^T$  m. The center of a stationary obstacle is set as  $\mathbf{r}_{obs} = [-70, 0, 0]^T$  m. Scaling factors and design parameters are set as  $\lambda_{str} = 0.5$ ,  $\lambda_{rep} = 0.5$ ,  $q_1 = q_2 = q_3 = q_4 = 10$ ,  $\lambda_{rot} = 0.15$ ,  $\lambda_r = 0.13$ ,  $\lambda_p = 0.1$ ,  $\lambda_v = 1$ ,  $\lambda_{vk,VL} = 2$ , and  $\lambda_{vk} = 5$ .

Figure 3.1.21a shows the trajectories of the four satellites and the virtual leader for 3500 seconds. A dashed line represents the virtual leader's trajectory, and solid lines represent the four satellites. A grey rectangular parallelepiped represents the obstacle. Figure 3.1.22 shows the minimum Euclidean distance between the satellites and the obstacle surface is kept higher than or equal to 14.410 m during the simulation time. In Figure 3.1.22, the distances between the obstacle and the satellites do not change smoothly because the satellites avoid an ellipse enclosing the rectangular obstacle. As shown in Figure 3.1.21a and Figure 3.1.22, the virtual leader and the four satellites safely avoid the obstacle. Figure 3.1.21b shows the formation of four satellites ( $\square$ ) around the virtual leader ( $\Delta$ ) through lines between the satellites at 200 sec, 600 sec, 1000 sec, 1400 sec, 1800 sec, 2200 sec, 2600 sec, and 3500 sec. Figure 3.1.23 shows the distance changes between the virtual leader and each of the four satellites. Figure 3.1.24 shows the distance changes between the four satellites.

The result of this example implies that if the virtual leader avoids the obstacle at a sufficiently long distance, the follower satellites do not have to maneuver of avoiding the obstacle.



**Figure 3.1.21a** Trajectories of four satellites (solid line), obstacle (grey face), reference trajectory of the virtual leader (dashed line), initial & final position of virtual leader ( $\Delta$ ) and four satellites ( $\square$ )



**Figure 3.1.21b** Lines between four satellites (solid line), obstacle (grey face), reference trajectory of the virtual leader (dashed line), instantaneous position of virtual leader ( $\Delta$ ) and four satellites ( $\square$ )

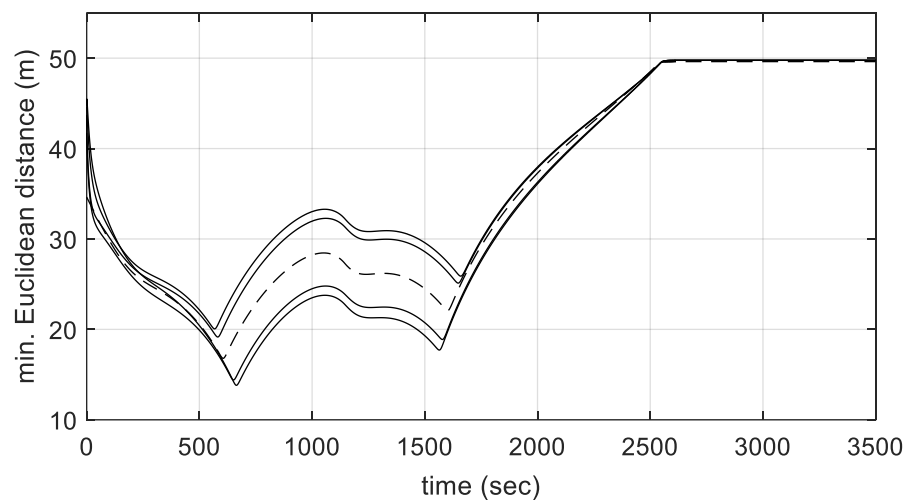


**Figure 3.1.22** Minimum Euclidean distance changes between four satellites and the obstacle surface

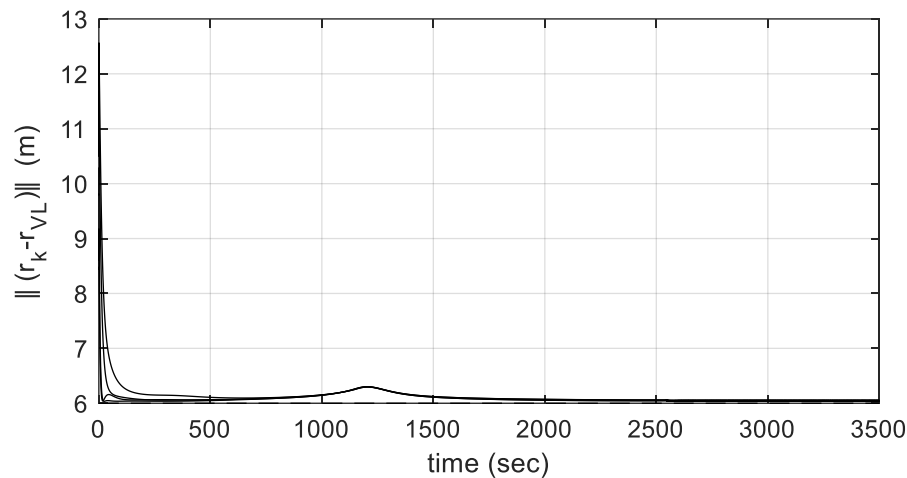


**Figure 3.1.23** Relative distances between virtual leader and four satellites (solid line) in a square formation and radius of circle  $R = 6$  m (dashed line)

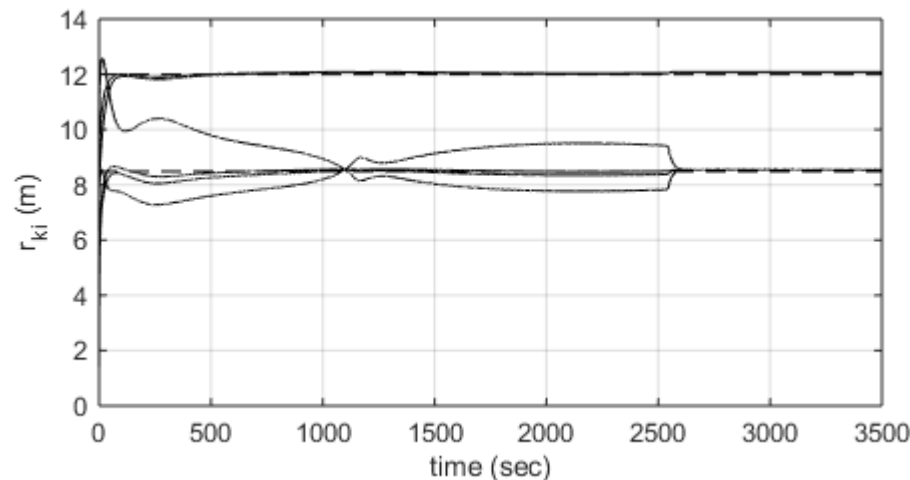


**Figure 3.1.24** Relative distances between satellites (solid line), side length of square,  $6\sqrt{2} \approx 8.49$  m (dashed line), and diagonal length of square, 12 m (dashed line)

## 3.2 Multiple Reconfigurations

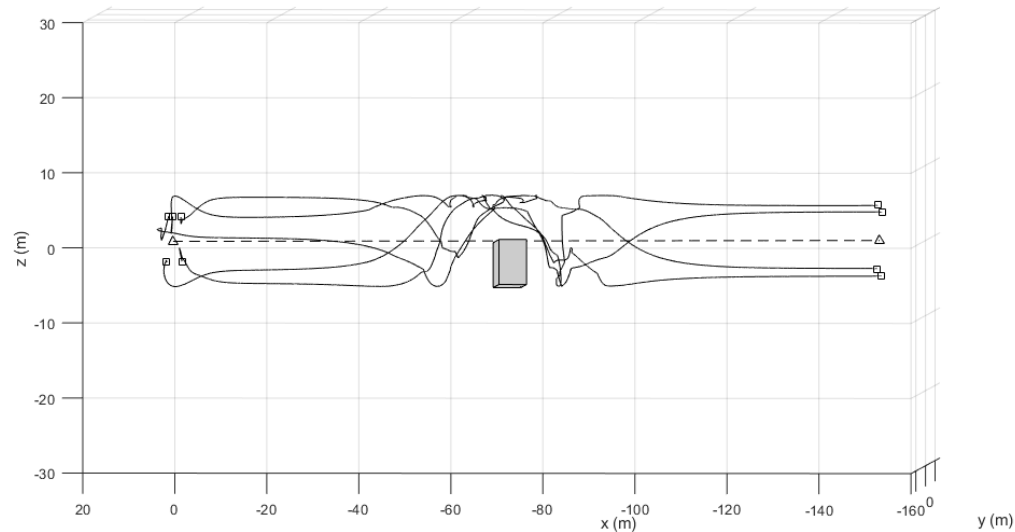
When defining the repulsive potential function in Section 2.2.2,  $N$  satellites are balanced by the repulsive force (Coulomb force) between the satellites without specifying the relative distance. By this definition, even if one or two satellites had problems and could no longer maneuver, the remaining satellites maintain equal distances between them without additional control. We verify this property through an example that the number of satellites changes from five to four.

Suppose that on a circle with a radius of  $R = 6$  m centered on the virtual leader in the  $yz$ -plane, five satellites ( $\mathbf{r}_1, \mathbf{r}_2, \mathbf{r}_3, \mathbf{r}_4, \mathbf{r}_5$ ) form a pentagon shape while avoiding a rectangular parallelepiped obstacle with side lengths of (6,12,6) m. The obstacle is not moving in the reference frame. The fifth satellite ( $\mathbf{r}_5$ ) suddenly stopped maneuvering while avoiding the obstacle. To make one of the satellites destroyed, we aim to keep the satellites at least 3m away from the obstacle surface. Check if the remaining four satellites can maintain a square formation without additional work.

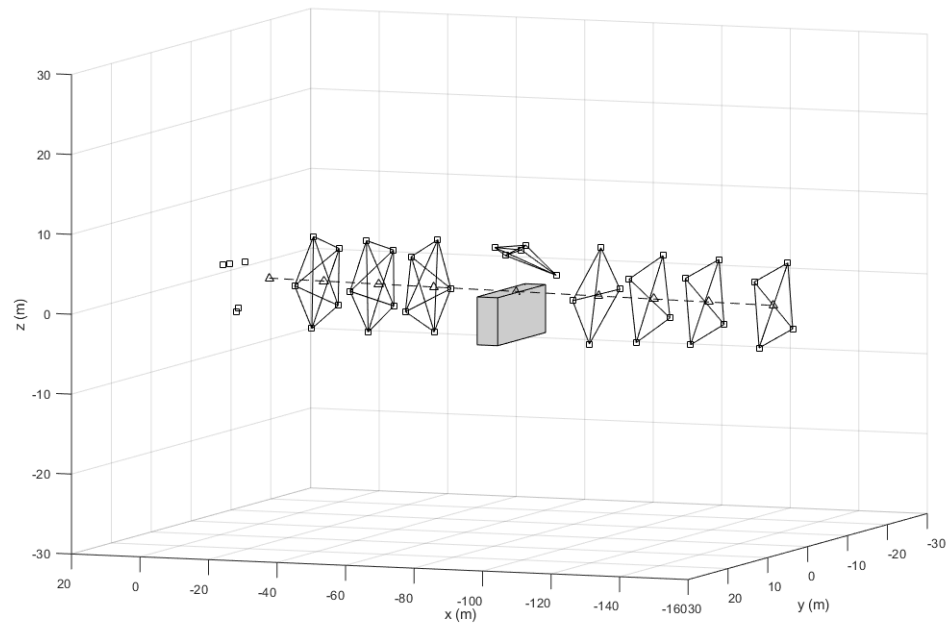
The initial positions of the five satellites at rest are set as  $\mathbf{r}_{1,0} = [2, 2, 3]^T$  m,  $\mathbf{r}_{2,0} = [2, 4, -3]^T$  m,  $\mathbf{r}_{3,0} = [4, 4, 3]^T$  m,  $\mathbf{r}_{4,0} = [5, 1, -3]^T$  m, and  $\mathbf{r}_{5,0} = [5, 5, 3]^T$  m. The initial position of the virtual leader at rest is set as  $\mathbf{r}_{VL,0} = [3, -5, 0]^T$  m and the target point of the virtual leader is set as  $\mathbf{r}_{VL,goal} = [-150, 0, 0]^T$  m. The center of a stationary obstacle is set as  $\mathbf{r}_{obs} = [-70, -3, -3]^T$  m. Scaling factors and design parameters are set as  $\lambda_{str} = 0.45$ ,  $\lambda_{rep} = 0.28$ ,  $q_1 = q_2 = q_3 = q_4 = 10$ ,  $\lambda_{rot} = 0.12$ ,  $\lambda_r = 5$ ,  $\lambda_p = 0.1$ ,  $\lambda_v = 1.2$ ,  $\lambda_{vk,VL} = 1$ , and  $\lambda_{vk} = 7$ .

Figure 3.2.1a shows the trajectories of the five satellites and the virtual leader for 2000 seconds. A dashed line represents the virtual leader's trajectory, and solid lines represent the five satellites. A grey rectangular parallelepiped represents the obstacle. Figure 3.2.1b shows the formation of five satellites ( $\square$ ) around the virtual leader ( $\Delta$ ) through solid lines between the satellites at 200 sec, 400 sec, 600 sec, 900 sec, 1200 sec,

1400 sec, 1600 sec, and 2000 sec. Figure 3.2.2 shows minimum Euclidean distances between the satellites and the obstacle surface. As shown in Figure 3.2.1a and Figure 3.2.2, the five satellites avoid the obstacle greater than or equal to 3.9 m until 900 seconds. In Figure 3.2.2, the fifth satellite indicated by a bold dotted line stopped maneuvering after 900 seconds. However, Figure 3.2.1b and Figure 3.2.4 demonstrate that the remaining four satellites without the fifth satellite successfully maintain their equal distances after 900 seconds. Figure 3.2.3 shows the distance changes between the virtual leader and each satellite. Figure 3.2.4 shows the relative distance changed between the satellites. In Figure 3.2.4, a dashed line represents the desired relative distance between the satellites in a pentagon formation and a square formation.



**Figure 3.2.1a** Trajectories of five satellites (solid line), obstacle (grey face), reference trajectory of the virtual leader (dashed line), initial & final position of virtual leader ( $\Delta$ ) and five satellites ( $\square$ )



**Figure 3.2.1b** Lines between five satellites (solid line), obstacle (grey face), reference trajectory of the virtual leader (dashed line), instantaneous position of virtual leader ( $\Delta$ ) and five satellites ( $\square$ )

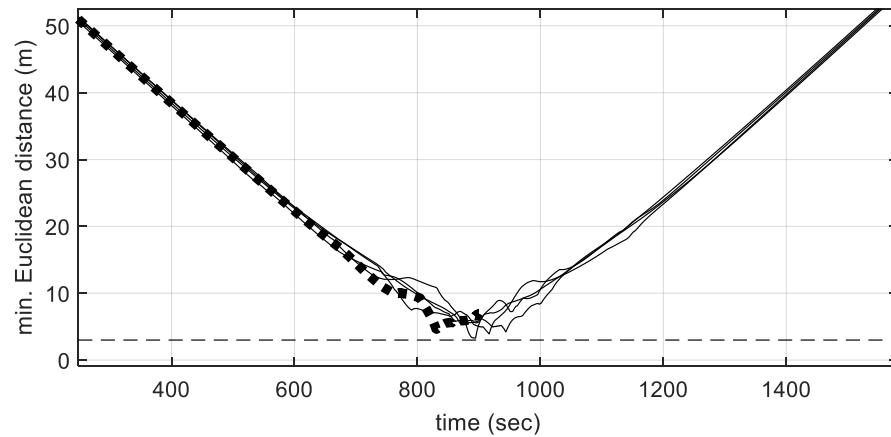


**Figure 3.2.2** Relative distances from the obstacle to four satellites (solid line) and the fifth satellite (bold dotted line)

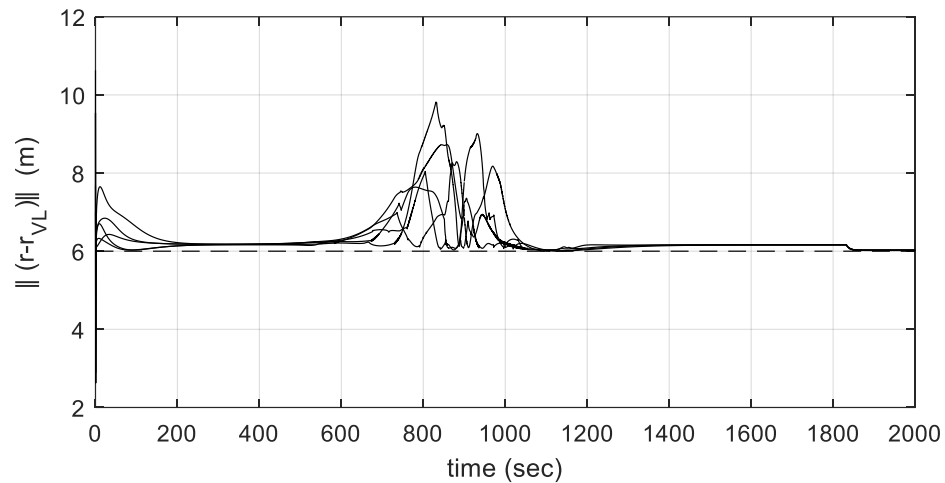


**Figure 3.2.3** Relative distances between virtual leader and five satellites (solid line) in pentagon & square formation, and radius of circle  $R = 6$  m (dashed line)

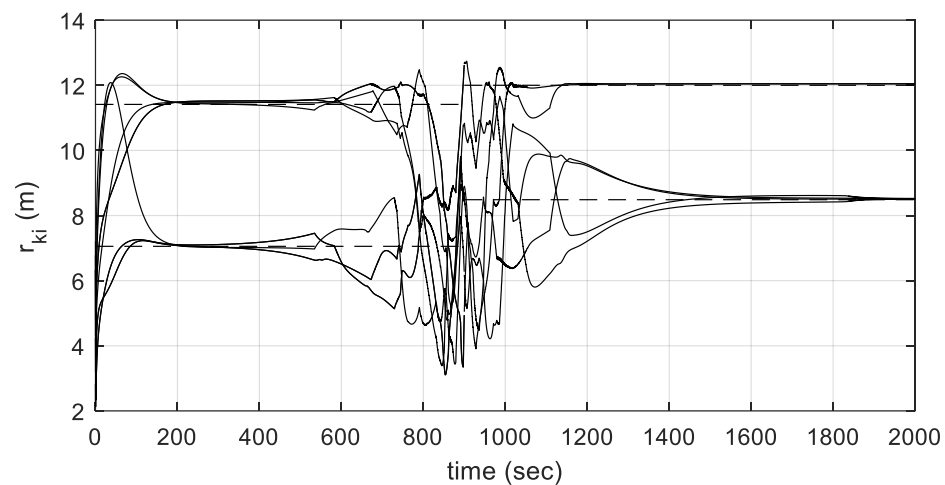


**Figure 3.2.4** Relative distances between five satellites (solid line), side length of pentagon, 7.053 m (dashed line) & diagonal length of pentagon, 11.413 m (dashed line) for 0~900 sec and side length of square, 8.485 m (dashed line) & diagonal length of square, 12 m (dashed line) after 900 sec

### 3.3 Improvement of Local Minima Problem

A local minimum is where a satellite stops before it reaches a target because the negative gradient of the total potential function becomes zero. Someone might think that the satellites do not fall into a local minimum and avoid obstacles easily owing to formation flying or effect of dynamic environment. To avoid the suspicion, we show that the satellite does not get into a local minimum through a single satellite's maneuver example.

Consider that a satellite with a position vector of  $\mathbf{r} = [x, y, z]^T$  is initially located at  $\mathbf{r}_0 = [-5, 0, 0]^T$  m in the inertial frame  $I: \{\hat{x}, \hat{y}, \hat{z}\}$  without dynamics. We want to make the satellite fly to the target point  $\mathbf{r}_{goal} = [-140, 0, 0]^T$  m while avoiding a rectangular parallelepiped obstacle located at  $\mathbf{r}_{obs} = [-70, 0, 0]^T$  m with side lengths of (40, 20, 20) m. The center of the obstacle ( $\mathbf{r}_{obs}$ ), the initial position of the satellite ( $\mathbf{r}_0$ ), and the target point ( $\mathbf{r}_{goal}$ ) are all located on a straight line.

Two types of control laws (Method A & Method B) are implemented by numerical simulations under the above situation. Method A uses the control law derived from our approach and Method B uses a control law based on APF [27] which is also developed for solving local minima problem. Before applying to the example, we derive the control laws of the two methods.

#### (1) Method A

In Method A, we use the control law developed in this research. Total potential function ( $V_{tot}$ ) and control law ( $\mathbf{u}$ ) are defined in the same way with the virtual leader's in Eq. (2.4.15) and Eq. (2.4.16) in Section 3.1.

$$V_{tot} = \lambda_p \|\mathbf{r} - \mathbf{r}_{goal}\| + \frac{1}{2} \lambda_v \dot{\mathbf{r}} \cdot \dot{\mathbf{r}} + V_{rot} \quad (3.3.1)$$

where  $\dot{\mathbf{r}} = [\dot{x}, \dot{y}, \dot{z}]^T$  is velocity vector of the satellite and  $V_{rot}$  is defined about the satellite.



$$\mathbf{u} = - \left( \frac{\lambda_p}{\lambda_v} \frac{(\mathbf{r} - \mathbf{r}_{goal})}{\|\mathbf{r} - \mathbf{r}_{goal}\|} + \frac{1}{\lambda_v} \dot{\mathbf{r}} + T^{-1} \cdot \nabla^* V_{rot} \right) \quad (3.3.2)$$

where transformation matrices  $T^{-1}$  and  $\nabla^* V_{rot}$  are defined about the satellite.

## (2) Method B

The most frequently used avoidance potential function ( $V_{avoid}$ ) is defined that the potential increases exponentially as the satellite approaches an obstacle, so that repulsive force increases exponentially.

$$V_{avoid} = \frac{\exp(-d)}{d} \quad (3.3.3)$$

where  $d$  is the distance between the obstacle and the satellite.

This avoidance potential function is the most used function for collision avoidance, but it has a disadvantage in certain situations. In case of defining the avoidance potential function for a rectangular obstacle, it is easier for the satellite to fall into the local minimum because the potential has an angular shape. In reference [27], the avoidance potential is newly defined to solve this issue by expressing the obstacle as superquadrics.

Total potential function ( $V_{tot}$ ) for the satellite is composed with the attractive potential function ( $V_{att}$ ) for reaching the target point, the velocity term for maintaining the velocity at the low level, and the avoidance potential function ( $V_{avoid}$ ) for collision avoidance.

$$\begin{aligned} V_{tot} &= V_{att} + \frac{1}{2} \lambda_v \dot{\mathbf{r}} \cdot \dot{\mathbf{r}} + V_{avoid} \\ &= \lambda_p \|\mathbf{r} - \mathbf{r}_{goal}\| + \frac{1}{2} \lambda_v \dot{\mathbf{r}} \cdot \dot{\mathbf{r}} + V_{avoid} \end{aligned} \quad (3.3.4)$$

Both the attractive potential function and the velocity term are defined in the same way as the Method A's, and the avoidance potential function is defined by representing the obstacle as superquadrics. Superquadric function for the obstacle is defined as [35, 36, 37]:

$$\left(\frac{x}{a_n}\right)^{2n} + \left(\frac{b_n}{a_n}\right)^2 \left(\frac{y}{b_n}\right)^{2n} + \left(\frac{c_n}{a_n}\right)^2 \left(\frac{z}{c_n}\right)^{2n} = 1 \quad \text{for } n \geq 1 \quad (3.3.5)$$

The semi-axes  $(a_n, b_n, c_n)$  of the superquadrics are defined as (3.3.6), and the superquadrics become a sphere containing the entire obstacle when  $n = 1$ . Details are given in [27].

$$a_n = \frac{40}{2} \left(2^{\frac{1}{2n}}\right), \quad b_n = \frac{20}{2} \left(2^{\frac{1}{2n}}\right), \quad c_n = \frac{20}{2} \left(2^{\frac{1}{2n}}\right) \quad \text{for } n \geq 1 \quad (3.3.6)$$

After expressing the superquadrics of the obstacle, the minimum distance ( $K$ ) from the point-mass satellite to the surface of the superquadrics is defined as follows:

$$K = \|\mathbf{r} - \mathbf{r}_{obs}\| \left[ 1 - \left( \left(\frac{x}{a_n}\right)^{2n} + \left(\frac{b_n}{a_n}\right)^2 \left(\frac{y}{b_n}\right)^{2n} + \left(\frac{c_n}{a_n}\right)^2 \left(\frac{z}{c_n}\right)^{2n} \right)^{\frac{1}{2n}} \right] \quad (3.3.7)$$

As the distance between the obstacle and the satellite decreases, the relationship between  $n$  and  $K$  is defined as follows to make the superquadrics close to the actual obstacle's shape by increasing  $n$ .

$$n = \frac{1}{1 - \exp(-\lambda_n K)} \quad (3.3.8)$$

where  $\lambda_n$  is a positive design parameter.

To determine  $n$  according to the distance  $K$ , we use the bisection method to find  $n$  where  $K$  in Eq. (3.3.7) and  $K$  in Eq. (3.3.8) are equal. The avoidance potential function is defined in the form of Eq. (3.3.3) using  $K$  that is obtained from  $n$ .

$$V_{\text{avoid}} = \lambda_{\text{avoid}} \frac{\exp(-\lambda_o K)}{K} \quad (3.3.9)$$

where  $\lambda_{\text{avoid}}$  is a positive scaling factor, and  $\lambda_o$  is a positive design parameter.

The total potential function of the satellite is defined as:

$$\begin{aligned} V_{\text{tot}} &= V_{\text{att}} + \frac{1}{2} \lambda_v \dot{\mathbf{r}} \cdot \dot{\mathbf{r}} + V_{\text{avoid}} \\ &= \lambda_p \|\mathbf{r} - \mathbf{r}_{\text{goal}}\| + \frac{1}{2} \lambda_v \dot{\mathbf{r}} \cdot \dot{\mathbf{r}} + \lambda_{\text{avoid}} \frac{\exp(-\lambda_o K)}{K} \end{aligned} \quad (3.3.10)$$

The control law ( $\mathbf{u}$ ) is defined as follows to make the time derivative of the total potential function negative semi-definite:

$$\mathbf{u} = - \left( \frac{\lambda_p (\mathbf{r} - \mathbf{r}_{\text{goal}})}{\lambda_v \|\mathbf{r} - \mathbf{r}_{\text{goal}}\|} + \frac{\lambda_{vk}}{\lambda_v} \dot{\mathbf{r}} + \nabla V_{\text{avoid}} \right) \quad (3.3.11)$$

For the implementation of the control laws in Method A & B, scaling factors and design parameters are set as  $\lambda_p = 0.1$ ,  $\lambda_v = 1$ ,  $\lambda_{vk} = 7$ ,  $\lambda_{\text{rot}} = 0.3$ ,  $\lambda_r = 2$ ,  $\lambda_{\text{avoid}} = 2$ , and  $\lambda_o = 40$ . Figure 3.3.1 shows the trajectories of the satellite for 1600 seconds using two methods. A solid line represents the resultant trajectory using Method A, and a dashed line represents the trajectory using Method B. A grey rectangular parallelepiped represents the obstacle, and a grey star represents the target point. The initial position of the satellite is represented by ( $\Delta$ ), and final position of the satellite is represented by ( $\circ$ ).

As shown in Figure 3.3.1, the satellite arrives at the target point without collisions in Method A. In Method B, on the other hand, the satellite stopped in front of the obstacle. The location where the satellite stopped is a local minimum. Even if defining the avoidance potential function using superquadrics, the satellite cannot avoid the obstacle because both the attractive and the avoidance forces are acted on a straight line in the opposite direction regardless of the shape of avoidance potential. After the satellite returns to the initial point



direction by the avoidance (repulsive) force, the satellite maneuvers again toward the obstacle by the attractive force. This process is repeated, and the satellite seems to be trapped at that point.

Figure 3.3.2 shows the minimum relative distances between the satellite and the obstacle's surface. In Method A, as the relative distance (solid line) decreases, the satellite moves away from the obstacle by the control law. In Method B, the relative distance (dashed line) is maintained constant from the moment when the satellite enters the local minimum. This result demonstrates that our approach improved the local minima problem in APF.

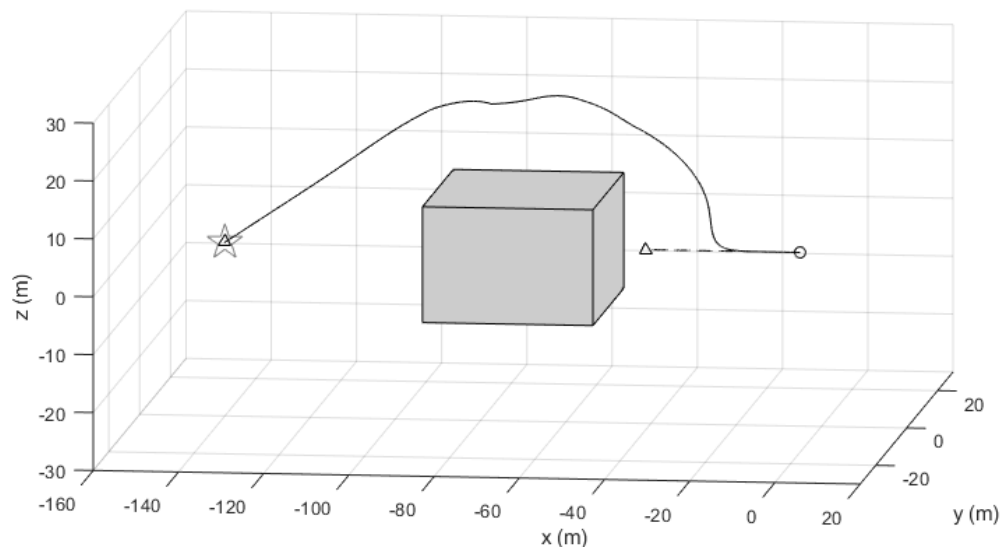


**Figure 3.3.1** Trajectories of the satellite by Method A (solid line) & Method B (dashed line), initial position ( $\Delta$ ) & final position ( $\circ$ ) of the satellite, the target point (grey star), and obstacle (grey face)

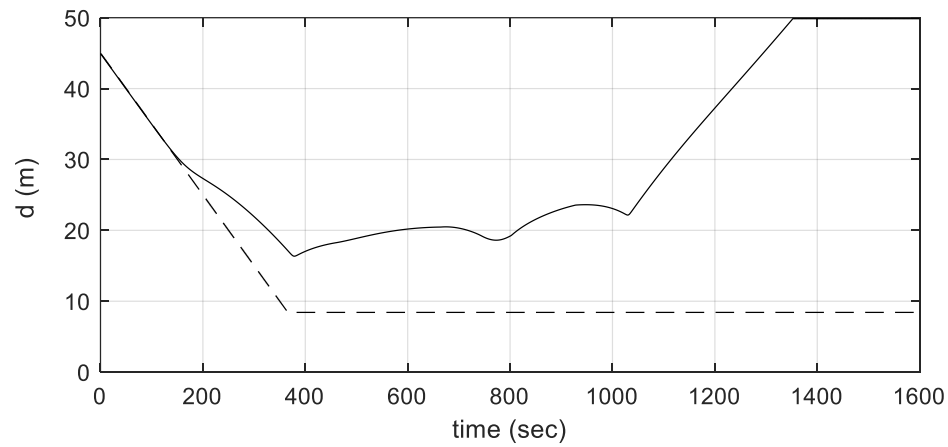


**Figure 3.3.2** Relative distances between the obstacle and the satellites by Method A (solid line) & Method B (dashed line)

## 4. Sliding Surface Application

Sliding Mode Control (SMC) is a classical method that allows robust control even with disturbances and uncertainties of the dynamic system. In the SMC methodology, n-dimensional differential equations are simplified into a one-dimensional system, which leads to a stable and consistent performance [34]. In this thesis, we apply the SMC technique to the APF-based control system [38, 39, 40]. This application makes four satellites maneuver maintaining more rigid tetrahedral formation despite the presence of disturbances or imperfections of the system.

### 4.1 Sliding Mode Controller Design

Inspired by [39], we apply our artificial potential function to Sliding Mode Control. First, we redefine a total potential function ( $V_{total,k}$ ) for the  $k$ -th satellite to maintain a regular tetrahedron formation while avoiding collisions where  $k \in \{1,2,3,4\}$ .

$$V_{total,k} = V_{structure,k} + V_{rep,k} + V_{rot,k} \quad (4.1.1)$$

The structural potential function ( $V_{structure,k}$ ), the repulsive potential function ( $V_{rep,k}$ ), and the rotational potential function ( $V_{rot,k}$ ) were defined in the Chapter 2. The total potential function is different from Eq. (3.1.2) in that the velocity term is removed. If four satellites maintained a regular tetrahedron formation, the total potential function ( $V_{total,k}$ ) becomes zero, and we can say that the total potential function is a positive definite function.

The time derivative of the total potential function ( $\dot{V}_{total,k}$ ) will be:

$$\begin{aligned} \dot{V}_{total,k} &= \dot{V}_{structure,k} + \dot{V}_{rep,k} + \dot{V}_{rot,k} \\ &= \nabla V_{structure,k}(\dot{\mathbf{r}}_k - \dot{\mathbf{r}}_{VL}) + \nabla V_{rep,k}(\dot{\mathbf{r}}_k - \dot{\mathbf{r}}_i) + \dot{\mathbf{r}}_k \cdot T^{-1} \cdot \nabla^* V_{rot,k} \end{aligned} \quad (4.1.2)$$

Previously, we assumed that the velocity of other satellites ( $\dot{\mathbf{r}}_i$ ) and virtual leader ( $\dot{\mathbf{r}}_{VL}$ ) are zero when defining the total potential function for the  $k$ -th satellite, but we do not use this assumption here.

The required velocity vector of the  $k$ -th satellite is defined as:

$$\dot{\mathbf{r}}_k = (\dot{\mathbf{r}}_{VL} - \alpha \nabla V_{structure,k}) + (\dot{\mathbf{r}}_i - \beta \nabla V_{rep,k}) - \gamma T^{-1} \cdot \nabla^* V_{rot,k} \quad (4.1.3)$$

where  $\alpha, \beta, \gamma$  are some positive constants.

As mentioned before, it is difficult to know the exact velocity of other satellites ( $\dot{\mathbf{r}}_i$ ) in real time. Thus, when deriving a control law for the  $k$ -th satellite, we assume that the speed of every satellite except the  $k$ -th satellite is bounded under some positive value,  $\sigma$ . To determine  $\sigma$ , we use the virtual leader's speed range that can be obtained through designing the reference trajectory of the formation group (i.e., the virtual leader's trajectory).

Assume that  $\|\dot{\mathbf{r}}_i\| \leq \sigma$  where  $\|\dot{\mathbf{r}}_{VL}\| \leq \sigma = \|\dot{\mathbf{r}}_{VL}\|_{max}$  for  $\sigma > 0$

where  $\sigma$  is chosen to be a maximum speed of the virtual leader. Under this assumption, the  $k$ -th satellite's required velocity is defined as:

$$\begin{aligned} \dot{\mathbf{r}}_k = & -\alpha \nabla V_{structure,k} - \alpha' sgn(\nabla V_{structure,k}) \\ & -\beta \nabla V_{rep,k} - \beta' sgn(\nabla V_{rep,k}) - \gamma T^{-1} \cdot \nabla^* V_{rot,k} \end{aligned} \quad (4.1.4)$$

where  $\alpha' > \sigma, \beta' > \sigma$  are positive constants and  $sgn(\mathbf{r})$  is the sign function that extracts the sign of each component of vector  $\mathbf{r}$ .

With the proposed velocity vector, the time derivative of the total potential function of the  $k$ -th satellite will be:

$$\begin{aligned}\dot{V}_{total,k} = & -\alpha \|\nabla V_{structure,k}\|^2 - \alpha' \|\nabla V_{structure,k}\| - \dot{\mathbf{r}}_{VL} \nabla V_{structure,k} \\ & - \beta \|\nabla V_{rep,k}\|^2 - \beta' \|\nabla V_{rep,k}\| - \dot{\mathbf{r}}_i \nabla V_{rep,k} \\ & - \gamma \|T^{-1} \cdot \nabla^* V_{rot,k}\|^2\end{aligned}\quad (4.1.5)$$

Because we set  $\alpha' > \sigma$ ,  $\beta' > \sigma$  for a positive constant  $\sigma$ , the time derivative of the total potential function will be:

$$\begin{aligned}\dot{V}_{total,k} \leq & -\alpha \|\nabla V_{structure,k}\|^2 - \alpha' \|\nabla V_{structure,k}\| + \sigma \|\nabla V_{structure,k}\| \\ & - \beta \|\nabla V_{rep,k}\|^2 - \beta' \|\nabla V_{rep,k}\| + \sigma \|\nabla V_{rep,k}\| \\ & - \gamma \|T^{-1} \cdot \nabla^* V_{rot,k}\|^2\end{aligned}\quad (4.1.6)$$

Then, the time derivative of the total potential function satisfies the inequality:

$$\begin{aligned}\dot{V}_{total,k} \leq & -\alpha \|\nabla V_{structure,k}\|^2 - \beta \|\nabla V_{rep,k}\|^2 - \gamma \|T^{-1} \cdot \nabla^* V_{rot,k}\|^2 \\ \leq & 0\end{aligned}\quad (4.1.7)$$

Equation (4.1.7) proves that the total potential function of the  $k$ -th satellite is negative semi-definite. Thus, Lyapunov stability is proven.

Next, we discuss how to apply the SMC technique to the APF [39]. Dynamical systems of the  $k$ -th satellite is defined as following equations of motion:

$$\ddot{\mathbf{r}}_k = g_k(\mathbf{r}_k, \dot{\mathbf{r}}_k) + \mathbf{u}_k \quad (4.1.8)$$

where  $\mathbf{u}_k$  is the control input.

Here,  $g_k(\mathbf{r}_k, \dot{\mathbf{r}}_k)$  includes uncertainties and disturbances that we do not know exactly. Assume that  $g_k(\mathbf{r}_k, \dot{\mathbf{r}}_k)$  consists of two parts, the known part  $g_k^a(\mathbf{r}_k, \dot{\mathbf{r}}_k)$  and the unknown part  $g_k^b(\mathbf{r}_k, \dot{\mathbf{r}}_k)$ :

$$g_k(\mathbf{r}_k, \dot{\mathbf{r}}_k) = g_k^a(\mathbf{r}_k, \dot{\mathbf{r}}_k) + g_k^b(\mathbf{r}_k, \dot{\mathbf{r}}_k) \quad (4.1.9)$$

We need an additional assumption here that the unknown part is bounded to a positive value,  $\bar{f}$ :

$$\|g_k^b(\mathbf{r}_k, \dot{\mathbf{r}}_k)\| \leq \bar{f} \quad (4.1.10)$$

In order to apply SMC to the APF, we need to define the sliding manifold for the  $k$ -th satellite [34]. The sliding manifold ( $s_k$ ) of the  $k$ -th satellite is defined as:

$$\begin{aligned} s_k = \dot{\mathbf{r}}_k + \alpha \nabla V_{structure,k} + \alpha' sgn(\nabla V_{structure,k}) + \beta \nabla V_{rep,k} + \\ \beta' sgn(\nabla V_{rep,k}) + \gamma T^{-1} \cdot \nabla^* V_{rot,k} \end{aligned} \quad (4.1.11)$$

In the sliding mode,  $s_k = 0$ , the velocity ( $\dot{\mathbf{r}}_k$ ) of the  $k$ -th satellite satisfies Eq. (4.1.4) so that the desired maneuver can be made. We need to properly select the control input ( $\mathbf{u}_k$ ) to make  $s_k = 0$  (i.e., to reach on the sliding surface). The control input is defined through a sliding condition that is a sufficient condition for the sliding mode,  $s_k = 0$ . [34]

$$s_k^T \dot{s}_k \leq -\eta \|s_k\| < 0, \quad (\eta > 0) \quad (4.1.12)$$

where  $\eta$  is a positive constant.

The time derivative of the sliding manifold is given by:

$$\begin{aligned} \dot{s}_k = \ddot{\mathbf{r}}_k + \frac{d}{dt} [\alpha \nabla V_{structure,k} + \alpha' sgn(\nabla V_{structure,k})] \\ + \frac{d}{dt} [\beta \nabla V_{rep,k} + \beta' sgn(\nabla V_{rep,k})] \\ + \frac{d}{dt} [\gamma T^{-1} \cdot \nabla^* V_{rot,k}] \end{aligned} \quad (4.1.13)$$

We need another assumption that the time derivative terms are bounded by some positive constants:

$$\left\| \frac{d}{dt} [\alpha \nabla V_{structure,k} + \beta \nabla V_{rep,k}] \right\| \leq J_1 \quad (4.1.14a)$$

$$\left\| \frac{d}{dt} [\alpha' sgn(\nabla V_{structure,k}) + \beta' sgn(\nabla V_{rep,k})] \right\| \leq J_2 \quad (4.1.14b)$$

$$\left\| \frac{d}{dt} [\gamma T^{-1} \cdot \nabla^* V_{rot,k}] \right\| \leq J_3 \quad (4.1.14c)$$

where  $J_1$ ,  $J_2$ , and  $J_3$  are known positive constants.

If the constants are chosen large enough, the assumption is valid because the maximum values of the left terms in Eq. (4.1.14a) and Eq. (4.1.14c) are actually determined [39]. However, Eq. (4.1.14b) is an exception.

The derivative of the  $sgn$  function in Eq. (4.1.14b) is unbounded because the sign can change continuously with a high frequency. Reference [39] solved this problem by using the appropriate low-pass filter:

$$\mu \dot{\mathbf{z}} = -\mathbf{z} + \alpha' sgn(\nabla V_{structure,k}) + \beta' sgn(\nabla V_{rep,k}) \quad (4.1.15)$$

where  $\mu$  is a sufficiently small positive constant.

In the system of Eq. (4.1.15), the term  $\alpha' sgn(\nabla V_{structure,k}) + \beta' sgn(\nabla V_{rep,k})$  denotes an input and  $\mathbf{z}$  denotes a filtered output. With an appropriate value of  $\mu$ , we can say that:

$$\mathbf{z} \approx \alpha' sgn(\nabla V_{structure,k}) + \beta' sgn(\nabla V_{rep,k}) \quad (4.1.16)$$

Then, the third term on the right term of Eq. (4.1.11) can be replaced by  $\mathbf{z}$ . The new sliding manifold is defined:

$$s_{k,new} = \dot{\mathbf{r}}_k + \alpha \nabla V_{structure,k} + \beta \nabla V_{rep,k} + \gamma T^{-1} \cdot \nabla^* V_{rot,k} + \mathbf{z} \quad (4.1.17)$$

The time derivative of sliding manifold is given by:

$$\dot{s}_{k,new} = \ddot{\mathbf{r}}_k + \frac{d}{dt} [\alpha \nabla V_{structure,k} + \beta \nabla V_{rep,k}] + \frac{d}{dt} [\gamma T^{-1} \cdot \nabla^* V_{rot,k}] + \dot{\mathbf{z}} \quad (4.1.18)$$

Instead of assumption in Eq. (4.1.14b), we assume that the time derivative of  $\mathbf{z}$  is bounded:

$$\begin{aligned} \|\dot{\mathbf{z}}\| &= \left\| \frac{1}{\mu} [-\mathbf{z} + \alpha' sgn(\nabla V_{structure,k}) + \beta' sgn(\nabla V_{rep,k})] \right\| \\ &\leq \frac{(\alpha' + \beta')}{\mu} \\ &\approx J_2 \end{aligned} \quad (4.1.19)$$

for a known constant  $0 < J_2 < \infty$

Using Eq. (4.1.18), the sliding condition equation is given by:

$$\begin{aligned} s_{k,new}^T \dot{s}_{k,new} &= s_{k,new}^T \left( \ddot{\mathbf{r}}_k + \frac{d}{dt} [\alpha \nabla V_{structure,k} + \beta \nabla V_{rep,k}] \right. \\ &\quad \left. + \frac{\partial}{\partial t} [\gamma T^{-1} \cdot \nabla^* V_{rot,k}] + \dot{\mathbf{z}} \right) \end{aligned} \quad (4.1.20)$$

If we substitute  $\ddot{\mathbf{r}}_k$  into Eq. (4.1.8), Eq. (4.1.20) will be:

$$\begin{aligned} s_{k,new}^T \dot{s}_{k,new} &= s_{k,new}^T \left( f_k(\mathbf{r}_k, \dot{\mathbf{r}}_k) + \mathbf{u}_k + \frac{d}{dt} [\alpha \nabla V_{structure,k} + \beta \nabla V_{rep,k}] \right. \\ &\quad \left. + \frac{d}{dt} [\gamma T^{-1} \cdot \nabla^* V_{rot,k}] + \dot{\mathbf{z}} \right) \end{aligned} \quad (4.1.21)$$

The control law ( $\mathbf{u}_k$ ) is chosen to satisfy the sliding condition in Eq. (4.1.12).

$$\mathbf{u}_k = -f_k^a(\mathbf{r}_k, \dot{\mathbf{r}}_k) - u_0 sgn(s_{k,new}) \quad (4.1.22)$$

where  $u_0$  is a positive constant.

If we substitute Eq. (4.1.22) into Eq. (4.1.12), we have

$$s_{k,new}^T \dot{s}_{k,new} < -\|s_{k,new}\|(u_0 - \bar{f} - J_1 - J_2 - J_3) \quad (4.1.23)$$

If we choose  $u_0$  to satisfy the inequality below for a positive constant  $\epsilon$ :

$$u_0 > \bar{f} + J_1 + J_2 + J_3 + \epsilon \quad (4.1.24)$$

the sliding condition is satisfied.

$$s_{k,new}^T \dot{s}_{k,new} < -\epsilon \|s_k\| < 0 \quad (4.1.25)$$

Satisfying a sliding condition means that once the sliding surface is reached, the SMC makes the system states to stay on the sliding surface,  $s_{k,new} = 0$ .

## 4.2 Simulation Results

In this section, the control law derived in the previous section is implemented by numerical simulations in an example. Suppose that on a circle with radius  $R = 6$  m centered on the virtual leader in the  $yz$ -plane, four satellites ( $\mathbf{r}_1, \mathbf{r}_2, \mathbf{r}_3, \mathbf{r}_4$ ) form a regular tetrahedron formation while avoiding a rectangular parallelepiped obstacle with side lengths of  $(6, 12, 6)$  m under random disturbances with a range of  $(-0.5 \sim 0.5)$  m/s<sup>2</sup>. The equations of motion in this example is defined as:

$$\ddot{\mathbf{r}}_k = g_k(\mathbf{r}_k, \dot{\mathbf{r}}_k) + \mathbf{u}_k, \quad k \in \{1, 2, 3, 4\} \quad (4.2.1)$$

where  $g_k(\mathbf{r}_k, \dot{\mathbf{r}}_k) = f_k(\mathbf{r}_k, \dot{\mathbf{r}}_k) + g_k^b(\mathbf{r}_k, \dot{\mathbf{r}}_k)$  is the HCW dynamic equation with the bounded disturbances.

In this example, a reference trajectory of the virtual leader is designed not to consider collision avoidance. The initial position of the virtual leader at rest is set as  $\mathbf{r}_{VL,0} =$

$[-5, -5, 0]^T$  m and the target point of the virtual leader is set as  $\mathbf{r}_{VL,goal} = [-140, 0, 0]^T$  m. The initial positions of the four satellites at rest are set the same as the example (4) in Section 3.2.1. The center of a stationary obstacle is set as  $\mathbf{r}_{obs} = [-70, -3, -3]^T$  m. We aim to keep the satellites at least 5m away from the obstacle surface.

We choose  $\alpha = 0.005$ ,  $\beta = 0.03$ ,  $\gamma = 10$ ,  $\alpha' = 0.001$ ,  $\beta' = 0.001$ , and  $\mu = 0.01$ .

The control law of the  $k$ -th satellite is defined as:

$$\mathbf{u}_k = -f_k(\mathbf{r}_k, \dot{\mathbf{r}}_k) - u_0 \tanh(\eta s_k) \quad (4.2.2)$$

Here,  $sgn$  function is replaced by  $tanh$  function with a positive constant  $\eta$  to make the smoother control [39].

As suggested in the previous section,  $u_0$  should be defined to satisfy the following inequality:

$$u_0 > \bar{f} + J_1 + J_2 + J_3 + \epsilon \quad (4.2.3)$$

Before choosing the constants in Eq. (4.2.3), we choose scaling factors and design parameters as  $\lambda_{str} = 1.6$ ,  $\lambda_{rep} = 1.6$ ,  $q_1 = q_2 = q_3 = q_4 = 10$ ,  $\lambda_{rot} = 0.1$ ,  $\lambda_r = 40$ ,  $\lambda_p = 0.1$ ,  $\lambda_v = 1.3$ ,  $\lambda_{vk, VL} = 2$ ,  $\lambda_{vk} = 8$ , and  $\eta = 10$ . Then, we can set  $\bar{f} = 0.5$ ,  $J_1 = 0.0036$ ,  $J_2 = 0.2$ ,  $J_3 = 0.5$ ,  $\epsilon = 0.1$ , and  $u_0 = 1.7$ .

Figure 4.2.1a shows the trajectories of the four satellites for 3500 seconds. A dashed line represents the virtual leader's reference trajectory, and solid lines represent the four satellites. A grey rectangular parallelepiped represents the obstacle. Figure 4.2.2 shows minimum Euclidean distances between the satellites and the obstacle surface. As shown in Figure 4.2.1a and Figure 4.2.2, the four satellites did not collide with the obstacle. The minimum relative distance between the obstacle and the satellites,  $\|\mathbf{r}_k - \mathbf{r}_{obs}\|_{min}$ , is

6.8 m. Figure 4.2.1b shows the formation of four satellites ( $\square$ ) around the virtual leader ( $\Delta$ ) through lines between the satellites. Figure 4.2.3 shows the distance changes between the virtual leader and each satellite. The four satellites should maintain a distance of 6 m (dashed line) which is the radius of the sphere. Figure 4.2.4 shows the distance changes between the four satellites. The maximum relative distance error between the satellites and the virtual leader in the final time,  $d\|\mathbf{r}_k - \mathbf{r}_{VL,goal}\|_{t=t_f,max}$ , is 0.090 m. The maximum relative distance error between the satellites in the final time,  $\|d\mathbf{r}_{ki}\|_{t=t_f,max}$ , is 0.026 m.

We analyze the results compared with the results of example (4) in section 3.2.1. Note that the variables and the simulation time are different with the example (4) and that the SMC example assumes some disturbances in the system. The results of the examples have two notable differences.

As depicted in Figure 4.2.1a, in the SMC example, one of the four satellites avoid the obstacle in the opposite direction with other satellites while all satellites avoid the obstacle in the same direction in the example (4). One of the four satellites was controlled to avoid the obstacle in the same direction as the other satellites due to the structural potential. As the satellite is closer to the obstacle than the other satellite, the satellite becomes closer to the other satellite by the greater rotational potential. Then, the satellite is repelled by the repulsive potential and avoid the obstacle in a different direction to the other satellites.

Another notable difference is that the relative distance changes are maintained with less chattering than in the example (4) as shown in Figure 4.2.3 and Figure 4.2.4. Figure 4.2.4 shows that the maximum relative distance error between each satellite is,  $\|d\mathbf{r}_{ki}\|_{t=t_f,max} = 0.026$  m, which is about 4.1 times smaller than in example (4). Also, Figure 4.2.3 shows that the maximum relative distance error between the virtual leader and satellites is,  $d\|\mathbf{r}_k - \mathbf{r}_{VL,goal}\|_{t=t_f,max} = 0.090$  m, which is about 1.5 times smaller than in example (4). Unlike the example (4), the SMC control law allows more precise control by considering the speed of the virtual leader and the other satellites.

The control law of SMC resulted in robust performances of the satellites despite the presence of disturbances with a range of  $(-0.5 \sim 0.5) \text{ m/s}^2$ . However, there are more parameters than before; thus it might take more time to fine-tune the parameters.

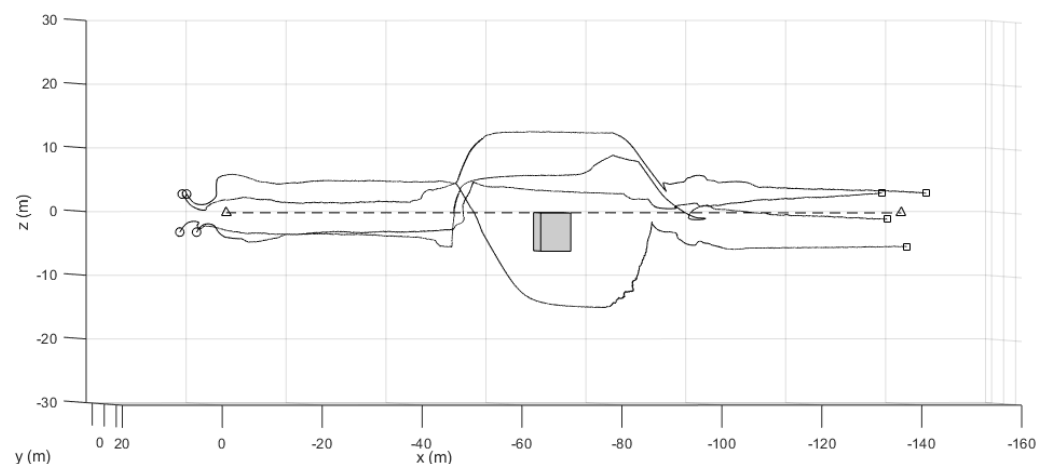


**Figure 4.2.1a** Trajectories of four satellites (solid line), obstacle (grey face), reference trajectory of the virtual leader (dashed line), initial & final position of virtual leader ( $\Delta$ ) and four satellites ( $\square$ )

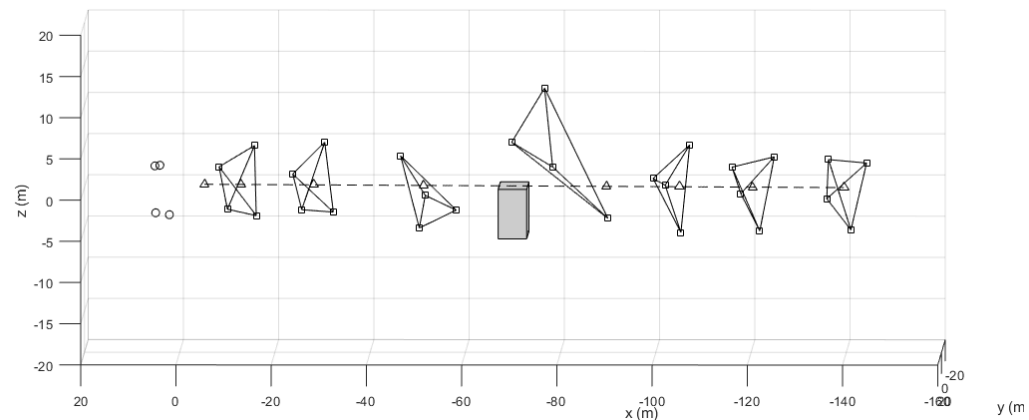


**Figure 4.2.1b** Lines between four satellites (solid line), obstacle (grey face), reference trajectory of the virtual leader (dashed line), instantaneous position of virtual leader ( $\Delta$ ) and four satellites ( $\square$ )

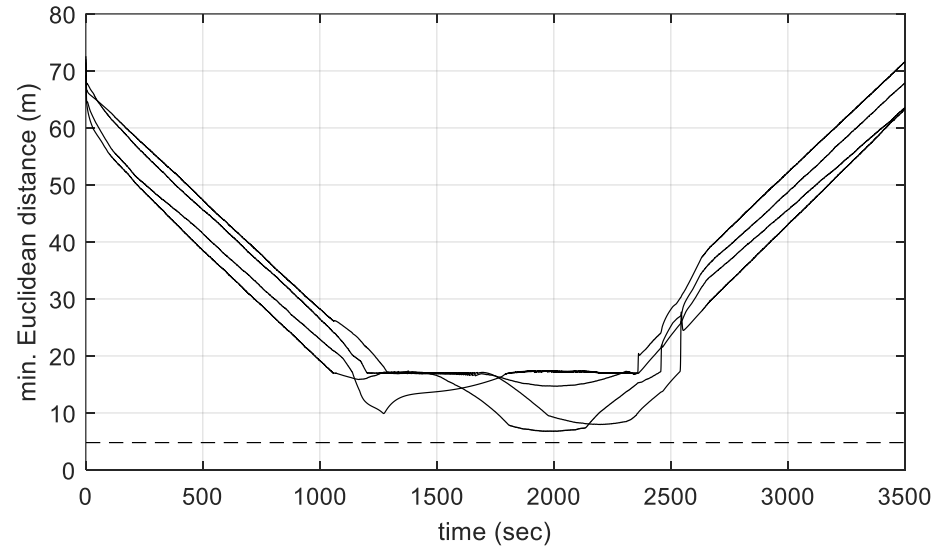


**Figure 4.2.2** Relative distances between the obstacle and four satellites

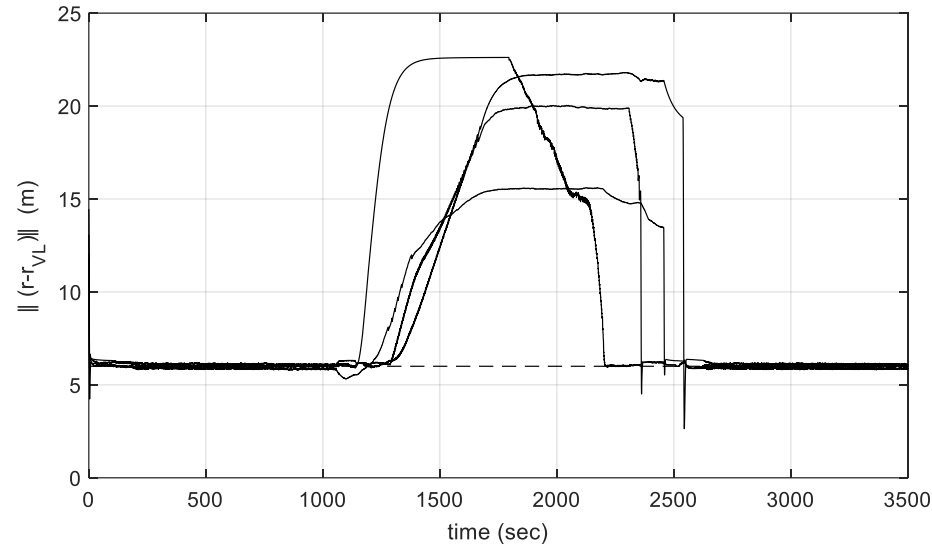


**Figure 4.2.3** Relative distances between virtual leader and four satellites (solid line) in a regular tetrahedron formation and radius of circle  $R = 6$  m (dashed line)

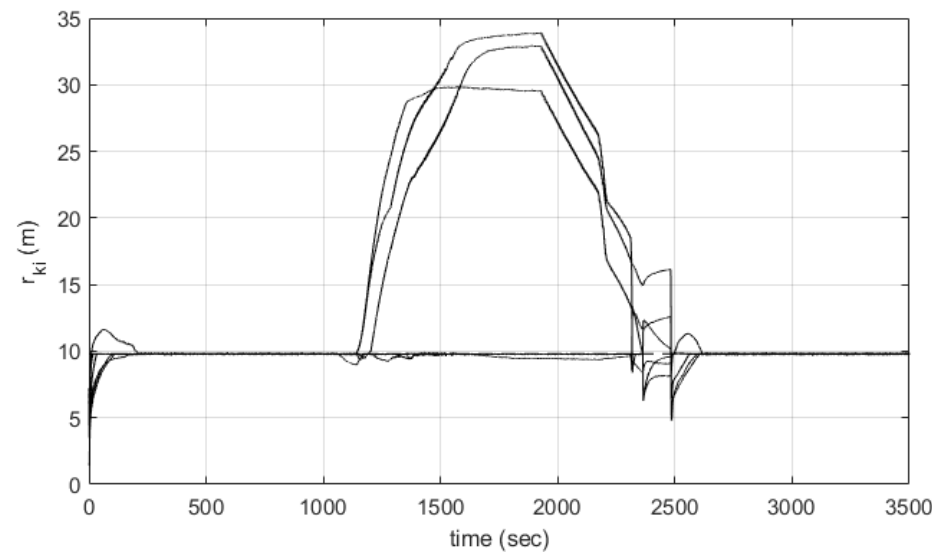


**Figure 4.2.4** Relative distances between satellites (solid line), side length of tetrahedron, 9.798 m (dashed line)

## 5. Conclusions

### 5.1 Summary and Contributions

We have presented a novel approach for collision-free trajectory design and control based on the Artificial Potential Field (APF) method for satellites formation flying in a regular polygonal and a tetrahedron shape. The formation potential function was defined for the formation flying through the virtual structure approach and the control law was derived referring to the Lyapunov stability theorem. The formation potential function consists of the structural and the repulsive potential function. The structural potential function is defined so that the multiple satellites can maintain a constant distance from the virtual leader. The repulsive potential function is defined to maintain equal distances between the satellites without specifying the distance between two satellites. This function allows the satellites to reconfigure into another regular polygonal formation without modifying control laws when some of the satellites in a group fail. The stability analysis was presented to ensure the stability of the control system.

Next, the rotational potential function was derived in the newly defined local coordinate frame for collision avoidance maneuvers through four-step process. The local frame which has the origin at the center of the obstacle is defined using the positions of the satellite and target point. The control law has been developed for formation control with collision avoidance by combining the formation potential function and the rotational potential function. The performance of the control law based on the Lyapunov theory was illustrated in the numerical simulation examples of formation keeping and reconfiguration. Simulation results imply that our collision avoidance strategy has more advantages when designing the reference trajectory of the formation group without detecting obstacles in advance. Our control law has shown to prevent convergence to a local minimum compared with the other APF-based approach in the simulation example. Furthermore, we augmented sliding mode controller to the developed control law to improve the formation flying performance in

terms of robustness, which was successfully verified by numerical simulations in the presence of disturbances.

In conclusion, we designed the integrated control law by newly defining the potential functions for formation flying and collision avoidance. This approach presents the rotational potential function which is newly defined to tackle the APF's local minimum issue. It can be easily applied to nonlinear control because the control law is fully developed under the APF system. By applying the SMC method additionally, the control law is developed as a robust control law to accommodate uncertainties and disturbances without losing the benefit of the APF-based control law. The proposed approach demonstrates practical usability to small satellites in that its formulas and calculations are relatively intuitive and straightforward, and that the stability of the control system is ensured. Since this method can be fully utilized in other dynamic systems, not only in the HCW dynamics, it suggests the possibility of application to various fields.

## 5.2 Future Work

*Reflect realistic characteristics of system dynamics.* The proposed control law does not reflect real space environments such as a variety of perturbations due to the additional gravitational effects of planets or asteroids. It is worth studying under more realistic space environments. It is also worthwhile to impose bounds on controller to reflect hardware characteristics of satellites such as fuel consumption or maximum possible thrust.

*Parametric study on the developed control law.* Since the proposed control law has many design parameters, it might be difficult to empirically select appropriate values. Therefore, it should be considered to investigate and analyze the relationships between parameters.



Mainly, we will analyze the change of parameters according to an obstacle size and a size of a polygonal formation and compare simulation results of reference trajectory design with/without consideration of obstacles.

## References

- [1] Scharf, Daniel P., Fred Y. Hadaegh, and Scott R. Ploen. "A survey of spacecraft formation flying guidance and control (part I): Guidance." (2003).
- [2] McInnes, Colin R. "Autonomous ring formation for a planar constellation of satellites." *Journal of Guidance, Control, and Dynamics* 18.5 (1995): 1215-1217.
- [3] Wang, P. K. C., and Fred Y. Hadaegh. "Coordination and control of multiple microspacecraft moving in formation." (1996).
- [4] Park, Jae-Pil, et al. "Mission analysis and cubesat design for canyval-x mission." *14th International Conference on Space Operations*. 2016.
- [5] Moreira, Alberto, et al. "Tandem-L: A highly innovative bistatic SAR mission for global observation of dynamic processes on the Earth's surface." *IEEE Geoscience and Remote Sensing Magazine* 3.2 (2015): 8-23.
- [6] Burch, J. L., et al. "Magnetospheric multiscale overview and science objectives." *Space Science Reviews* 199.1-4 (2016): 5-21.
- [7] Giulietti, Fabrizio, Lorenzo Pollini, and Mario Innocenti. "Autonomous formation flight." *IEEE Control Systems* 20.6 (2000): 34-44.
- [8] Balch, Tucker, and Ronald C. Arkin. "Behavior-based formation control for multirobot teams." *IEEE transactions on robotics and automation* 14.6 (1998): 926-939.
- [9] Ren, Wei, and Nathan Sorensen. "Distributed coordination architecture for multi-robot formation control." *Robotics and Autonomous Systems* 56.4 (2008): 324-333.
- [10] Stilwell, Daniel J., and Bradley E. Bishop. "Platoons of underwater vehicles." *IEEE control systems* 20.6 (2000): 45-52.
- [11] Pham, Viet Hoang, Minh Hoang Trinh, and Hyo-Sung Ahn. "Formation control of rigid graphs with flex edges." *International Journal of Robust and Nonlinear Control* 28.6 (2018): 2543-2559.

- [12] Scharf, Daniel P., Fred Y. Hadaegh, and Scott R. Ploen. "A survey of spacecraft formation flying guidance and control (Part II): Control." *Control*. (2004).
- [13] Hirata, Yasuhisa, et al. "Decentralized control of mobile robots in coordination." *Control Applications, 1999. Proceedings of the 1999 IEEE International Conference on*. Vol. 2. IEEE, 1999.
- [14] Lewis, M. Anthony, and Kar-Han Tan. "High precision formation control of mobile robots using virtual structures." *Autonomous robots* 4.4 (1997): 387-403.
- [15] Leonard, Naomi Ehrich, and Edward Fiorelli. "Virtual leaders, artificial potentials and coordinated control of groups." *Decision and Control, 2001. Proceedings of the 40th IEEE Conference on*. Vol. 3. IEEE, 2001.
- [16] Chen, Yang Quan, and Zhongmin Wang. "Formation control: a review and a new consideration." *Intelligent Robots and Systems, 2005.(IROS 2005). 2005 IEEE/RSJ International Conference on*. IEEE, 2005.
- [17] Rezaee, Hamed, and Farzaneh Abdollahi. "A decentralized cooperative control scheme with obstacle avoidance for a team of mobile robots." *IEEE Transactions on Industrial Electronics* 61.1 (2014): 347-354.
- [18] Crowther, Richard. "Orbital debris: a growing threat to space operations." *Philosophical Transactions of the Royal Society of London. Series A: Mathematical, Physical and Engineering Sciences* 361.1802 (2002): 157-168.
- [19] Starek, Joseph A., et al. "Spacecraft autonomy challenges for next-generation space missions." *Advances in Control System Technology for Aerospace Applications*. Springer, Berlin, Heidelberg, 2016. 1-48.
- [20] Feron, Eric, ed. *Advances in Control System Technology for Aerospace Applications*. Springer, 2016.
- [21] Lee, Kwangwon, Chandeok Park, and Youngho Eun. "Real-time collision avoidance maneuvers for spacecraft proximity operations via discrete-time Hamilton–Jacobi theory." *Aerospace Science and Technology* 77 (2018): 688-695.
- [22] Khatib, Oussama. "Real-time obstacle avoidance for manipulators and mobile robots." *Autonomous robot vehicles*. Springer, New York, NY, 1986. 396-404.

- [23] Rimon, Elon, and Daniel E. Koditschek. "Exact robot navigation using artificial potential functions." *IEEE Transactions on robotics and automation* 8.5 (1992): 501-518.
- [24] Vail, Douglas, and Manuela Veloso. "Multi-robot dynamic role assignment and coordination through shared potential fields." *Multi-robot systems* (2003): 87-98.
- [25] 남현성, et al. "전위장을 이용한 로봇 경로계획의 구조적 Local Minimum에 대한 연구 (A Study on the Structural Local Minimum Problem in Robot Path Planning Using Potential Field)." *대한전자공학회 학술대회* (1994): 58-63.
- [26] Zhu, Qidan, Yongjie Yan, and Zhuoyi Xing. "Robot path planning based on artificial potential field approach with simulated annealing." *Intelligent Systems Design and Applications, 2006. ISDA'06. Sixth International Conference on*. Vol. 2. IEEE, 2006.
- [27] Badawy, Ahmed. *On-orbit manoeuvring using superquadric potential fields*. Diss. University of Strathclyde, 2007.
- [28] Kelasidi, Eleni, Kristin Ytterstad Pettersen, and Jan Tommy Gravdahl. "A waypoint guidance strategy for underwater snake robots." *Control and Automation (MED), 2014 22nd Mediterranean Conference of*. IEEE, 2014.
- [29] Osborne, John, and Rolf Rysdyk. "Waypoint guidance for small UAVs in wind." *Infotech@ Aerospace*. 2005. 6951.
- [30] Matoui, Fethi, Boumedyen Boussaid, and Mohamed Naceur Abdelkrim. "Local minimum solution for the potential field method in multiple robot motion planning task." *Sciences and Techniques of Automatic Control and Computer Engineering (STA), 2015 16th International Conference on*. IEEE, 2015.
- [31] Kim, Yong Hwi, et al. "Smooth Path Planning by Fusion of Artificial Potential Field Method and Collision Cone Approach." *MATEC Web of Conferences*. Vol. 75. EDP Sciences, 2016.
- [32] Vallado, David A. *Fundamentals of astrodynamics and applications*. Vol. 12. Springer Science & Business Media, 2001.

- [33] Bate, Roger R., Donald D. Mueller, and Jerry E. White. *Fundamentals of astrodynamics*. Courier Corporation, 1971.
- [34] Slotine, Jean-Jacques E., and Weiping Li. *Applied nonlinear control*. Vol. 199. No. 1. Englewood Cliffs, NJ: Prentice hall, 1991.
- [35] Barr, Alan H. "Superquadrics and angle-preserving transformations." *IEEE Computer graphics and Applications* 1.1 (1981): 11-23.
- [36] Volpe, Richard, and Pradeep Khosla. "Manipulator control with superquadric artificial potential functions: Theory and experiments." *IEEE Transactions on Systems, Man, and Cybernetics* 20.6 (1990): 1423-1436.
- [37] Jaklic, Ales, Ales Leonardis, and Franc Solina. *Segmentation and recovery of superquadrics*. Vol. 20. Springer Science & Business Media, 2013.
- [38] Saaj, Chakravarthini M., Vaios Lappas, and Veysel Gazi. "Spacecraft swarm navigation and control using artificial potential field and sliding mode control." *Industrial Technology, 2006. ICIT 2006. IEEE International Conference on*. IEEE, 2006.
- [39] Gazi, Veysel, and Raúl Ordóñez. "Target tracking using artificial potentials and sliding mode control." *International Journal of Control* 80.10 (2007): 1626-1635.
- [40] Yao, Jingyi, Raúl Ordóñez, and Veysel Gazi. "Swarm tracking using artificial potentials and sliding mode control." *Journal of Dynamic Systems, Measurement, and Control* 129.5 (2007): 749-754.

## 국문요약

군집 위성의 충돌회피를 고려한  
인공전위장 기반의 편대비행 제어 방법

연세대학교 대학원

천문우주학과

황지윤

본 논문은 인공전위장(Artificial Potential Field, APF) 기법을 가상 구조(Virtual Structure) 방법에 적용하여 군집 위성의 충돌회피를 고려한 편대비행 케적 설계 및 제어 방법을 제시한다. 가상 구조 방법을 이용한 위성의 다각형 및 정사면체 편대비행 케적을 APF 기법을 통해 설계 및 제어하기 위해 편대 전위장 함수(Formation Potential Function)를 정의하고 제어기를 개발한다. 리아푸노프 안정성 정리(Lyapunov stability theorem)와 밸바랫의 보조 정리(Barbalat's lemma)를 통해 개발된 제어기의 안정성(stability) 분석을 수행한다. 기존의 APF 기법에서 장애물 회피를 고려할 때 발생할 수 있는 국부 최적해로의 수렴 문제를 개선하기 위해 장애물을 중심으로 정의한 3 차원의 국부 좌표계에서 기존 연구를 바탕으로 충돌 회피를 위한 회전력 함수(Rotational Force Function)를 정의하고 APF 기법을 적용할 수 있도록 회전 전위장 함수(Rotational Potential Function)를 유도한다. 충돌 회피를 고려한 편대비행 케적 설계 및 제어를 위하여 편대 전위장 함수와 회전 전위장 함수를 더하여 전체 전위장 함수(Total Potential



Function)를 정의하고 제어기를 개발하여 소프트웨어 시뮬레이션을 통해 제어기의 성능을 검증 및 분석한다.

힐-클로헤시-월셔 동역학 방정식(Hills-Clohessy-Wiltshire Dynamics) 하에 장애물을 배치하여, 다양한 형태로 편대비행하는 다수의 위성이 국부 최적해에 수렴하기 쉬운 시뮬레이션 환경을 구성한다. 대형유지비행 및 대형 재배치 예제를 통해 다양한 경계조건에 대한 다수의 위성의 충돌회피와 편대비행 유지 여부를 확인하고, 다른 APF 기반의 기법과 비교하여 국부 최적해 문제의 개선을 확인했다. 추가로 편대 비행 성능을 높이기 위해 앞서 APF 기법을 위해 정의한 전체 전위장 함수에 슬라이딩 모드 제어(Sliding Mode Control) 방법을 적용하여 제어 시스템의 불확실성과 외란에도 강건 제어(robust control)가 가능하도록 제어기를 개발한다. 소프트웨어 시뮬레이션을 통해 개발된 제어기를 통해 대형 유지 성능이 향상됨을 확인했다.

이 논문은 국부 최적해 문제를 개선할 수 있는 충돌 회피 전위장 함수를 새롭게 유도했다는 점에 의의가 있다. 충돌 회피와 편대비행 제어를 위해 정의한 전위장 함수를 하나의 함수로 통합하여 표현함으로써 제어 시스템의 안정성을 보장하는 APF 기반의 제어기 설계가 가능했다. 이와 같이 전위장 함수를 정의하여 SMC 방법 적용이 가능하게 되어 제어기의 성능을 더 높일 수 있었다.

---

핵심어: 인공전위장, 충돌 회피, 편대비행, 슬라이딩 모드 제어